This is to certify that the
dissertation entitled

Free Stream Surface Methods for Stabilizing Mixed-Compression Inlets

presented by

David Benjamin Benson

has been accepted towards fulfillment
of the requirements for the

Ph.D. degree in Mechanical Engineering

Major Professor's Signature

August 9, 2004

Date

Fre

Free Stream-Surface Methods for Stabilizing Mixed-Compression Inlets

By

David Benjamin Benson

A DISSERTATION

Submitted to
Michigan State University
in partial fulfillment of the requirements
for the degree of

DOCTOR OF PHILOSOPHY

DEPARTMENT OF MECHANICAL ENGINEERING

2004

ABSTRACT

FREE-STREAM SURFACE METHODS FOR STABILIZING MIXED-COMPRESSION INLETS

By

David Benjamin Benson

Mixed-compression inlets are needed by turbojet engines powering aircraft intended to cruise at Mach numbers exceeding about 2.5 for efficient conversion of inlet air's dynamic pressure to static pressure. Unfortunately, mixed-compression inlets are not very stable because of flow separation from shock-wave / boundary-layer interactions, which changes the effective inlet surface geometry. In this study, two methods for controlling the effective inlet geometry for stable fluid flow in a mixed-compression inlet are proposed and investigated by using computational fluid dynamics (CFD). CFD simulations were performed to (1) characterize the near-throat flow of the mixed-compression inlet under critical flow conditions with bleed and (2) examine free-stream surfaces formed by two proposed control methods.

In the first set of simulations, critical flow through an axisymmetric, mixed-compression inlet was examined using two different bleed boundary conditions to model the flow through the cowl and centerbody bleed holes. In one bleed boundary condition, the locations of the bleed holes were discerned. In the

other. e

numbe

rate. T

the inle

bleed r

this reg

and su

stream

Key pr

the su

the in

inject

driven

modif

param

cross

flow r

impor

solve

mod

a the

equa

other, each row of bleed holes was modeled as a porous surface, where the number of bleed holes in each row was accounted for to give the correct bleed rate. These simulations characterized the shock structure in the throat region of the inlet and indicated that the bleed-hole configuration, in addition to the overall bleed rate, is a central element in determining the shock structure and strength in this region. The second set of simulations uses combined supersonic injection and suction in a turbulent, supersonic crossflow to generate a desired free-stream surface that behaves like a wall of the inlet except with a slip surface. Key properties of the jet structure were well-captured and results for the height of the surface generated indicate that there is little impact as the Mach number of the injected fluid is increased. The third set of simulations uses subsonic injection into a recessed cavity placed in a turbulent, supersonic crossflow. The driven fluid is used to control the deflection of the crossflow by the cavity and to modify the boundary layer downstream of the cavity. For the range of parameters investigated, results indicate that the deflection of the separated crossflow is only modestly influenced by either the Mach number or the mass flow rate of the injected fluid and that the shape of the cavity is the most important parameter in determining the downstream profile of the boundary layer.

The CFD simulations were generated by using the CFL3D code, which solves the Reynolds-averaged continuity, compressible Navier-Stokes (using a modified form the thin-shear layer approximation), and total energy equations for a thermally perfect gas. The turbulent stresses were modeled by the one-equation Spalart-Allmaras model and the shear-stress transport (SST) model.

To my wife, Tamara, and to the Laughter which we share.

ACKNOWLEDGEMENTS

I would like to extend my special thanks to my thesis advisor, Dr. Tom I-P. Shih, for his guidance and assistance during my graduate studies. I would also like to thank the members of my committee for their guidance and their willingness to commit their time to this process: Dr. Manoocher Koochesfahani, Dr. Farhad Jaberi, Dr. Mei Zhuang, and Dr. Guowei Wei.

In addition, I would like to thank Fred Hall for his patience and assistance with all of the computer and network glitches that occupied my time in graduate school and Dr. Robert Stein for his advice and for his assistance in helping me turn CFL3Dv6.1 into CFL3Dv6.2. I would also like to thank Dr. Charles Petty for his interest and approach to students and education.

I would like to thank my spouse, Tamara, for her support and my son, Isaac, for his patience. He grew up with this research and was an excellent assistant. A note of thanks also goes to C&J Editing of Chevy Chase, MD for they're excellent work.

Finally, I would like to thank David O. Davis and Brian Wills from NASA Glenn for their funding of the mixed-compression inlet simulations. The inlet research was supported by grant NAG 3-2234 from NASA Glenn Research Center and I am grateful for this support.

TABLE OF CONTENTS

LIST OF FIGURES

Images in this dissertation are presented in color.

Figure

Figure

Figure

Figure

Figure

Figure

Figure

Figure

Figure

Figure

Figure

Figure

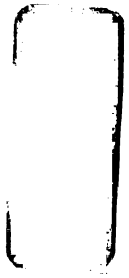

Figure

Figure

Figure

Figure

Figure

Figure

Figure

Figure

Figur

Figur

Figur

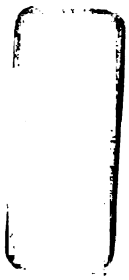

Figure

Figure

Figure

Figure

Figure

Figure

Figure

Figur

Figur

Figur

Figur

Figur

Figur

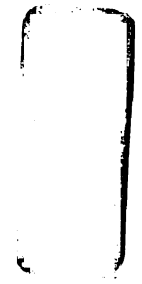

LIST OF TABLES

KEY TO SYMBOLS AND ABBREVIATIONS

b	spanwise spacing between bleed holes
c	crossflow property
C_D	discharge coefficient
d	injection/bleed hole diameter
D	inlet capture diameter
f	freestream property
inf	freestream property
j	jet property
J	jet-to-crossflow momentum ratio
k	turbulent kinetic energy
M	Mach number
P	pressure
R	inlet capture radius
SST	shear-stress transport
V	velocity
W	normal velocity
x	x-coordinate
x_c	streamwise distance as measured from cowl lip
y	y-coordinate
y+	wall coordinate
z	z-coordinate
Z_0	local wall coordinate as measured from centerbody surface
Z_{wall}	local wall coordinate as measured from cowl surface

Greek Symbols

ρ	density
τ	flap angle
θ	angle of injection measured relative to x-coordinate
Δy	normal distance from first grid point to wall
ω	dissipation rate per unit turbulent kinetic energy
γ	ratio of specific heats

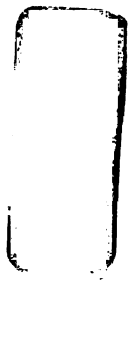

1.1 O

upon
Golds
as we
comp
supe
by th
disto

types
mixe
a str
entra
is fu
comp
comp

CHAPTER 1

Introduction

1.1 Objectives

The performance and efficiency of a turbojet engine depends strongly upon the design and performance of the engine's inlet (*cf.* Seddon and Goldsmith, 1985). The inlet determines the amount of air entering each engine as well as the velocity and pressure of the air when it reaches the engine's compressor face. Since the compressor requires air at low subsonic speeds, supersonic air entering the inlet must be decelerated to the conditions required by the compressor with a maximum of pressure recovery and a minimum of flow distortion.

To accomplish these objectives during supersonic flight, there are two types of inlets available for turbojet engines: external compression inlets and mixed-compression inlets. In an external compression inlet, the fluid undergoes a strong shock at the entrance or just outside the entrance to the inlet. From the entrance of the inlet to the compressor face, therefore, the fluid is subsonic and is further decelerated by the shape of the inlet to the conditions required by the compressor. When the flight Mach number exceeds about 2.5, however, mixed-compression inlets are the preferred approach because they can effectively

convert dynamic pressure of the high Mach number flow to static pressure over relatively compact space. In a mixed-compression inlet, the flow is first decelerated through a series of oblique shocks. Just downstream of the throat, these oblique shocks culminate in a weak terminal shock. From this point, the remainder of the inlet is a subsonic diffuser and the flow is further decelerated to the conditions required by the compressor (**Figure 1.1**). In this way, the objectives of the inlet can be obtained with a minimum of internal drag and a large pressure recovery.

The ideal flow through a mixed-compression inlet is one in which the inlet captures all of the air approaching the inlet's cross-section and the normal (terminal) shock is stabilized just downstream of the inlet's throat. At this location, the Mach number is only slightly above unity and the loss across the terminal shock is minimized. This flow, referred to as critical flow, is preferred, but is difficult to maintain because small perturbations in the flow field can move the terminal shock upstream of the throat.

If the terminal shock should move upstream of the throat for any reason, the shock will continue to move upstream until the flow is subsonic throughout the inlet and a bow shock is formed outside of the inlet. For a mixed-compression inlet, this situation causes most of the flow approaching the inlet to be diverted away from the inlet and is known as the unstart condition since the engine will shut down from an insufficient amount of air. When this occurs, the engine is shut down and the inlet needs to be reconfigured so as to re-initialize the flow in the inlet.

Figur

Opera

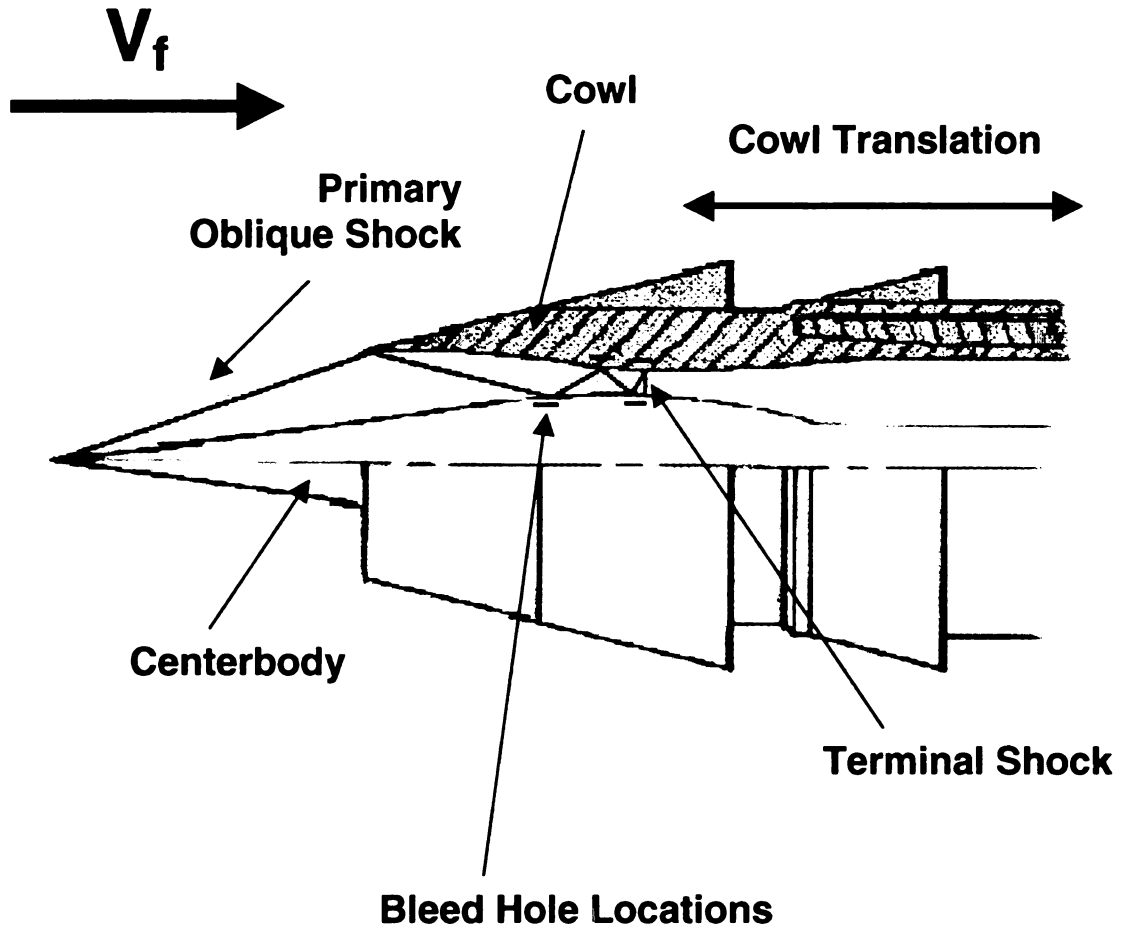

Figure 1.1 General flow pattern observed in the mixed-compression inlet operating at design conditions.

In order to maintain critical flow with the terminal shock stabilized just downstream of the throat, it is necessary to bleed (i.e., suction away) some of the air in the boundary layer about all locations on the inlet where shock waves impinge on the boundary layer (**Figure 1.1**). Bleeding makes the velocity profile in the boundary layer "fuller" so that the flow can overcome the adverse pressure gradient created by the incident and terminal shock waves without separating.

An additional issue associated with the operation of a mixed-compression inlet is the method by which the flow through the inlet is initialized. Since the mixed-compression inlet is designed to operate at supersonic speeds, special measures must be taken to bring the aircraft and the inlet up to the design speeds. During the initialization of flow through the inlet, the geometry of the inlet is changed to maintain operating conditions at the engine face as the speed of the aircraft increases. In a mixed-compression inlet, this is accomplished by moving the cowl to change the geometric profile of the inlet. As a result, designing a mixed-compression inlet requires that certain trade-offs be made in the profiles that are generated as the cowl is translated: the inlet profile requirements for high-speed flight are quite different for those at low-speed flight. This inherently means that, to achieve efficient flight at the design speed, sacrifices are made during flight at lower speeds.

As a result of the need to restructure the inlet profile by physically changing the geometry of the inlet, both inlet unstart and the flow initialization procedure are awkward aspects of mixed-compression inlet operation. This research into the operation and improvement of mixed-compression inlets,

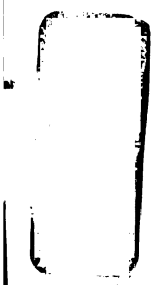

therefore, has two objectives. The first objective is to improve the current state of the art in the numerical simulation of flow through mixed-compression inlets by implementing a set of bleed boundary conditions to model the bleed process that is central to inlet operation. Currently, much of the computational investigation into the flow within mixed-compression inlets has resorted to simulating the bleed holes, used to control the boundary-layer growth within the inlet, as slots or porous walls. This simplification omits many of the three-dimensional aspects that are present in the inlet flow. By modeling the bleed regions as discrete holes, the three-dimensional nature of the flow within the mixed-compression inlet can be more accurately captured, thereby improving our understanding of the nature of the shock structure within the inlet and its relationship with the boundary layer. Improving the numerical simulation of the mixed-compression inlet will also permit the development of alternative control methods for these types of inlets.

This work also presents a method for initializing the flow through a mixed-compression inlet in CFD simulations. The nature of critical flow with in the inlet, with its subsonic and supersonic domains, as well as the complicated boundary-layer/shock wave interactions, presents exceptional difficulties when initializing the flow through the inlet. The methods that are available to the experimentalist in starting the flow though the inlet, involving the translation of the cowl or centerbody to change the shape of the inlet, are not reasonable for use in CFD simulations. In addition, this problem is also complicated by issues associated with the positioning of the terminal shock just downstream of the throat and inlet

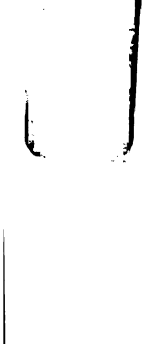

unstart. As a result, a general method is needed to initialize the flow through the inlet for computations.

The second objective of this research is to examine the feasibility of implementing a free stream-surface control method in flow conditions that are similar to the near-throat region of a mixed-compression inlet. In the first approach, the free stream-surface control method is implemented as a supersonic jet injected into a supersonic flow over the inlet centerbody or cowl surface with the addition of downstream bleed. The injected plume forms a free stream-surface that penetrates some distance into the freestream flow and then reconnects to the flat plate at the downstream bleed location. This captured free stream-surface traps a region of the fluid beneath it and causes the exterior flow to be diverted past the reconnected structure. In several respects, this system is similar to the aeroshaping work that has been done in aerodynamics for changing wing shapes. In the previous work, however, the injected plume is used to change the shape of the wing to affect its lift and drag characteristics or to prevent flow separation. In the current situation, however, it is suggested that the injected plume would be used for internal control to change the effective-area ratio of an inlet.

The second approach taken in generating a free stream-surface in a mixed-compression inlet uses injection within a recessed cavity that is placed in the centerbody or cowl surface of the inlet. In this approach, the injected fluid serves to drive the recirculating flow that is already present in the cavity. In this manner, either the thickness of the boundary layer as the freestream flow

reconnects to the surface or the height of the recirculation region within the cavity can be altered to control the effective-area ratio of the inlet. The advantage of this approach, however, is that the injection process is shielded from the high momentum fluid present in the crossflow. To complete the circuit, downstream bleed is provided by the bleed holes that would ordinarily be used within the inlet to control boundary layer separation.

In conducting this research, it is proposed that a free stream-surface control method can be used to address both of the main issues facing the operation of a mixed-compression inlet: inlet unstart and the flow initialization procedure. For example, a free stream-surface control method, implemented in the converging portion of a mixed-compression inlet, could be used to replace or reduce the amount of cowl translation needed to bring the aircraft to its operational speed. By methodically changing the amount and/or angle of injection or by modifying the number of active bleed holes, the free stream-surface can be controlled in such a way as to replicate the necessary changing geometry of the inlet, mimicking the effect of the translating cowl (**Figure 1.2**). A free stream-surface control method could also be implemented to respond to the initial stages of unstart so as to change the effective area ratio of the inlet upstream of the shock and to re-establish favorable operating conditions. The simulations conducted here seek to establish the relevant parameters of the free stream-surface control method and to set the stage for future research into implementing the concept.

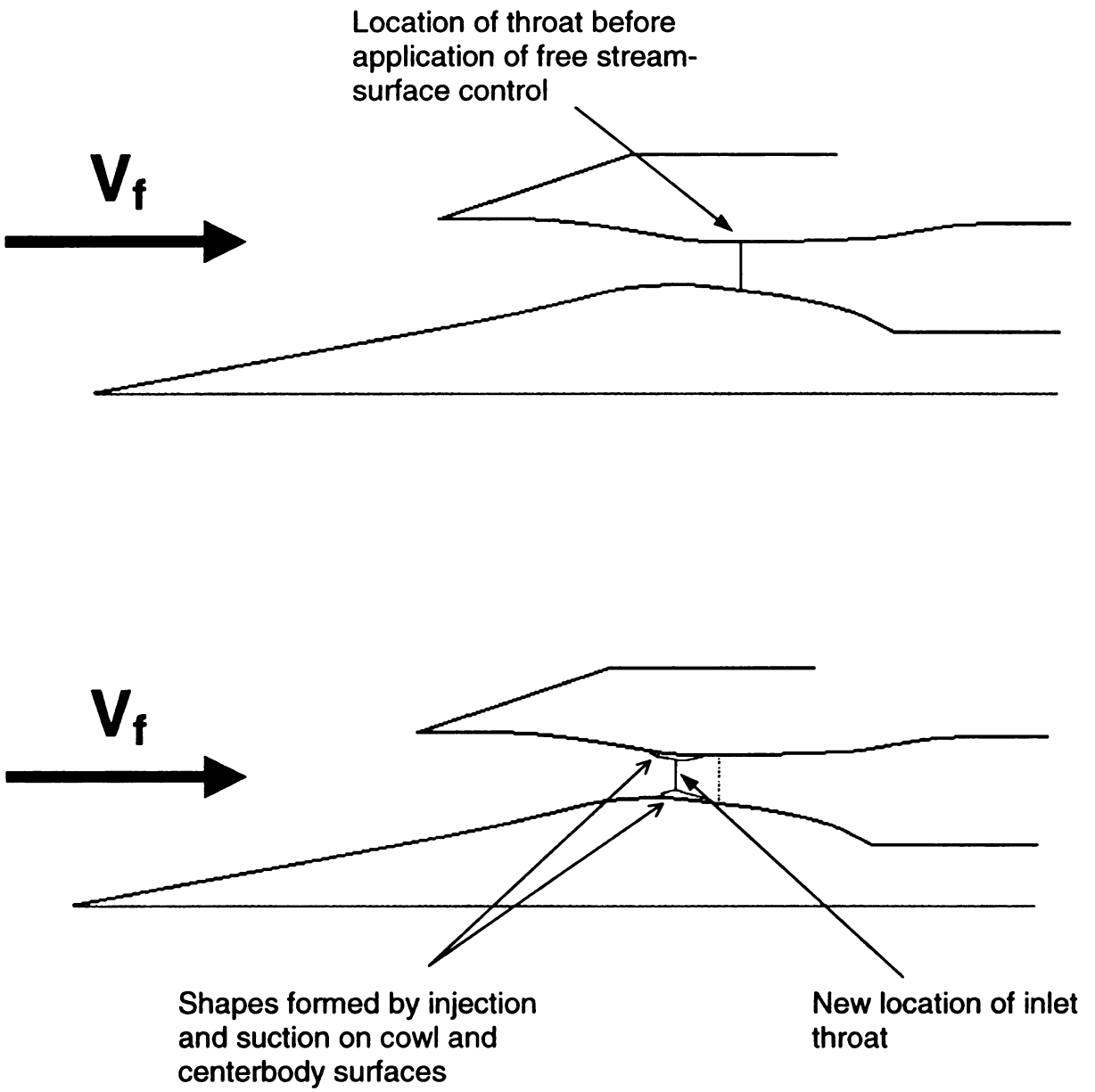

Figure 1.2 Illustration of one of the proposed free stream-surface control method as implemented in the throat region of a mixed-compression inlet. Top: Before the addition of control mechanism. Bottom: After addition of control mechanism.

In the first set of simulations conducted, the free stream-surface is generated by a transverse supersonic jet injected into a supersonic turbulent flow over a flat plate coupled with a series of bleed holes located at some distance downstream of the injection port. The injected plume forms the free stream-surface that enters into the crossflow and then reconnects to the flat plate at the downstream bleed location. In these simulations, the downstream bleed region is modeled, using a bleed boundary condition suitable for choked bleed, as a configuration of discrete bleed holes and the injected jet is modeled as simple square injection port using a supersonic patch boundary condition. The shape of the injected plume is controlled by varying the Mach number and total pressure of the injected fluid or by varying the size, location and pattern of the bleed holes.

In the second set of simulations, the driven cavity portion of a free stream-surface control mechanism is generated by injecting a high-subsonic fluid into a recessed cavity that is placed in a supersonic, turbulent crossflow. In these simulations, the injection occurs on the leading face of the cavity (streamwise face). The Mach number of the injected fluid, the amount of injected fluid and the angle of injection are used to control both the deflection of the crossflow as it separates off the leading edge of the cavity and the boundary layer profile downstream of the cavity. The influence of these parameters on the flow are examined for several cavity length-to-depth ratios (L/h) and for several ratios of the approaching boundary layer height to the cavity depth (δ/L). An additional study was conducted investigating the influence of grid structure on the simulation results.

Taken as a whole, these three studies form the beginnings of a much larger research project. Central to any future research on the development of a viable free stream-surface control mechanism are: (1) the characterization of the free stream-surface profile as a function of the injection and bleed rates; (2) the generation the system's response to an incident, oblique shock; and (3) the response of the core flow within the inlet to changes in the effective area. These research areas are the logical next steps in the process. Additional future research directions indicated are as follows: a characterization of the response of the system in the presence of a normal shock; an investigation of the drag and mixing effects of the free stream-surface system; an exploration into the possible uses of a localized high Mach region that has been observed; and the insertion of the control structure into an inlet.

1.2 Theory and Background

Active flow control is a broad term that describes many different methods used to achieve responsive control of a fluid environment beyond its static design. For example, boundary-layer suction is often used on airfoils to delay the onset of the airfoil's natural separation point. Some of the active flow control methods currently in development include variable geometry techniques, such as MEMs-based active flow manipulators (AFM) and flexible surfaces; the use of combined injection and suction to generate appropriate free stream surfaces; and piezoelectric actuators used to drive oscillations within a flow. In some circles, the term pseudo-active flow control (Joslin *et al.*, 1999) is applied to methods

such as constant boundary-layer bleed and vortex generators, where the control method is not continually evolving to respond to inputs from the flow field. While the control method included in this study could be realized in either category, it is here presented as a pseudo-active control mechanism.

Free stream-surface control methods have been employed in many circumstances where a main flow needs to negotiate a complex geometry. Classical engineering examples include cusp-surface configurations for diffusers and split flaps for airfoils (Chang, 1976). In the suction split flap example, shown in **Figure 1.3**, a hinged portion of an airfoil is detached from the surface on the suction side of an airfoil. As the flow over the upper surface of the airfoil reattaches to the split flap, a standing vortex is trapped in the wedge between the airfoil and the flap. The effect of the split flap, in this case, is to change the shape of the airfoil, thereby changing its lift and drag properties.

Free stream-surface control can also be found in nature. Two examples of this are flow over snow cornices and silt deposits past dams (Chang, 1976). In snow cornices, blown snow piles up on the leading edge of a surface and a trapped vortex is generated as the wind blows across the structure. As a result, any additional blown snow is diverted past the region where the vortex is trapped and builds up on the downwind side of the cornice. This process is self-reinforcing and ends up exaggerating the pointed structure of the snow cornice. In each of these situations, the shape of a trapped (standing) vortex serves to change the main flow in such a way as to improve its passage over an obstacle (Chang, 1976).

Figu

(sta

Figure 1.3 Diagram of a suction spit flap on an airfoil indicating the trapped (standing) vortex and the diverted flow pattern (Chang, 1976).

In 1961, Hurley developed a potential flow analysis for the generation of a free streamline flap (two-dimensional analysis) that, in practice, could be used to change the effective profile of a thin airfoil. By utilizing injection on the leading edge of the airfoil and suction on the trailing edge, the free streamline generates a "thick pseudo-body shape" (**Figure 1.4**) and can, therefore, alter the lift characteristics of the thin airfoil. In Hurley's analysis, the line CD_1 is initially closed and resting on line BD_2. At some later time, the two are separated by an angle τ and fluid is injected tangentially from point B. Suction applied at point C serves to generate a streamline that begins and ends on the two physical surfaces. Within the two lines, a trapped vortex region exists, and the net effect is that the system now has a thick wing shape. This system was designed for use in improving the take-off (low-speed) characteristics of thin airfoils such as those used in supersonic aircraft. Subsequent experiments utilizing injection slots served to confirm the two-dimensional analysis.

One potential application for the free stream-surface, generated by either the direct action of combined injection and suction or by injection within a cavity, is in the near throat region of a mixed-compression inlet. Control methods implemented in this environment could be used to initiate flow through the inlet without having to physically move or change the cowl or centerbody shape and to aid in the prevention of unstart by influencing the effective-area ratio of the inlet. In either circumstance, these control methods would have direct application to supersonic flight projects such as the high-speed civil transport (HSCT).

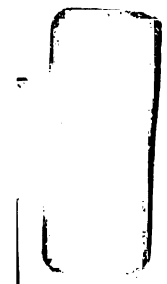

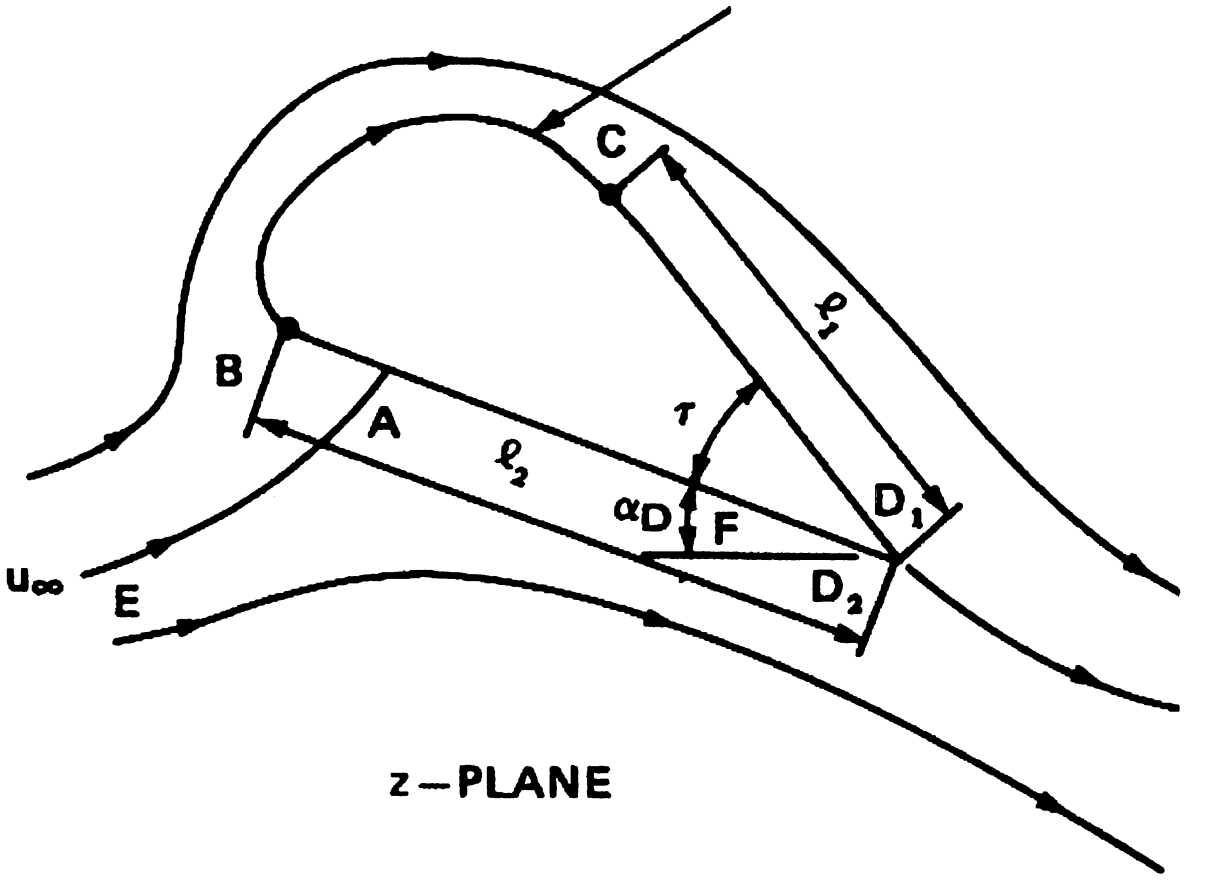

Figure 1.4 A potential flow model for the generation of a free streamline for use in altering the shape of an airfoil (Hurley, 1961).

In high-speed flight, at speeds greater than Mach 2.5, mixed-compression inlets are the preferred method for bringing the supersonic air entering the inlet to the low subsonic speeds required by the compressor (*cf.* Seddon and Goldsmith, 1985). These inlets are very effective at converting the dynamic pressure of the high Mach number flow into the static pressure needed by the compressor. They are also capable of achieving this goal over a relatively short length, thereby decreasing the internal drag of the inlet. However, numerous complications arise when using mixed-compression inlets.

The ideal flow through a mixed-compression inlet is one in which the inlet captures all of the air approaching the inlet cross-section and where the normal (terminal) shock is stabilized just downstream of the inlet's throat. Within the inlet, the flow is decelerated through a series of oblique shocks until it reaches the throat region where it terminates in a strong shock (**Figure 1.5**).

At the terminal shock location, the local Mach number is only slightly above unity so that the loss across the terminal shock is minimized. This flow, referred to as critical flow, is preferred, but it is difficult to maintain because small perturbations in the flow field can move the terminal shock upstream of the throat. Once the terminal shock moves upstream of the throat, it will continue to move upstream until the flow is subsonic throughout the inlet and a bow shock forms outside the inlet. This causes most of the flow approaching the inlet to be diverted away and is known as the unstart condition since the engine will shut down from an insufficient amount of air.

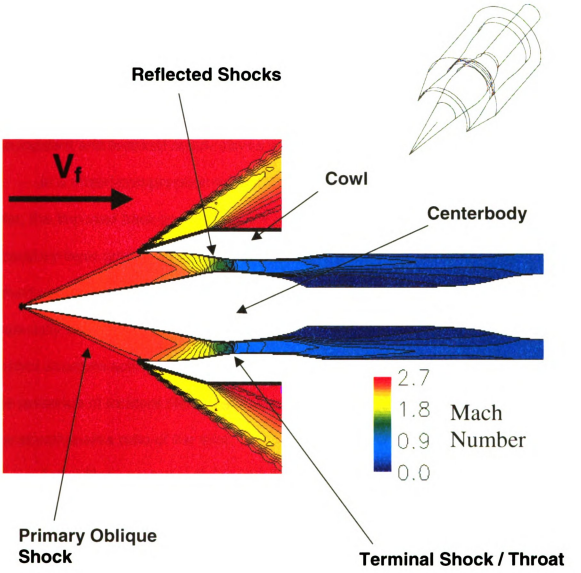

Figure 1.5 Mach Number contours for CFD simulation of flow through a mixed-compression inlet (Benson *et al.*, 2003). Inset: Perspective view of a 180 degree slice of the inlet.

downs

air in t

on the

"fuller"

the inc

inlet. t

bound

mixed-

especi

contro

the pr

the eff

injecti

dimen

is also

some

comp

mech

inlet.

Harlo

In order to maintain critical flow with the terminal shock stabilized just downstream of the throat, it is necessary to bleed (i.e., suction away) some of the air in the boundary layer at all locations on the inlet where shock waves impinge on the boundary layer. Bleeding makes the velocity profile in the boundary layer "fuller" so that the flow can overcome the adverse pressure gradient created by the incident and terminal shock waves without separating.

In a mixed-compression inlet, the flow responds to the geometry of the inlet, the imposed back-pressure at the engine face, and the effect of the boundary-layer growth on top of the geometry. Since the terminal shock in a mixed-compression inlet is held (ideally) very close to the throat, the inlet is especially sensitive to disturbances and area changes. A free stream-surface control structure acting in the near-throat region of the inlet needs to be stable in the presence of incident oblique shock waves and capable of appreciably altering the effective-area ratio of the inlet.

Active/Pseudo-Active flow control with free stream-surfaces utilizing injection and bleed through discrete holes is highly dependent on the three-dimensional behavior of the flow. This three-dimensional behavior of the system is also of interest to this study since the injection and suction regions are to be, in some cases, modeled by boundary conditions. This is necessary from a computational efficiency standpoint, especially if, in future research, the control mechanism is to be implemented within a simulation of a mixed-compression inlet. For the modeling of bleed through discrete holes, various authors (cf. Harloff and Smith, 1985; Paynter *et al.*, 1994; Benson *et al.*, 2000) have already

done extensive work developing the bleed boundary conditions to accurately capture the physics of the bleed process.

In 1968, Spaid and Zukoski developed an analytical model for the interaction of a supersonic transverse jet with a supersonic cross-flow and were able to develop relationships for, among other things, the jet penetration height (**Figure 1.6**). This analytical model, developed for two-dimensional flow, compared well with slot injection experiments. In these experiments, the injected jet caused the boundary-layer flow upstream of the jet to separate and generated a trapped region of recirculating flow in front of the jet. Within the jet, a series of shocks were observed as the flow turned and was swept downstream. The pattern of shocks was also observed to be dependent on the degree of under-expansion of the jet. Downstream of the jet, another trapped region of recirculating flow was observed and a compression shock was generated as the flow reattached.

In 1970, Povinelli *et al.* and Billig *et al.* (Chang, 1976) investigated the penetration of a single, normal gas jet injected into a supersonic crossflow. The authors classified the shape of the resulting shock structure within the jet and developed methods for ascertaining the penetration height as a function of the Mach number ratio, momentum ratio, nozzle diameter, and downstream distance from the injection point.

The study identified the momentum flux ratio was identified as the most important parameter in determining the penetration of the jet into the crossflow.

STATI
PRESS

Figur
(slot)

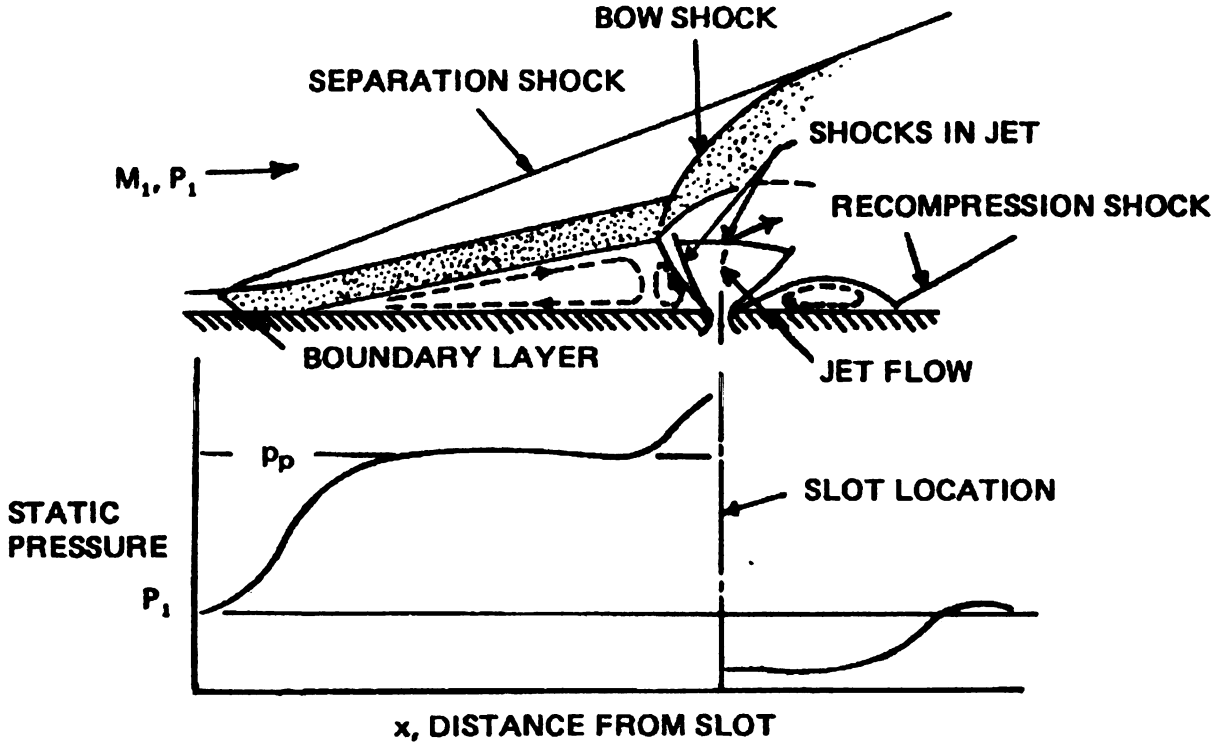

Figure 1.6 Schematic and pressure profile of the interaction of a transverse jet (slot) with a supersonic main flow (Spaid and Zukoski, 1968).

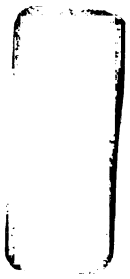

The mo

where

Schetz

expand

termina

identif

also at

cross-

et al.,

single

exper

divert

near t

that f

at the

role i

The momentum flux ratio, J, is determined as

$$J \equiv \frac{\rho_j V_j^2}{\rho_c V_c^2}$$

where j and c refer to the transverse jet and crossflow properties, respectively.

Figure 1.7 displays the details the internal jet structure as described by Schetz and Billig (1966). In these experiments, they observed that the jet expanded as it entered the crossflow and this structure had a barrel shape that terminated in a disk-shaped shock referred to as the barrel shock. In addition to identifying qualitative features of the jet structure, Schetz and Billig (1966) were also able to develop models for the width and location of the Mach disk and the cross-sectional area distribution of the jet.

Other jet-in-crossflow research (*cf.* VanLerberghe *et al.*, 2000 and Huang *et al.*, 1990) has focused on the mixing aspects associated with injection by a single transverse jet at various angles of injection. In these simulations and experiments, the jet causes a bow shock to form that allows the crossflow to divert around the jet. A horseshoe vortex is also seen to develop as the flow near the surface is diverted around the jet (**Figure 1.8**).

The jet plume is also observed to consist of a counter-rotating vortex pair that forms in response to the deflection of flow around the jet and the separation at the rear of the jet. The flow is clearly three-dimensional, and this plays a large role in the mixing behavior of the jet. Much of the previous referenced research

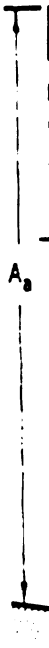

Figu
(slot)

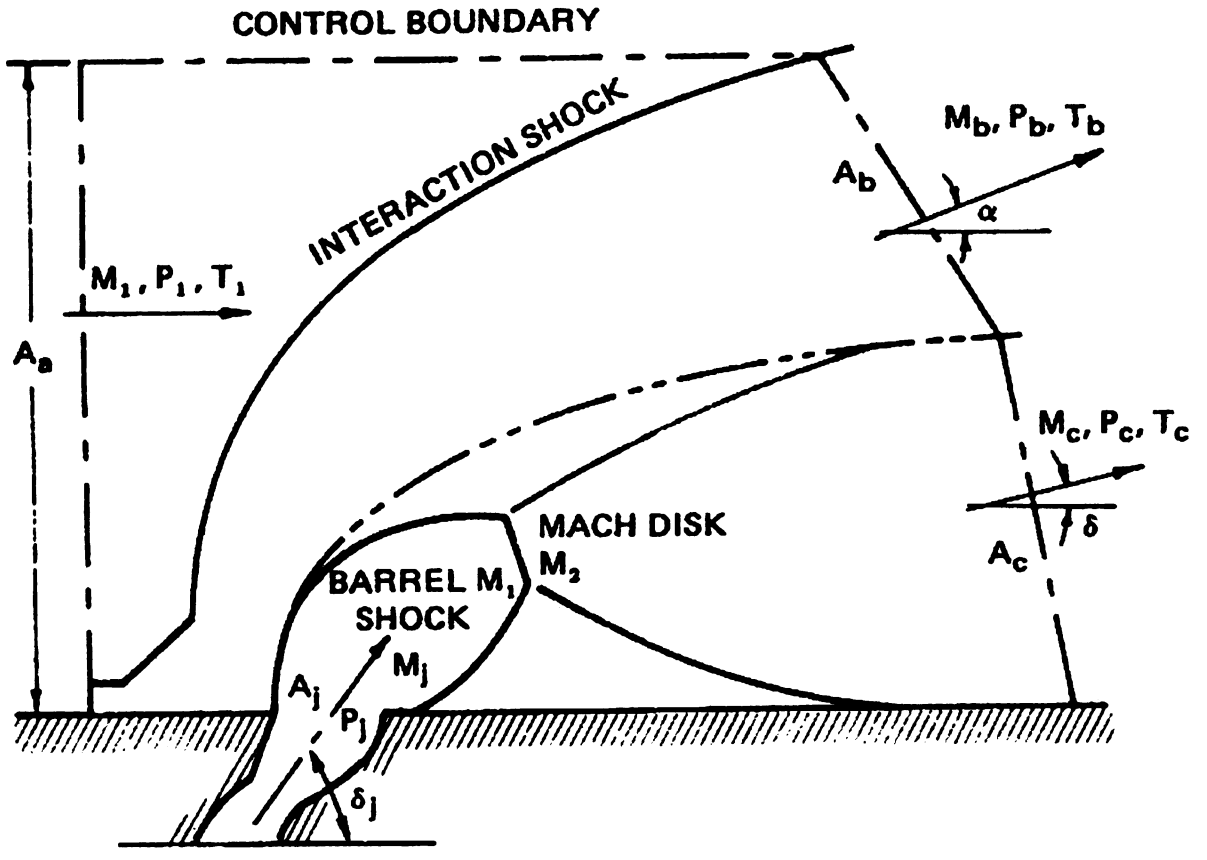

Figure 1.7 Schematic and pressure profile of the interaction of a transverse jet (slot) with a supersonic main flow (Schetz and Billig, 1966).

Su

Cr

H

V

Figu

supe

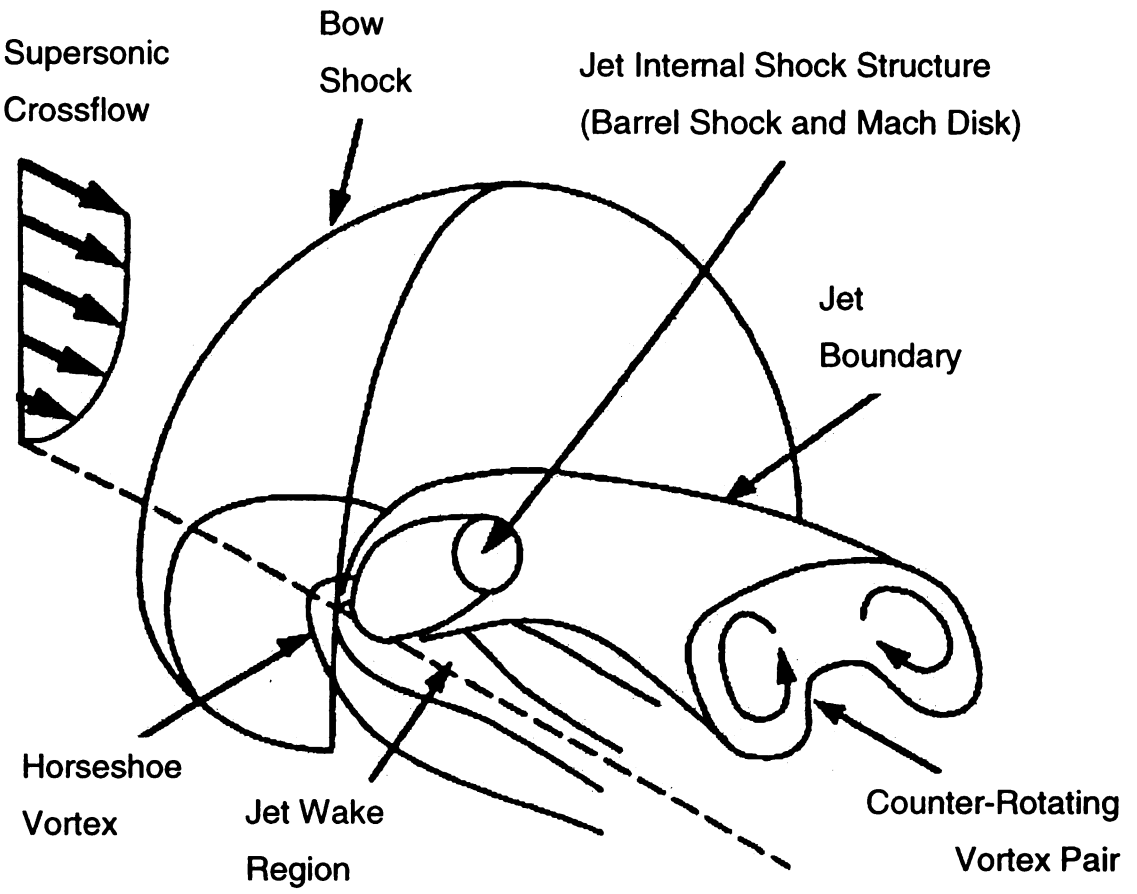

Figure 1.8 Three-dimensional flowfield due to transverse injection into a supersonic crossflow (VanLerberghe *et al.*, 2000).

involved two-dimensional simulations and experiments; as a result, this horseshoe vortex and the counter-rotating vortex pair in the jet were not present. While these jet-in-crossflow experiments have not employed an associated bleed region, they have done extensive work in identifying the three-dimensional features of the injected flow. Their results are of use in identifying salient features of the free stream-surface control mechanism and in assessing the influence of the bleed region on the main flow.

Early work on cavity insertion in supersonic flow focused primarily on reducing the heat transfer rate for protection of hypersonic vehicles. Chang (1976) reports that experimenters were able to reduce the heat transfer rate by a factor of two when a laminar cavity flow replaced a laminar boundary layer flow. However, Chang also that these same studies showed that the changes in the downstream heat transfer rates tended to nullify the positive effects of the injection into the cavity. In 1965, Nicholl (Chang, 1976) conducted experimental studies with helium injection in an annular cavity on a conic re-entry vehicle at Mach 11 (**Figure 1.9**). Nicholl found that by increasing the height of the separation shoulder above the line of the conic surface, the injected fluid was able to pass into the downstream boundary layer flow and dramatically reduce the downstream heat transfer rates.

Current interest in cavity flow fields at supersonic speeds has focused on the issues associated with stores separation from high-speed aircraft. Recent developments in stealth technologies and the desire to reduce radar cross-section from the external store carriages in military aircraft are the motivating

Figu

conic

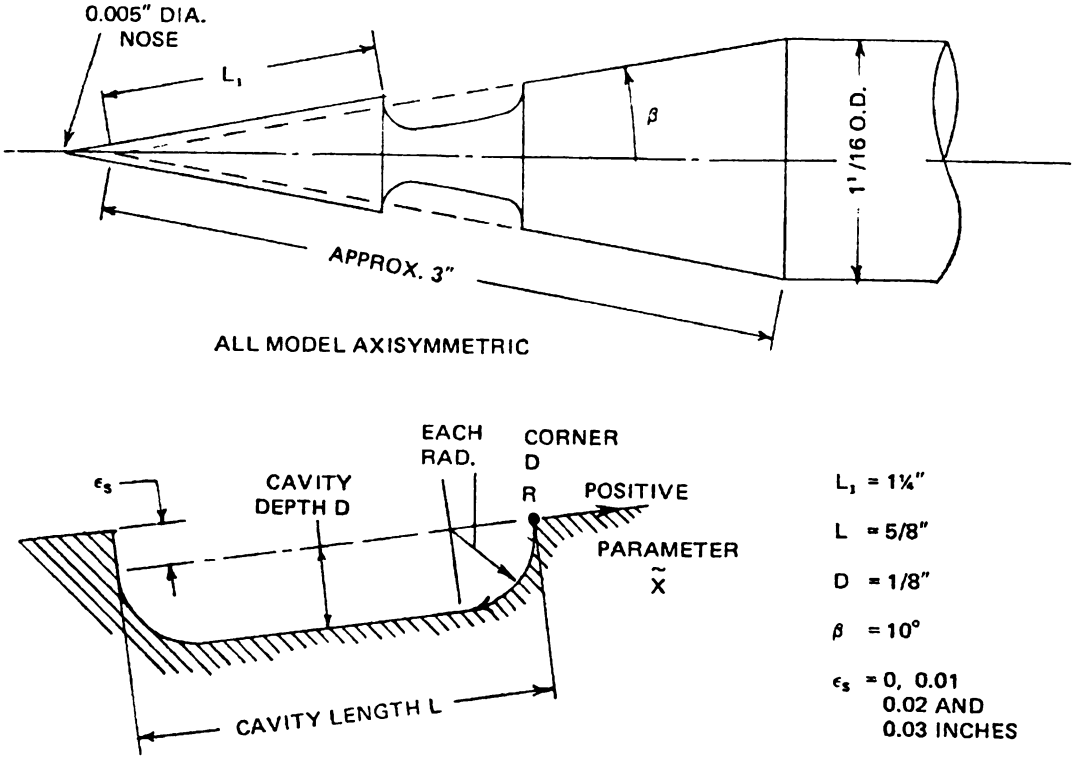

Figure 1.9 Schematic for helium injection into an annular cavity placed in a conic re-entry vehicle (Nicholl, as referenced in Chang, 1976).

factors in the examination of internal store carriages for supersonic aircraft. Research by various authors (*cf.* Wilcox, 1990; Stallings *et al.*, 1991; Plentovich *et al.*, 1993) has focused on quantifying the flow field in the cavity by measuring the pressure, force and moment distributions on a generic store separating from within a box cavity. Various researchers have also proposed different methods to control of the moments and drag experienced by the stores. For example, Wilcox (1990) presented an approach using a cavity with a porous-floor to modify the cavity flow field. By venting the high-pressure fluid in the rear of the cavity to the low-pressure fluid in the front, the objective was to reduce the overall drag characteristics of the cavity. Each of these approaches, however, has involved the passive control of the fluid within the cavity for the purpose of drag reduction or the prevention of flow oscillation.

1.3 Dissertation Outline

This study is an investigation into the three-dimensional aspects of a mixed-compression inlet and of a free stream-surface control method for use in these types of inlets. Chapter 2 focuses on the implementation of bleed boundary conditions within a mixed-compression inlet to examine the three-dimensional aspects of the flow and to provide a background for the control method described. Simulations where the bleed holes are modeled as slots are used for comparison. In Chapter 3, three-dimensional simulations are conducted to assess the structure and form of the proposed free stream-surface control method generated by combined injection and suction directly into the crossflow.

In this
qualita
structu
prese
placed
cross
functi
An ac
grid s

In this study, various features of the free stream-surface control mechanism are qualitatively characterized and the degree of penetration and shape of the structure is examined as a function of jet speed and pressure. Chapter 4 presents the results of several three-dimensional simulations of driven cavity placed in a crossflow. The influence of the driven cavity on the deflection of the crossflow and on the downstream boundary layer profile is examined as a function of jet speed and mass flow rate for several cavity length-to-height ratios. An additional aspect of this study is that it is the examination of the importance of grid structure on the simulation results.

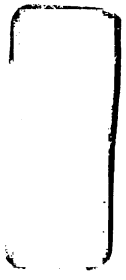

2.1

thro

blee

blee

othe

surf

adju

data

the

three

for i

guid

type

CHAPTER 2

CFD Simulations of Critical Flow Through an Axisymmetric Mixed-Compression Inlet with Bleed Through Discrete Holes

2.1 Summary

CFD simulations were performed to investigate boundary-layer control through bleed patches in an axisymmetric mixed-compression inlet in which the bleed patches are modeled by two global bleed boundary conditions. In one bleed boundary condition, the locations of the bleed holes are discerned. In the other bleed boundary condition, each row of bleed holes is modeled as a porous surface where the number of bleed holes in each row is accounted for by an adjusted discharge coefficient that gives the correct bleed rate. Experimental data for the mixed-compression inlet is used as a basis for comparison between the two boundary conditions.

In this study of critical flow through mixed-compression inlets, there are three main objectives. The first objective is to describe a method or procedure for initializing critical flow through mixed-compression inlets and to develop guidelines on the type of grid system needed to capture the flow physics in this type of inlet. This explicit detailing of the method for initializing the flow through

the inlet will be of use in any future experimentation. The second objective of this research is to present results for two bleed boundary conditions and to compare the results from modeling discrete bleed holes with the more conventional approach using bleed slots. Finally, this research serves as an introduction to the problem of controlling effective-area through the use of combined suction and bleed that will be presented in later sections.

Results are presented for the predicted bleed rates, pressure on the cowl and centerbody surfaces, and Mach number profiles at several key points. Mach number and pressure contours are also presented for the entire flow field. Comparisons were made with available experimental data. Also presented is a method based on one-dimensional isentropic and normal shock solutions to get the flow "started" in CFD simulations of critical flow in mixed-compression inlets.

This computational study is based on the Reynolds-averaged conservation equations of mass (continuity); momentum, using a modified form of the thin-shear layer, compressible Navier-Stokes equations (Biedron *et al.*, 1986); and total energy. These equations are closed by the shear-stress transport (SST) turbulence model of Menter, where integration is to the wall. Solutions were generated by a cell-centered, finite-volume method that uses third-order accurate flux-difference splitting of Roe with limiters, multigrid acceleration of a diagonalized ADI scheme with local time stepping, and patched/overlapped structured grids.

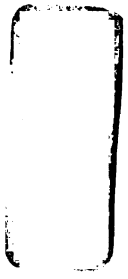

2.2 Introduction

The performance and efficiency of a turbojet engine depends strongly upon the engine's inlet (*cf.* Seddon and Goldsmith, 1985). The inlet determines the amount of air entering each engine as well as the velocity and pressure of the air at the engine's compressor face. Because the compressor requires air at low subsonic speeds, supersonic air entering the inlet must be decelerated with a maximum of pressure recovery and a minimum of flow distortion.

To accomplish this, turbojets utilize two main types of inlets: external compression inlets and mixed-compression inlets. At flight Mach numbers above Mach 2.5, mixed-compression inlets are preferred because they can effectively convert the dynamic pressure of a high Mach number flow to static pressure over relatively compact space. In addition, with proper design, mixed-compression inlets can achieve a very high pressure recovery with a minimum of flow distortion.

The ideal flow through a mixed-compression inlet occurs when the inlet captures all the air approaching the inlet cross-section and the normal (terminal) shock is stabilized just downstream of the inlet's throat. At this location, the Mach number is only slightly above unity and the loss across the terminal shock is minimized.

This ideal flow, referred to as critical flow, is preferred, but it is difficult to maintain because small perturbations in the flow field can move the terminal shock upstream of the throat. Once this happens, the terminal shock will continue to move upstream until the flow is subsonic throughout the inlet and a

bow shock is formed outside of the entrance to the inlet. This causes most of the flow approaching the inlet to be diverted and is known as the 'unstart condition' because the engine will shut down from an insufficient amount of air. In order to maintain critical flow with the terminal shock stabilized just downstream of the throat, some of the air in the boundary layer must be bled (i.e., suctioned away) at all of the locations on the inlet where shock waves impinge on the boundary layer. Bleeding "thickens" the velocity profile in the boundary layer so that the flow can overcome, and not be separated by, the adverse pressure gradient created by the incident and terminal shock waves.

Although many investigators have performed numerical studies of inlet flows (*cf.* Presley, 1975; Knight, 1977; Chen and Caughey, 1980; Buggeln, *et al.*, 1980; Paynter and Chen, 1983; Vaydak *et al.*, 1984; Chyu *et al.*, 1986), relatively few investigators (Kawamura *et al.*, 1987; Vaydak *et al.*, 1987; Chyu *et al.*, 1992) have reported simulations of critical flow through mixed-compression inlets. One of these studies, by Chyu *et al.* (1992), investigated numerous bleed boundary conditions for a two-dimensional, axisymmetric slice of a mixed compression inlet. However, because their study was two-dimensional, their results were limited to modeling the bleed holes as slots.

In simulating mixed-compression inlets, a researcher using numerical methods to study the flow encounters two areas of difficulty. The first area of difficulty is associated with the initialization of flow within the inlet and the method by which the position of the terminal shock is controlled. A physical inlet begins from rest, and the flow through the inlet is gradually increased to the operating

conditions. In this process, the physical inlet is brought through all of the stages of development in the flight. The flow begins as subsonic in the freestream and throughout the inlet. Gradually, the flow is transitioned to a state where the freestream flow is supersonic and the flow throughout the inlet is both supersonic and subsonic.

In addition, with a physical inlet the terminal shock is positioned downstream of the throat by translating either the centerbody or the cowl to change the inlet profile to match the flight conditions. At first glance, the translation of the cowl or centerbody may appear be a suitable control for the unstart condition; however, when the inlet unstarts, the process occurs at such a rapid rate that there would be no way for a mechanical system to respond. To accommodate the changing position of the shock within the inlet and the various possible operational speeds of the aircraft, the final design of a mixed-compression inlet is, therefore, a compromise based on several optimized designs for static inlets.

In summary, the methods employed to initialize the flow in the physical inlet case require that both the inflow boundary conditions and the inlet geometry are functions of time. The flight conditions change as the inlet is brought from rest to operating speeds and the shape of the inlet is changed to hold the terminal shock just downstream of the throat. To an investigator conducting numerical simulations of the flow through a mixed-compression inlet, neither of the methods that are available to the experimentalist for initializing the flow within the inlet are feasible. Even if these methods were available to the CFD

researcher, the time costs in damping out transients that occur after each change in either the freestream conditions or the geometry of the inlet would be prohibitive.

The second main difficulty in simulating mixed-compression inlets is in modeling the bleed patches where the boundary layer flow is suctioned away. With different patterns of circular holes, each bleed hole and its associated plenum would have to be numerically modeled and the flow through them simulated. The level of complexity introduced by this is considerable. Rimlinger *et al.* (1996) conducted simulations that studied supersonic boundary layer bleed through discrete bleed holes in a variety of configurations and environments. In these simulations, the surface of the bleed hole, or bleed half-hole because of symmetry considerations, typically required 32 grid points to appropriately capture the physics of the bleed process. To model the flow past and through a region consisting of six rows of holes, over 1.5 million grid points were used. Extending this level of grid refinement to a full mixed-compression inlet with four or five distinct bleed regions would require a prohibitively large number of grid points. An additional complication to the explicit modeling of the flow through the holes and plenum involves the configuration of the bleed holes being studied. If the patterns of bleed holes is modified in any way, a major reconstruction of the grid as well as the grid patching and overlapping information would be required, especially if multigrid methods are used.

A standard practice in the simulation of mixed-compression inlets, as well as in other devices that use bleed through discrete holes, is to replace the bleed

through discrete holes with a bleed-slot or porous-wall boundary condition. With this boundary condition, the effect of the bleed is distributed along a patch of the bleed surface. In a typical bleed-slot boundary condition, the mass flow rate through the boundary (as a percentage of the freestream) is a free parameter. Unfortunately, when the bleed-slot boundary condition is used to approximate bleed through discrete holes, much of the physics associated with the shape and configuration of the bleed holes, as well as the three-dimensional aspects of the flow, are lost.

To accurately capture the dynamics of the bleed process, Benson *et al.* (2000 and 2001) presented results for a bleed boundary condition that could be used to replace the simulation of flow through choked bleed holes. This boundary condition, applied only at the locations where the bleed is known to occur, treats the flow in the normal direction through the boundary as a function of the local sound speed above the hole. In this research, replacing the hole and its associated plenum with a bleed boundary condition was determined to be acceptable even in the most extreme cases where a single grid point was used to model a bleed hole. In doing so, Benson *et al.* (2000 and 2001) were able to model the flow turning that occurs in the bleed process and to capture the barrier shocks that form on the downstream edge of each bleed hole.

In this current research, the bleed process within the mixed-compression inlet will be simulated using two bleed boundary conditions. The first method uses the bleed boundary condition developed by Benson *et al.* (2000 and 2001)

where each of the bleed holes is discretely modeled. The second approach, common in practice, models each row of bleed holes as a porous surface or slot.

With these two approaches, this study of critical flow through a mixed-compression inlet has three main objectives. The first objective is to describe a method or procedure for initializing critical flow through mixed-compression inlets and to develop guidelines on the type of grid system needed to capture the flow physics in this type of inlet. This explicit detailing of the method for initializing the flow through the inlet will be of use in any future experimentation. The second objective is to present results for two bleed boundary conditions and to compare the results from modeling discrete bleed holes with the more conventional approach using bleed slots. The third and final objective of this research is to introduce the problem of controlling the effective-area through use of combined suction and bleed; this will be presented in later sections.

2.3 Description of Problem Studied and Methods Employed

2.3.1 Problem Description

The flow simulation studied involves a uniform, supersonic freestream flow incident upon and passing through an axisymmetric mixed-compression inlet. The main features of the inlet (**Figure 2.1**) consist of a centerbody, a cowl with both interior and exterior surfaces, bleed holes on both the centerbody and interior cowl surfaces, and an engine compressor face that is downstream of the throat. Other features of the inlet, such as the bypass valves and the bleed hole plenums, are not utilized in this study.

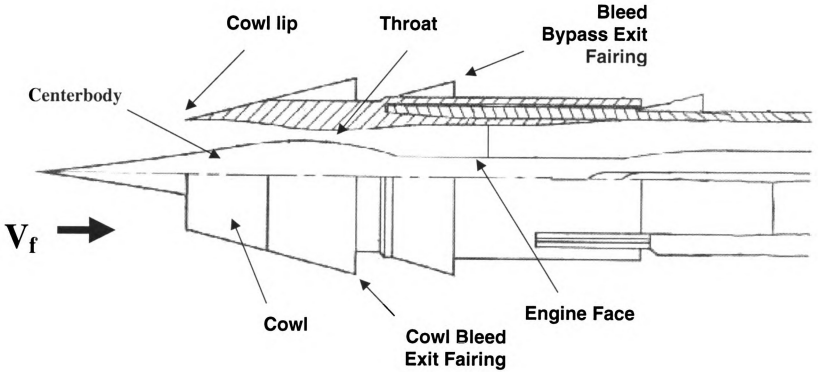

Figure 2.1 Schematic of the mixed-compression inlet.

Within the inlet, the approaching supersonic flow is first decelerated and turned by an oblique shock that forms from the centerbody tip (**Figure 2.2**). At the inlet's designed operating conditions, the primary oblique shock terminates on the lip of the cowl, thereby preventing any of the turned flow from being diverted past the inlet. This defines a capture diameter (D) for the inlet because all of the freestream flow within this capture diameter is passed through the inlet. If, for some configuration, the primary oblique shock does not terminate on the cowl lip, some of the flow that would have been available for use by the engine is diverted over the cowl; this is referred to as "spillage." When "spillage" is present, the inlet is less efficient.

The flow that was turned by the primary oblique shock travels up the centerbody ramp and enters the supersonic diffuser section of the inlet. Upstream of the throat, in the converging section of the inlet, a series of weak oblique shocks are formed and the flow is decelerated as it approaches the throat. Just past the throat, a normal shock forms and the flow transitions from supersonic flow to subsonic flow. In the configuration studied, the terminal shock is intentionally held close to the throat and the terminal shock is a weak normal shock. The remainder of the diverging section of the inlet now functions as a subsonic diffuser and the flow is further decelerated as it approaches the engine face.

To maintain the flow through the inlet, the low-momentum fluid near the wall is suctioned (bled) through a series of discrete bleed holes. Without this boundary layer bleed, shock waves interacting with the boundary layer will cause

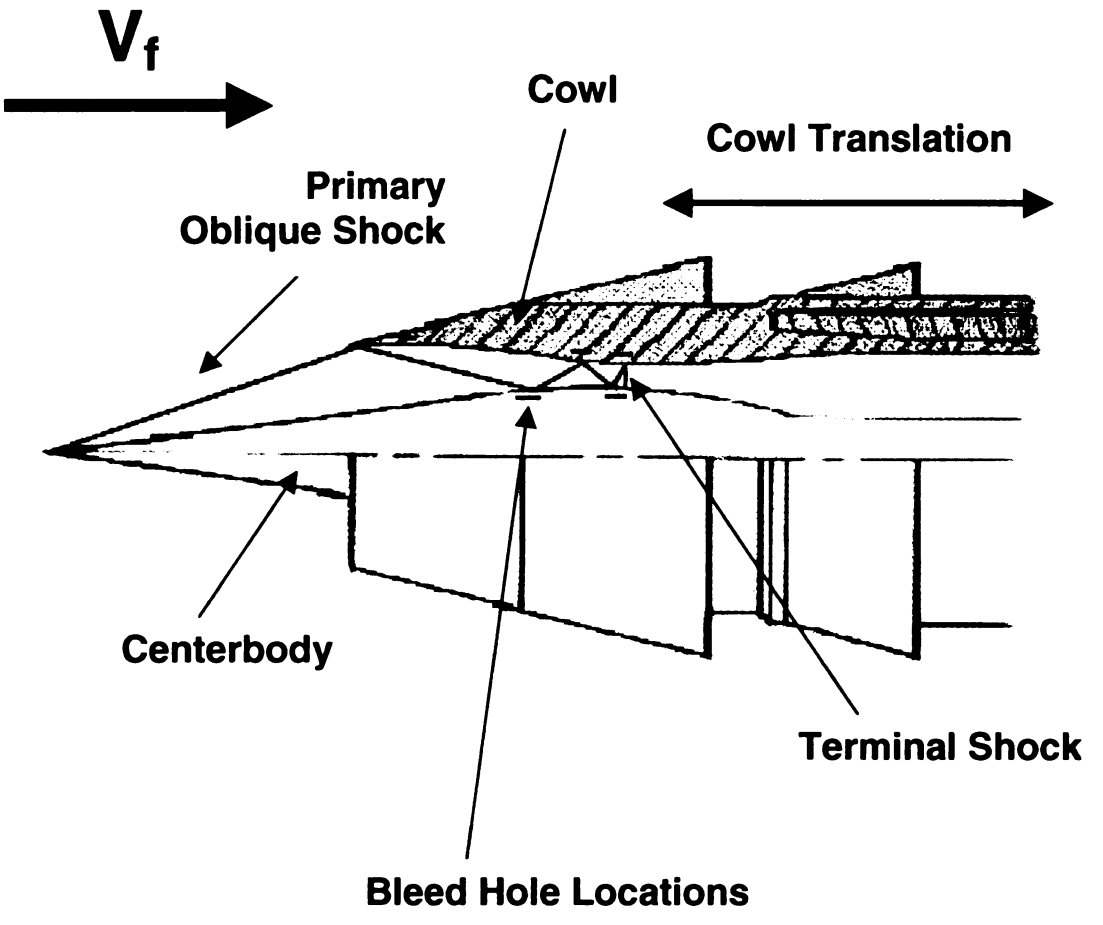

Figure 2.2 General flow pattern observed in the mixed-compression inlet operating at design conditions.

the flow to separate and the inlet will unstart. For the configuration studied in this research, no spillage is indicated, and the experimental bleed rate was given as 8.2 percent of the mass flow rate for the captured flow.

The prototype inlet simulated in this study was acquired from wind tunnel studies done by Smeltzer and Sorensen (1973). The prototype inlet is approximately one-quarter scale and has a capture diameter of D = 38.8 cm (R = 19.4 cm). The supersonic diffuser was designed for operation at a Mach number of 2.65. It was also designed with the objective of achieving optimal efficiency at the design conditions while permitting a large mass flow rate at a low Mach number flight and minimizing the length of the inlet to address internal drag issues. With this prototype inlet, the cowl was translated to change the inlet profile during the initialization of the flow within the inlet.

For this research, the properties of the inlet were examined at the design condition (Mach 2.65) and for a single configuration of the bleed holes (configuration C). At the design condition, the cowl lip is positioned downstream of the centerbody tip at x/R=2.325 (**Figure 2.3**), where x is the distance as measured from the centerbody tip. The engine face, fixed for all configurations, is located at x/R = 6.800 as measured relative to the centerbody tip.

The location of the bleed holes on the inlet cowl and centerbody walls, for the configuration studied (bleed hole configuration C), are shown in **Figure 2.4**. Each bleed hole has a diameter of d = 0.0125R, where R = D/2. For the inlet's design Mach number, this hole diameter is anticipated to be of the same order as the momentum thickness at the throat and is typical for this type of problem.

Figu
Sore

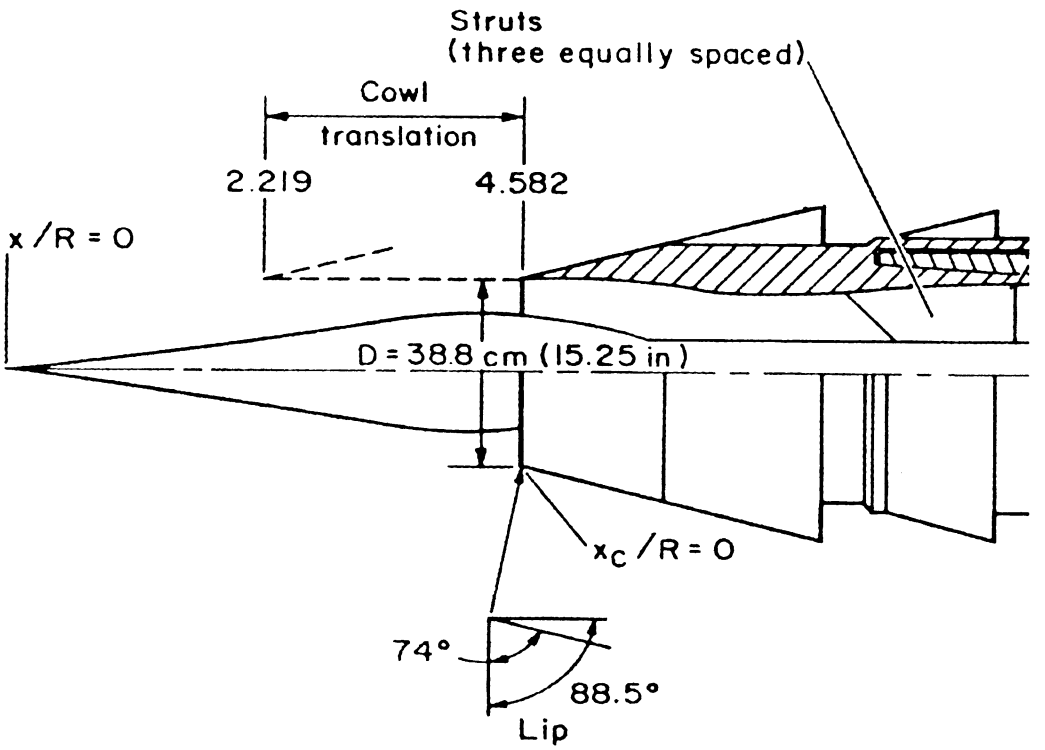

Figure 2.3 Model schematic for the mixed-compression inlet (Smeltzer and Sorensen, 1973).

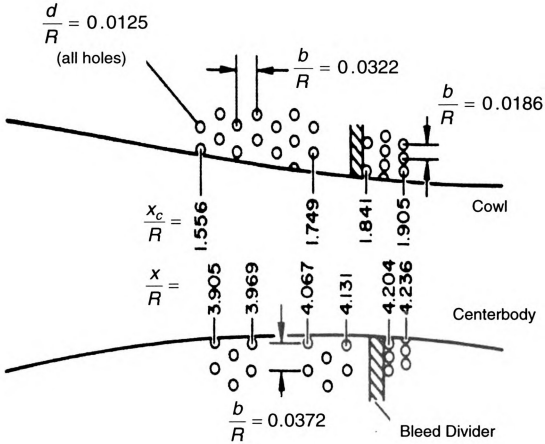

Figure 2.4 Bleed hole configuration (configuration C) on cowl and centerbody (Smeltzer and Sorensen, 1973).

For the bleed configuration studied, there are four discrete bleed zones. Zones 1 and 2 are upstream of the throat region and are located on the cowl and the centerbody, respectively. On the centerbody, the bleed has been divided in to two clusters. The first is placed significantly upstream of the throat to minimize the boundary layer growth. The second cluster of bleed holes is placed just upstream of the throat and is intended to prevent separation that will arise from the dynamics of the shock-wave/boundary-layer interaction because of the persistent reflecting oblique shocks. Bleed zones 3 and 4 are placed at the throat region and are intended to control the boundary layer thickening that will occur both before and after the terminal shock. In **Figure 2.4**, the measurements of x_c/R for the cowl surface reference the distance from the cowl lip, whereas those measurements on the centerbody surface are referenced from the centerbody tip. Additional details regarding the geometry of the inlet, the bleed configuration, and the design of the inlet can be found in Smeltzer and Sorensen (1973).

For the simulations described in this paper, the inlet described in the previous paragraphs is taken to be stationary and a uniform flow approaches at zero angle of attack. The freestream static temperature, pressure, and Mach number are 129.8 K, 4,700 Pa, and 2.65, respectively. This leads to a total pressure of approximately 1 atmosphere (1 atm). The Reynolds number per meter, based on the freestream conditions, is 8.53×10^6.

2.3.2 Problem Formulation

The problem described in the previous section is modeled by the Reynolds-averaged conservation equations of mass (continuity); momentum (a modified form of the thin-shear layer, compressible Navier-Stokes equations), and total energy for a thermally and calorically perfect gas with Sutherland's model for thermal conductivity. Turbulence is modeled by the shear-stress transport (SST) model of Menter (Menter, 1992 and Menter, 1993). Additional details of the governing equations are available in the CFL3D User's Manual (Version 5.0) by Biedron et al. (1996).

2.3.3 Boundary Conditions

Although the mixed-compression inlet studied is geometrically axisymmetric and the angle of attack is zero, the inclusion of the discrete bleed hole configuration in the simulation makes the problem three-dimensional. In these simulations, a 2.5 degree wedge of the inlet is modeled; this angle of the wedge is just large enough for the bleed hole patterns to repeat in the azimuthal direction for bleed configuration C. **Figure 2.5** details the bleed hole patterns on both the cowl and the centerbody and indicates several key measurement locations. At the two boundary planes in the azimuthal direction (solid lines in **Figure 2.5**), periodic boundary conditions were imposed.

The boundary conditions applied at the other boundaries of the flow domain (shaded area in **Figure 2.6**) are as follows. At the inflow boundary, all flow variables were specified at the freestream conditions. At the freestream

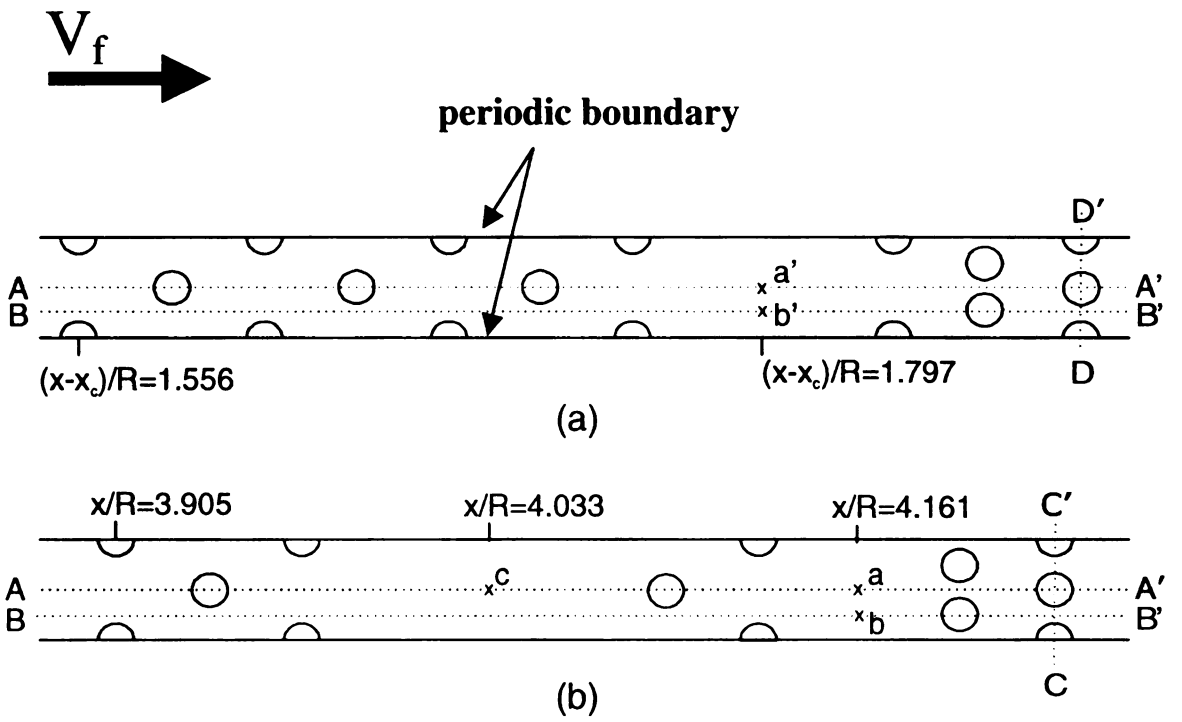

Figure 2.5 Details of the bleed hole configuration (configuration C) and measurement locations for (a) the cowl surface and (b) the centerbody surface of the axisymmetric, mixed-compression inlet. Freestream flow is from left to right. R = capture radius, x_c = location of cowl lip.

inf
bo

Fig

Sim

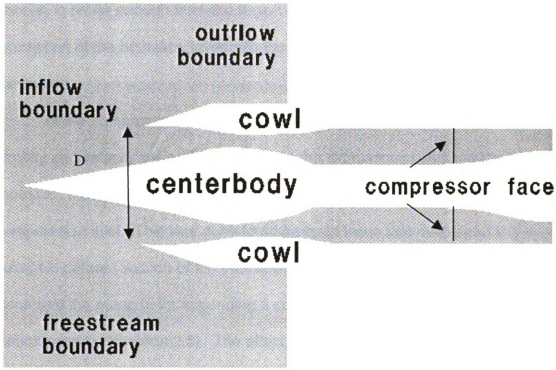

Figure 2.6 Boundary condition schematic for the mixed-compression inlet simulations.

boundary, exterior to the cowl, all of the flow variables were also specified at the freestream conditions. At the outflow boundary, the flow is supersonic, except within the very thin boundary layer that forms on the exterior surface, and all of the flow variables were extrapolated. The location for the outflow boundary was chosen to be far enough from the region of interest so that any effects due to the interaction of the boundary layer with the boundary condition would be minimized.

At the compressor face, a back-pressure (P_b) was imposed, and the density and velocity were extrapolated. In the simulations conducted in this research, a converging section was appended to the engine face of the mixed-compression inlet. This was done to address an issue that developed in the subsonic diffuser section of the inlet downstream of the terminal shock. This issue and the reasons for appending a converging section are addressed in the Results section (Section 2.5). The effect of adding this converging section is equivalent to simply shifting the compressor face boundary downstream from its actual location; the flow is still subsonic as it exits the domain. At all solid surfaces, the no-slip condition was imposed. These surfaces were treated as adiabatic walls and a zero normal-pressure gradient was also imposed.

The boundary conditions used for the turbulence model are as follows. On the wall, the turbulent kinetic energy (k) is set to zero, and ω (the dissipation rate per unit k) is set equal to $60\nu/(\beta\,\Delta y^2)$. In that boundary condition, β equals to 3/40, and Δy is the normal distance of the first grid point from the wall. The first grid point from the wall must be within a y^+ of unity. At the inflow, k is set to zero

and ω is set so that the flow is effectively laminar. At all other boundaries, k and ω were extrapolated.

To address the bleed through the discrete holes that occur on both the cowl and centerbody surfaces, two approaches are available when conducting numerical simulations. The first approach is to simulate the flow in the entire bleed system, including the flow through each bleed hole and the plenum (*cf.* Hahn *et al.*, 1993; Shih *et al.*, 1993; Chyu *et al.*, 1995; Hamed *et al.*, 1995; Rimlinger *et al.*, 1996; Rimlinger *et al.*, 1996; Lin *et al.*, 1997; Flores *et al.*, 1999). The advantage of this approach is that the physics of the bleed process is simulated by using first principles. The disadvantage, however, is that a very large number of grid points or cells would be needed to resolve the flow in the holes and the plenum. The second approach is to model instead of simulate the flow in the bleed holes and the plenum by using what are referred to as bleed boundary conditions, which are applied on surfaces where bleed is to occur (*cf.* Abrahamson *et al.*, 1988; Paynter *et al.*, 1994; Lee *et al.*, 1994; Harloff *et al.*, 1995; Benson *et al.*, 2000; Shih *et al.*, 1997). By not resolving the bleed holes and the plenum, fewer grid points are needed and this leads to greatly reduced memory and CPU-time requirements. From a computational efficiency point of view, the second approach based on bleed boundary conditions is preferred; however, its usefulness hinges on the accuracy of the bleed boundary conditions in modeling the relevant physics (Shih *et al.*, 1997).

Until only just recently, most bleed boundary conditions have treated each bleed patch (i.e., a region with bleed holes) as a porous surface. With these

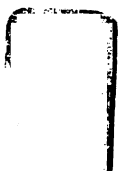

types of models, the information on hole geometry and arrangement is not represented (cf. Chyu *et al.*, 1986; Kawamura et al., 1987; Chyu *et al.*, 1992; Abrahamson *et al.*, 1988; Benhachmi *et al.*,1989). The focus of these bleed boundary conditions has been on acquiring the correct bleed rate, which is considered to be the most important part of the bleed process. However, by disregarding the bleed hole geometry some aspects of bleeding a supersonic boundary layer are lost. In particular, the "barrier" shocks that occur inside the bleed holes and the influence of those shocks on boundary-layer control are not accounted for in these models. Paynter *et al.* (1994) and Lee *et al.* (1994) improved the porous-wall type bleed boundary conditions by adding a partial differential equation that resembles a one-equation turbulence model to model the roughness effects induced by the bleed process. Benson *et al.* (2000 and 2001) presented a non-porous-wall bleed boundary condition in which at least one grid point is within each bleed hole. With such a bleed boundary condition, it was shown that it is possible to get the bleed rate correct and to account for many of the effects of the "barrier" shock.

In this current study, the bleed boundary condition developed by Benson *et al.* (2000 and 2001) is employed to model the effect of bleed through the discrete holes without having to simulate the flow through the bleed hole and its associated plenum. The investigators developed this bleed boundary condition using simulations of choked bleed that resolve the holes and the plenum as a guide and they demonstrated that the bleed boundary condition was effective at capturing the relevant physics of the bleed process and its effects on the flow,

even in a coarse grid simulation where the bleed is modeled with only one point per hole.

In this bleed boundary condition, the normal velocity, W, is calculated as a function of the local sound speed at one grid point above the bleed hole by using a discharge coefficient, that is, $W = - C_D \sqrt{\gamma P/\rho}$, where C_D, the discharge coefficient, is a constant over the entire hole, and γ is the ratio of the specific heats. Its value is chosen to ensure the correct average normal velocity over the bleed hole on the basis of simulations that resolved the flow through each bleed hole and plenum. The density (ρ), pressure (P), and the other two velocity components in each hole are extrapolated by assuming zero normal derivatives. The total energy is then computed by using the equation of state.

In these simulations, the above bleed boundary condition was implemented in two ways. In the first method, the locations of the bleed holes are discerned (i.e., at least one grid point represents the location of each bleed hole with the C_D distributed over a cell face about that grid point). In the other bleed boundary condition employed, each row of bleed holes is modeled as a porous surface (bleed slot) with a width equal to the hole diameter and where the number of bleed holes in each row is accounted for by adjusting the discharge coefficient to give the correct bleed rate. For the porous-surface bleed boundary condition, the problem becomes two-dimensional axisymmetric with a corresponding reduction in the number of grid points in the azimuthal direction from 13 to 2.

2.3.4 Numerical Method of Solution

Solutions to the governing equations described in the previous section were obtained by using a cell-centered, finite-volume code called CFL3D (Thomas *et al.*, 1990 and Rumsey *et al.*, 1993). All inviscid terms were approximated by the flux-difference splitting of Roe (1981 and 1983) (third-order accurate) with the slope limiter of Chakravarthy and Osher (1983). All of the diffusion terms were approximated conservatively by differencing derivatives at cell faces. Since only steady-state solutions were of interest, time derivatives were approximated by the Euler implicit formula. The system of nonlinear equations that resulted from the aforementioned approximations to the space- and time-derivatives were analyzed by using a diagonalized alternating-direction scheme (Pulliam *et al.*, 1981) with local time-stepping (local Courant number always set to unity) and a three-level V-cycle multigrid (Ni, 1981 and Ramsey *et al.*, 1988).

2.3.5 Grid Structure

The multi-block structured grid system used is shown in **Figure 2.7**. It has 1,391,676 grid points and is made up of four blocks that are connected through both grid patching and overlapping. In addition, all dimensions are designed so that multigrid methods can be used and accommodations have been made so that each patch and overlapping region, as well as bleed hole, can be fully included in the multigrid.

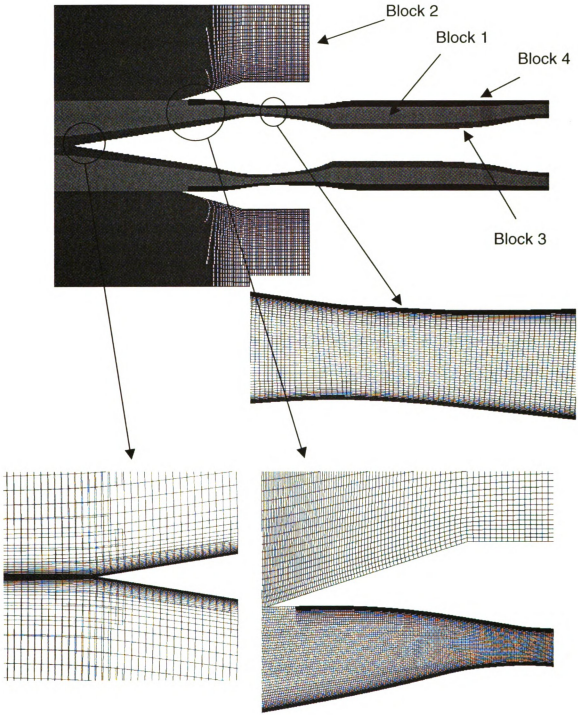

Figure 2.7 The four block, multigrid system employed in simulations of the mixed-compression inlet.

Block 1 fills the region between the centerbody and the cowl from the inflow boundary to the compressor face/inlet exit. This grid with dimensions 861 x 13 x 41 (13 grid points in the azimuthal direction) provides a fairly uniform distribution of grid points. Within Block 1, the aspect ratio is near unity everywhere so that shock reflections and interactions can be accurately resolved.

To capture the flow exterior to the cowl surface in the event of spillage, a second grid, Block 2, was patched to Block 1 and continues along the exterior surface of the cowl until such a point where the shock from the cowl lip would pass out of the downstream, outflow boundary. Block 2 has dimensions 333 x 13 x 33 and is similar to Block 1 in that it has a fairly uniform distribution of grid points with near unity aspect ratio near the patched surface. Because of its limited use in the analysis of the simulation, the grid for Block 2 is intentionally not of sufficient grid spacing to resolve any of the boundary layer development on the exterior cowl surface.

The third grid, Block 3, has dimensions 621 x 13 x 41 and overlaps Block 1 near the centerbody surface. Block 3 is included to provide the fine grid resolution needed to resolve the boundary layer that develops next to the centerbody. Near the surface, large aspect ratios exist because of the difference between the normal spacing required to capture the boundary layer and the coarser streamwise grid spacing. With this grid, it was determined that the streamwise spacing should be as close as possible to the main interior grid, Block 1. One reason for this restriction is that the length scales for these two directions are so disparate that any attempt to satisfy one of them would lead to

large aspect ratios in either the middle of the inlet or near the walls. This restriction on the streamwise spacing was also necessary to prevent interpolation errors that might result as the oblique shocks pass from one grid to the other. Another feature of Block 3 is that it was extended forward of the centerbody tip to the inflow boundary so as to properly capture the oblique shock forming off of the centerbody tip.

To resolve the boundary layer that forms adjacent to the interior cowl surface, a fourth grid, Block 4, is overlapped to the first grid, Block 1. Block 4, with dimensions 145 x 13 x 41, also overlaps Block 1 and provides the fine grid resolution needed to resolve the boundary layer next to the cowl. Block 4, however, cannot be extended forward to the inflow boundary in the same manner that Block 3 was extended.

For both Block 3 and Block 4, the first grid points away from the centerbody and cowl all have a y+ value less than unity. In addition, the first five grid points away from these walls all have y+ values less than 10. For these simulations, an initial value for y+ was determined by treating the inlet as a flat plate. As the simulations progressed, the value of y+ was re-assessed and corrections were made to the grids to provide appropriate adjustments.

2.4 Method for Initialization of Flow within the Inlet

One of the more difficult aspects of simulating flow through mixed-compression inlets is the method used to initialize the flow field within the inlet. Although the problem appears to be amenable to a solution using one-

dimensional isentropic theory, the presence of oblique shocks in the flow complicates matters to such a degree that special considerations need to be developed and implemented to initialize the flow throughout the inlet.

Simulating critical flow in a mixed-compression inlet is difficult for several reasons. The first problem involves the transients that may develop during the initialization of the flow. In the converging section of the mixed-compression inlet, the flow rate through the inlet is a constant, but the flow is supersonic and the cross-sectional area changes along the flow direction. If the initial conditions are inappropriate, then complicated transients may create disturbances that either cause the flow to unstart or require the need for an exorbitantly large number of iterations to damp or remove the disturbances. A second difficulty arises from the fact that, for a given area ratio between the capture area and the throat area, only a range of flow rates and Mach number distributions are possible. The problem here is that any deviations from this distribution that arise during the flow initialization procedure may be unrecoverable.

In addition to the above difficulties, several other problems arise from the dynamics of the flow through the inlet. For example, once the flow has been established, the shock-wave/boundary-layer interactions and the boundary-layer bleed cause the displacement thickness within the inlet to change. This change in the displacement thickness will affect the effective-area ratio of the inlet and, in turn, cause all the flow properties of the inlet to adjust to the new configuration. As the flow is developing, the interaction of the boundary layer with the effective-area ratio of the inlet becomes a critical and difficult parameter for control.

In addition to the problem associated with the displacement thickness, the location of the terminal shock is another complicating factor. The location of the terminal shock depends strongly on the back-pressure imposed at the compressor face; however, it also depends on several other factors such as the bleed rate, bleed hole configuration and the geometry of the inlet. In addition, if the terminal shock is moving, the effects of any compensatory changes in the back-pressure will not arrive at the terminal shock location in time to arrest its motion because the compressor face boundary is so far away from the throat. Finally, although the mass flow rate for the boundary-layer suction is known for this problem, the physics of the flow field above the bleed holes is not. Changing bleed locally to stabilize the shock location can, therefore, cause transient disturbances that end up destabilizing the location of the terminal shock.

The method described below outlines the best of the approaches that were used in initializing the flow through the mixed-compression inlet. Care has been taken to illuminate the special problems that occur at each junction in the solution process and to explain the reason for the proposed steps. Since each problem and the geometry associated with it is unique, knowledge of the general issues faced will allow future users to anticipate and prepare for all eventual problems. The method proposed takes special advantage of a slow start boundary condition to move from CFL3D's default initial condition, where all values set to freestream conditions everywhere, to a situation where the flow upstream of the throat region is converged. The slow-start boundary condition is a solid-wall boundary condition where the effects of the wall are gradually faded

into the simulation. In other words, with the slow-start boundary condition, the fluid can initially pass through the surface as if it were not present in the flow. As the number of iterations increases, the normal velocity of the fluid passing through the surface is reduced until the wall is completely "faded in" and impenetrable.

The method for initializing the flow proceeds as follows:

1. Beginning with a coarse and uniform grid, the freestream conditions are used as the initial condition for entire flow field. Supersonic inflow boundary conditions are applied at the inflow boundary (all variables are specified), and supersonic outflow boundary conditions are applied at the outflow boundary and compressor face (all variables extrapolated).
2. Before initiating the code, it should be decided where the terminal shock should be located downstream of the throat. We suggest choosing a location substantially downstream of the desired final position. The reasons for this are explained in step 10.
3. Slow-start, inviscid wall boundary conditions are applied on the inlet walls and the code is run until the flow upstream of the intended terminal shock location has converged. It should be noted that it is unnecessary for the entire flow field to be converged because the geometry and the grid employed in the diffuser section of the mixed-compression inlet is not intended to resolve supersonic flows with embedded shocks. At the conclusion of this step, a solution that involves supersonic flow throughout the mixed-compression inlet is obtained. This is referred to as

supercritical flow. The slow-start, inviscid wall boundary condition initially treats all solid walls as completely porous so that flow can penetrate the walls and then, over a finite number of time steps, the walls are made less and less porous until they are impermeable.

4. From this intermediate solution, the average static pressure, Mach number, and temperature are calculated just upstream of the intended terminal shock location. These values will be used in one-dimensional normal shock relations to determine the flow conditions on the downstream side of the terminal shock.
5. One-dimensional isentropic relations are applied to determine the solution from the downstream side of the shock wave to the compressor face, taking into consideration changes in inlet's cross-sectional area. Since the geometry in the subsonic diffuser may not meet the slowly varying requirements of the one-dimensional isentropic relations, some leeway should be accounted for when imposing the theoretical solution.
6. The solution obtained under step (3) for the region upstream of the terminal shock is combined with the solution obtained under step (5) for the solution downstream of the terminal shock. The combined solution is used as the new initial condition for the inlet.
7. Slow-start inviscid wall boundary conditions are applied from the location of the terminal shock to the compressor face and the code is run again. At the conclusion of this step, a converged, inviscid critical-flow through a mixed-compression inlet is obtained.

8. To speed up steps (1) through (7), a coarse grid could be used. If a coarse grid is used in these steps, the solution must now be interpolated to a fine mesh to account for viscous effects and bleeding next to the centerbody and cowl. In this study, Blocks 1 and 2 were used to carry out steps (1) to (7). Blocks 3 and 4 were then added to account for viscous effects and bleeding. To make the code more robust, first-order upwind could be used in the beginning and then later transitioned to higher-order accurate differencing formulas.
9. Using the converged, inviscid critical-flow solutions as initial conditions, the code is run with viscous wall boundary conditions and bleed initiated simultaneously. This will allow for the development of the boundary layer and prevent separation that may arise from the interaction between the oblique shock waves and the boundary layer.
10. The terminal shock location is then adjusted by fine-tuning the imposed back-pressure and the amount of bleed. Unfortunately, there is a difference in the response delay between the bleed and the back-pressure. Because bleed is a local phenomenon, changing the amount of bleed causes the terminal shock to move almost instantaneously. However, when the back-pressure is changed at the compressor face or inlet outflow boundary, the changes in back-pressure take time to be felt at the terminal shock location. Since the final terminal shock location depends on the combination of imposed back-pressure and bleed, the

process of moving the shock should be accomplished incrementally. This difficulty can be accentuated if large pressure waves are present.

2.5 Results

The computed Mach number and pressure distributions for an axisymmetric mixed-compression inlet at zero angle of attack with boundary-layer bleed are shown in **Figure 2.8** and **Figure 2.9**. **Figure 2.9** also displays pressure contours along the cowl and centerbody surfaces in the bleed region. Both of these figures represent the results of the simulations where the bleed regions were modeled as discrete holes. These figures show that the expected shock-wave structure involving oblique shock waves, their reflections, and the terminal shock are well resolved. For example, the oblique shock generated by the centerbody tip terminates on the cowl lip with near zero spillage; the reflected shocks within the supersonic diffuser are well defined; and the terminal shock is held by the bleed just downstream of the throat. The shock exterior to the cowl surface is not as well resolved as the interior shocks; however, as was noted previously, the exterior features were only included to allow for spillage to exist, if present at all, and not for measuring surface drag or for any other analysis.

Although not obvious in **Figure 2.8**, a large separated region exists in the subsonic diffuser section next to the centerbody. This separated region extends all the way to the compressor face and was unaccounted for in the prototype experiments: there was no experimental evidence to suggest that it did or did not exist. Several methods were employed to test the legitimacy of the separated

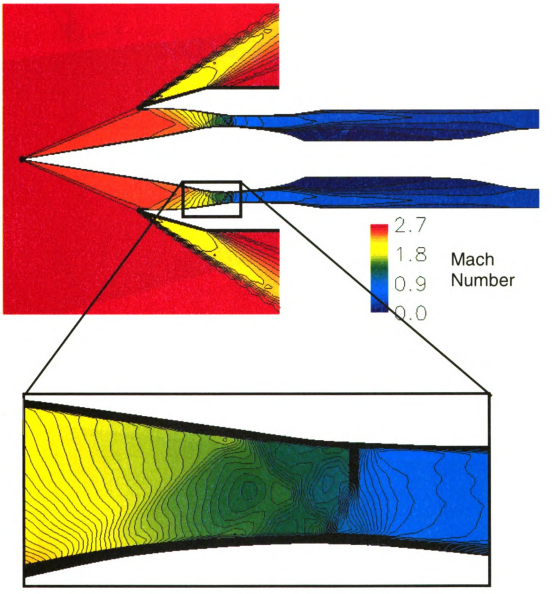

Figure 2.8 Mach number contours along centerline for the bleed boundary condition that resolves individual bleed holes (bleed-hole boundary condition).

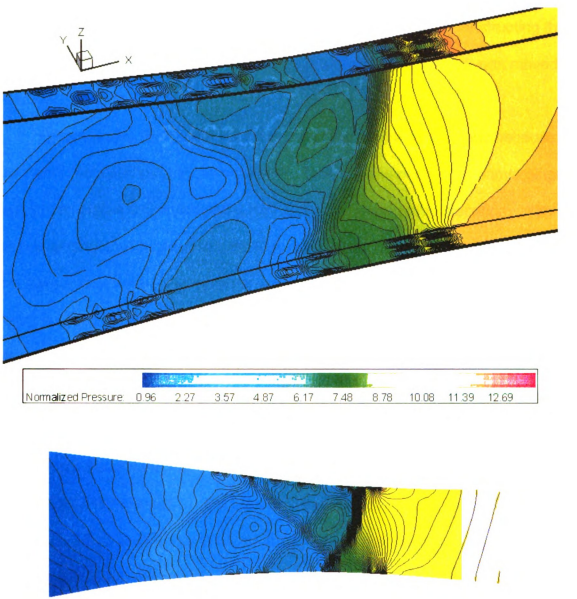

Figure 2.9 Pressure contours along centerline and solid surfaces for the bleed boundary condition that resolves individual bleed holes (bleed-hole boundary condition).

region, and the results from all of these tests were inconclusive. It is supposed that the separation could be a result of (1) a coarse database for constructing the geometry or (2) an artifact of the start-up procedure when the shock was moved to the throat region.

Re-circulating flows at the outflow boundary can be problematic because flow both enters and exits at the boundary. To solve this problem, a converging section was added to the end of the inlet at the compressor-face location. With this converging section attached, the flow re-attaches downstream of the compressor face before exiting the computational domain. Although the pressure at the outflow boundary is no longer comparable with the back-pressure referenced in the experimental literature, all of the flow will be moving outwards at the outflow boundary.

When a comparison is made between the hole-discerning bleed boundary condition results and the row-slot bleed boundary condition results that shown in **Figure 2.10** and **Figure 2.11**, it is clear that the hole-discerning bleed boundary condition predicts a more complicated shock structure in the bleed region than does the slot-row bleed boundary condition. With both bleed boundary conditions generating the same bleed rate, this more complicated shock structure in the bleed region is most likely the result of the bleed variation in the azimuthal direction that is produced when the holes are discretely modeled.

Figure 2.12 compares the average total pressure within a cross-section of constant x/R between the hole-discerning bleed boundary condition and the row-slot bleed boundary condition. The data, normalized to the average total

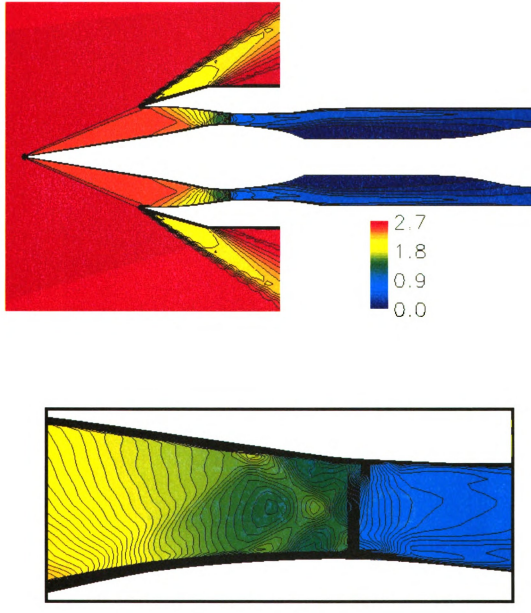

Figure 2.10 Mach number contours along the centerline for the bleed boundary condition that treats each row of bleed holes as a slot (bleed-slot boundary condition).

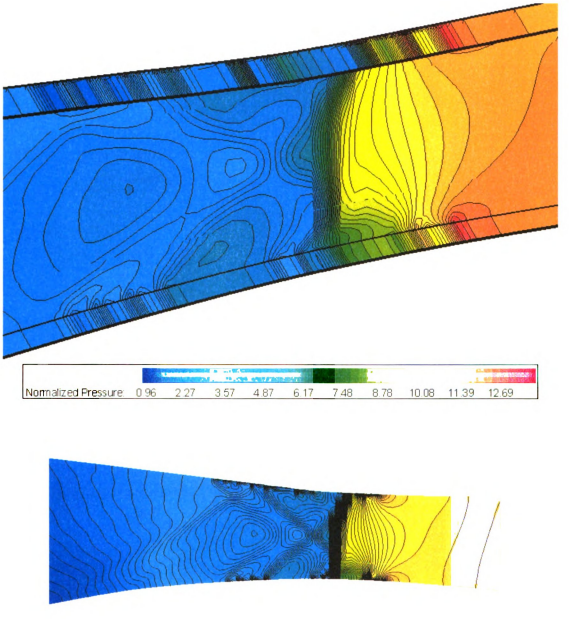

Figure 2.11 Pressure contours along the centerline and solid surfaces for the bleed boundary condition that treats each row of bleed holes as a slot (bleed-slot boundary condition).

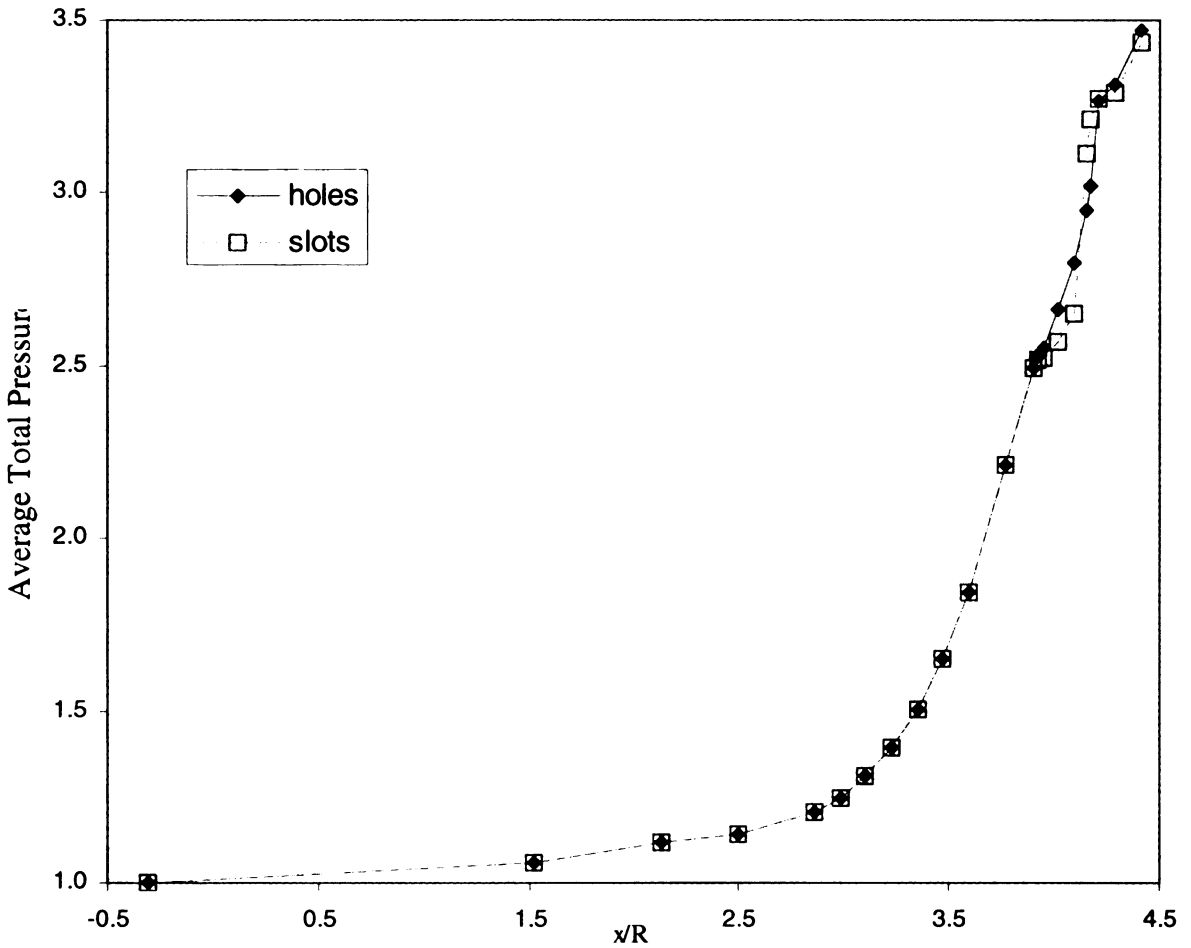

Figure 2.12 Average total pressure within a cross-section of constant x/R. Normalization is with respect to the average total pressure within a cross-section of the freestream capture-area of the inlet. The cowl lip is located at x/R = 1.

pressure in a cross-section of the freestream capture area, indicates that the flow upstream of the bleed region (x/R = 3.87 – 4.23) is identical for each of the bleed boundary conditions studied. The differences in the average total pressure observed in the bleed region of **Figure 2.12** are due to the differences that exist in the shock-wave structure formed by these two bleed boundary conditions. Downstream of the bleed region, the hole-discerning bleed boundary condition yields a slightly higher average total pressure than the row-slot bleed boundary condition.

Figure 2.13 compares the predicted surface pressure on the centerbody and cowl with experimentally measured values. The comparison is reasonable considering that the CFD study bled 10.2 percent of the captured flow, whereas the experimental study bled 8.2 percent. However, the CFD study predicts oscillations in the surface pressure created by the bleed process. that were not evident in the experimental measurement. The two bleed boundary conditions yielded similar results, although the row-slot bleed boundary condition yielded a slightly higher pressure downstream of the bleed region.

Regarding the oscillations in pressure about the bleed region that were predicted by the CFD study but not observed in the experimental results (**Figure 2.13**), it should be noted that CFD simulations that resolve the flow through each bleed in detail (Shih *et al.*, 1993; Chyu *et al.*, 1995; and Rimlinger *et al.*, 1996) show that the bleed process creates a "barrier" shock in each bleed hole. This process is a source of pressure oscillations and it is therefore possible that the measurements in the experiment were not made over the bleed holes.

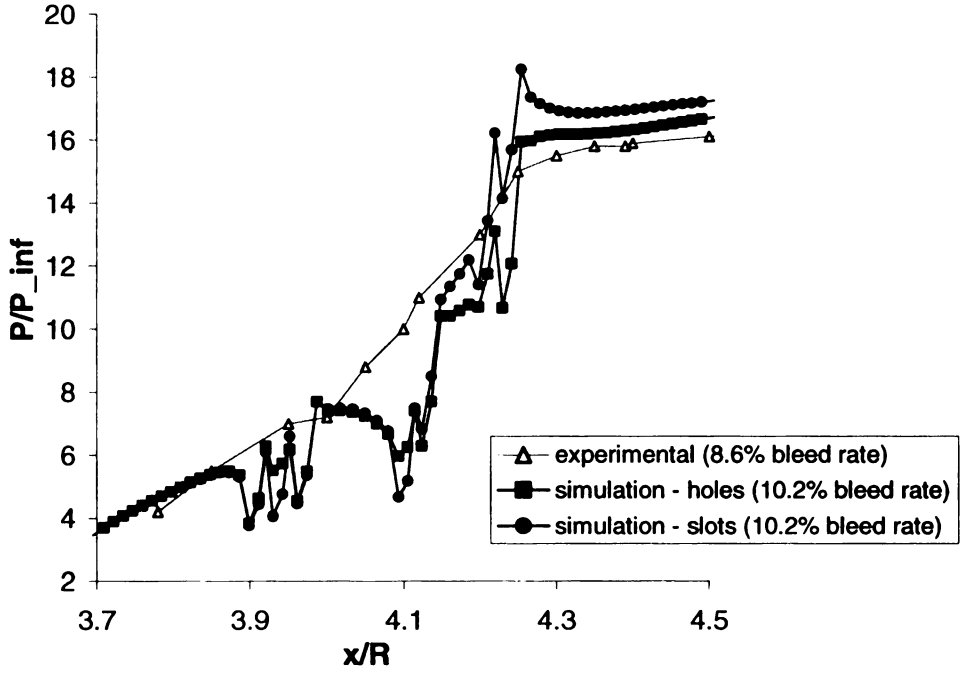

(a) centerbody

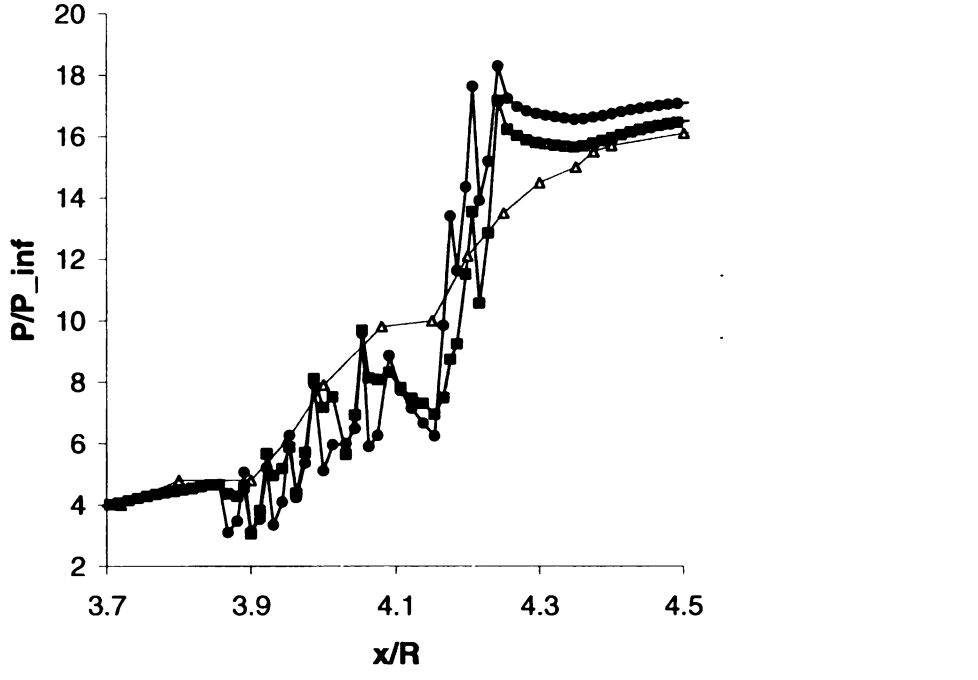

(b) cowl

Figure 2.13 Surface pressure, predictions versus measurements.

Figure 2.5 details the bleed configuration for the hole-discerning bleed boundary condition and indicates the locations selected for comparing the Mach number and pressure profiles of the two simulations. **Figure 2.14** and **Figure 2.15** compare the Mach number profiles on the cowl and centerbody predicted by the two different methods of implementing the bleed boundary condition. From these figures, it can be seen that at 10d upstream of the bleed region (d = bleed-hole diameter), the Mach number profiles are identical for the hole-discerning and the row-slot bleed boundary conditions. At a point midway between the two bleed patches, a significant difference can be seen. In this region, the row-slot bleed boundary condition and the hole-discerning bleed boundary condition produce nearly identical profiles near the surface; however, the row-slot bleed boundary condition generates significantly higher Mach number flow near the centerline. At 5d and 15d downstream of the bleed region, the hole-discerning bleed boundary condition produces a fuller Mach number profile than predicted by the row-slot bleed boundary condition. This result indicates that the bleed rate, on its own, does not determine the velocity profile downstream of the bleed region. It also demonstrates that concentrated bleed at selected locations, such as bleed holes, is more effective in creating a fuller profile than the same bleed spread out over a slot.

Figure 2.16 and **Figure 2.17** illustrate the variation of the Mach number profiles in the azimuthal direction on the centerbody. The data in **Figure 2.16**, comparing the hole-discerning and the row-slot bleed boundary conditions, were acquired at the same streamwise locations as in **Figure 2.15**, but on a different

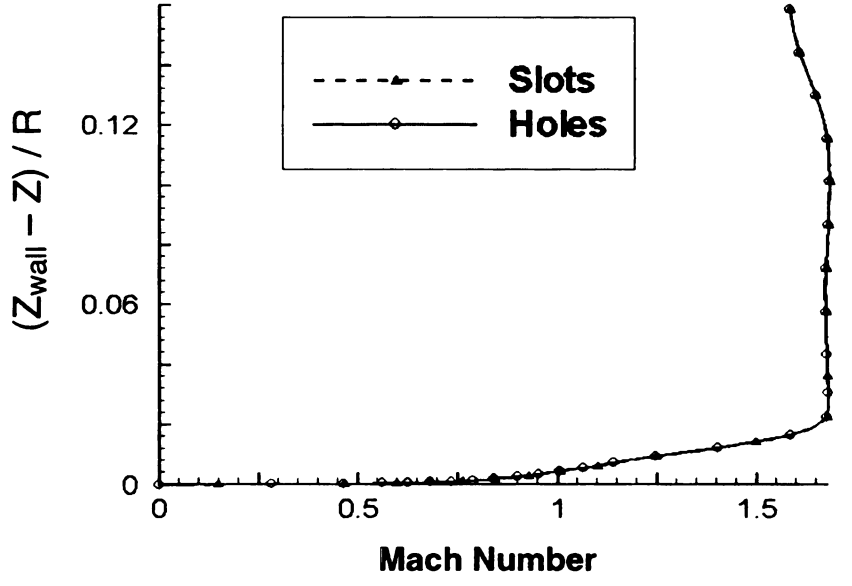

(a)

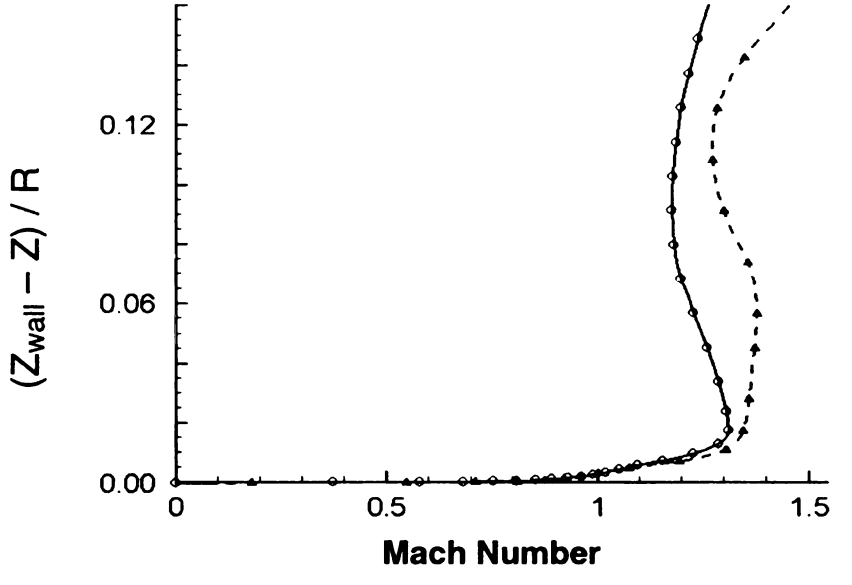

(b)

Figure 2.14 Mach number profile on cowl surface along centerline (A-A', Fig. 8) at (a) 10d upstream of bleed, (b) mid-way between 2 bleed patches (point a', Fig. 7), (c) 5d downstream of last row of bleed holes (D-D'), and (d) 15d downstream of last row of bleed holes.

Z = radial coordinate, Z_{wall} = local wall coordinate, d = bleed-hole diameter

Figure 2.14 (cont'd)

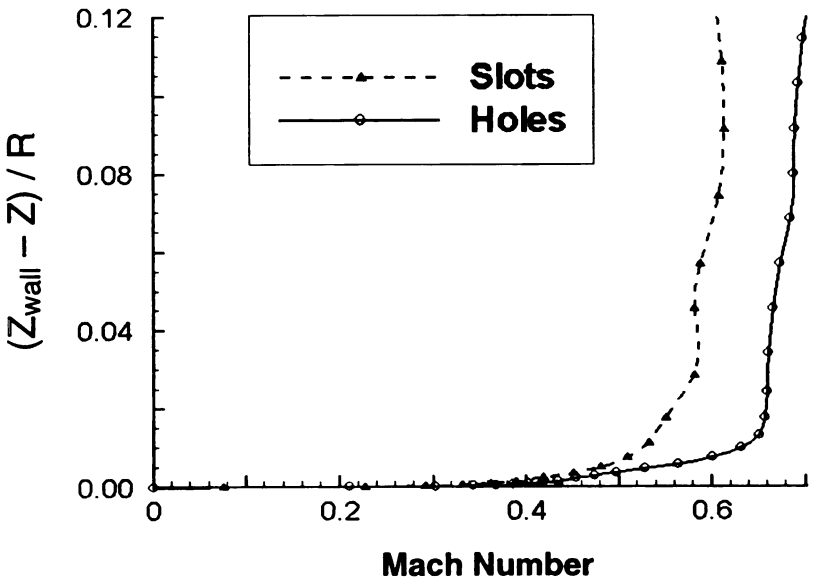

(c)

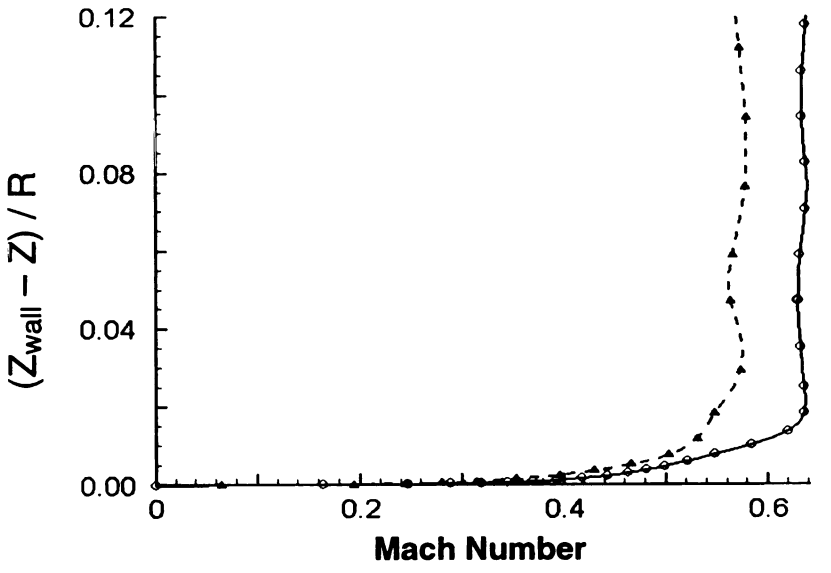

(d)

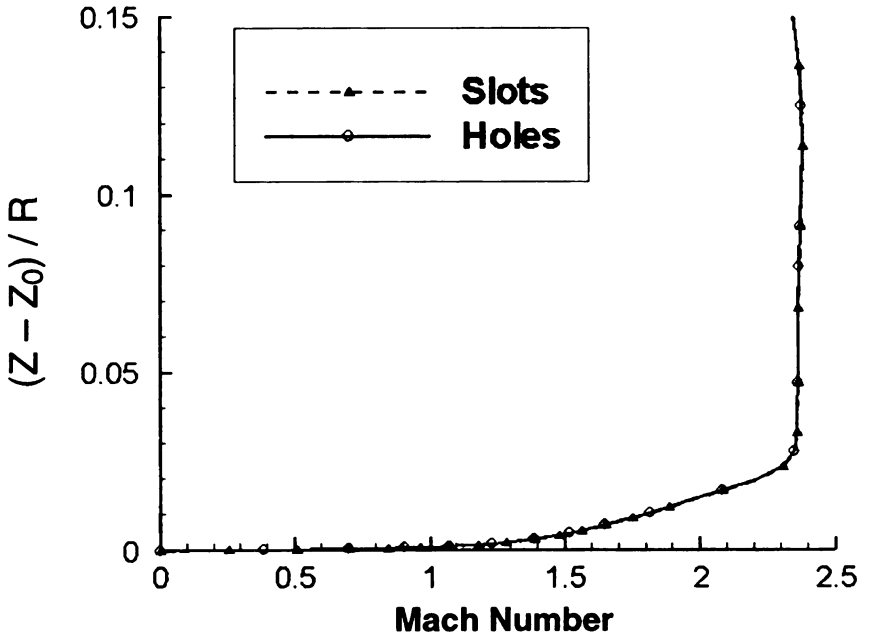

(a)

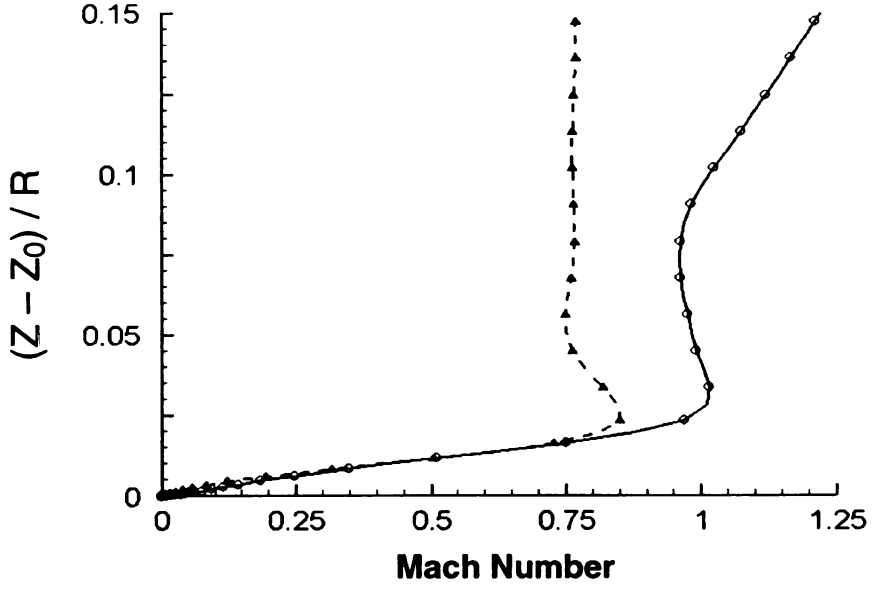

(b)

Figure 2.15 Mach number profiles on centerbody surface along centerline (A-A', Fig. 8) at (a) 10d upstream of bleed, (b) mid-way between 2 bleed patches (point a, Fig. 7), (c) 5d downstream of last row of bleed holes (C-C'), and (d) 15d downstream of last row of bleed holes.

Z = radial coordinate, Z_0 = local wall coordinate, d = bleed-hole diameter.

Figure 2.15 (cont'd)

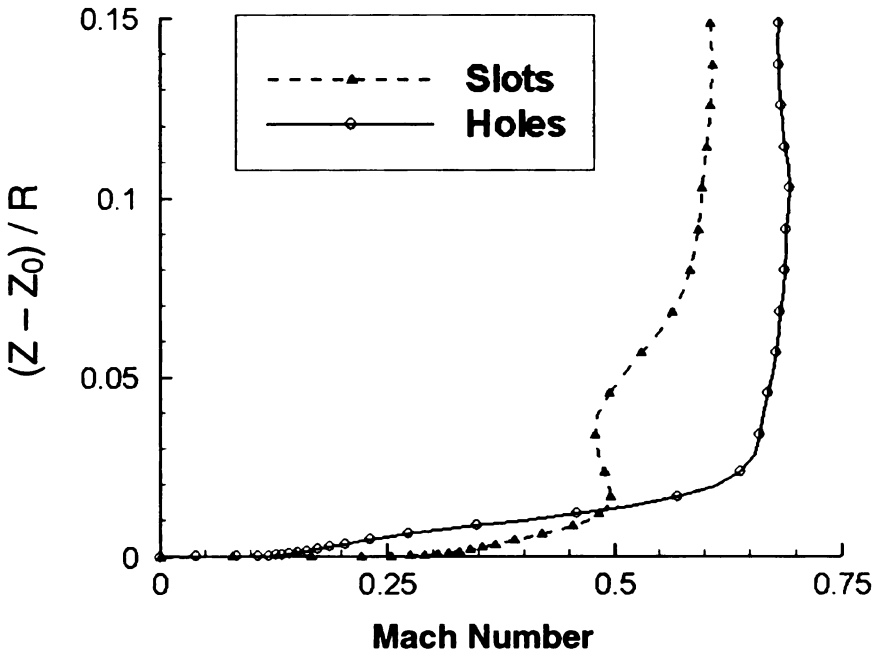

(c)

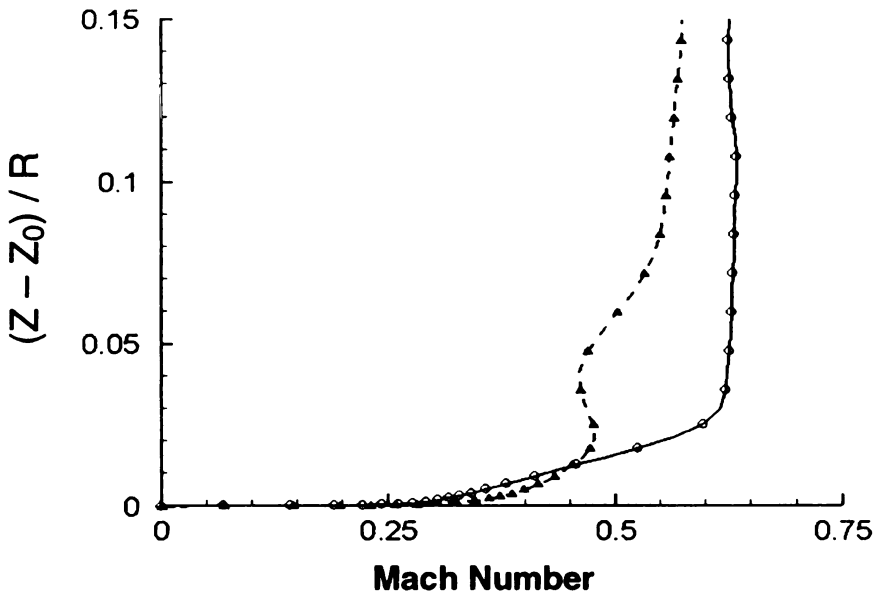

(d)

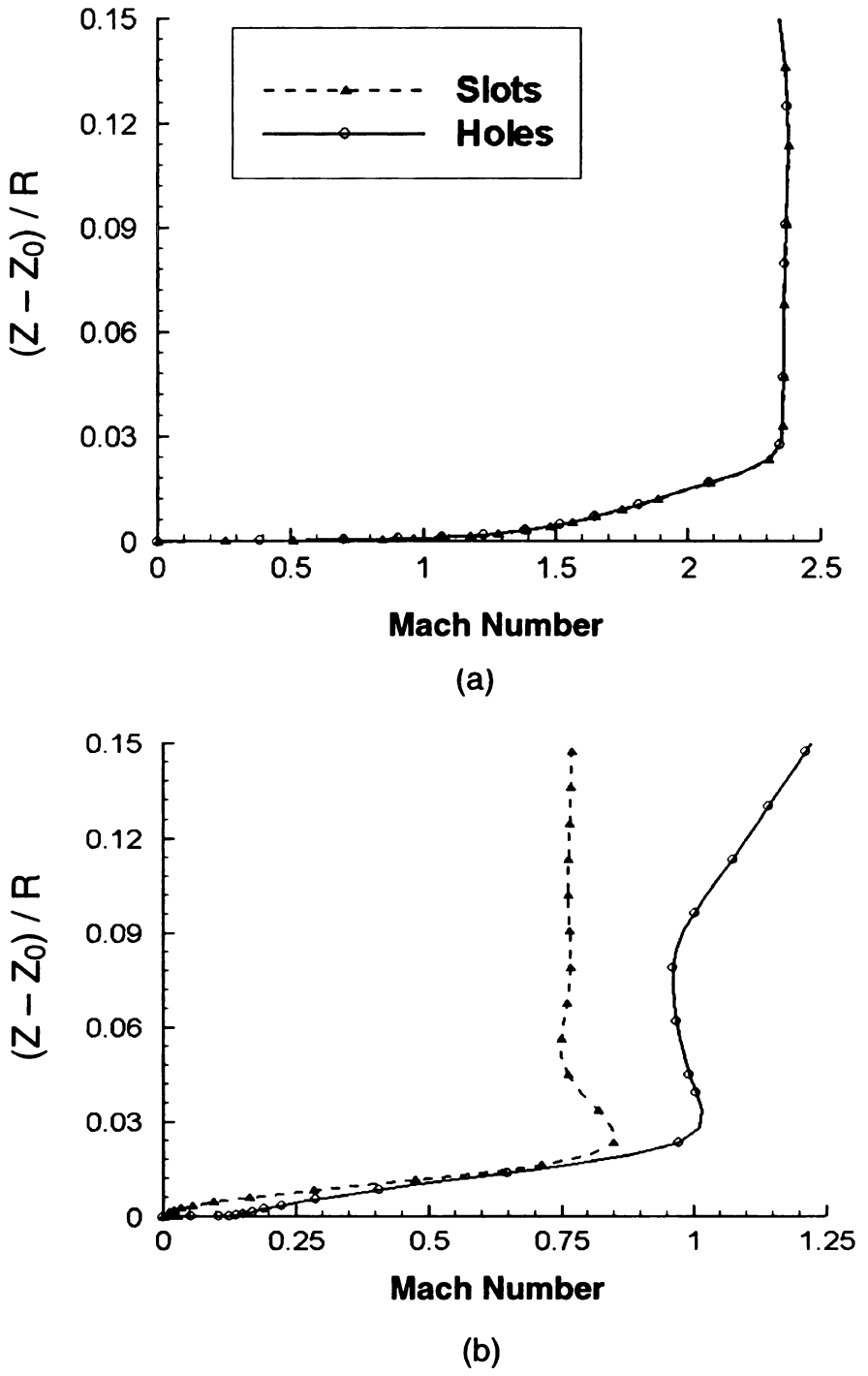

Figure 2.16 Mach number profile on centerbody surface along B-B' (Fig. 8) at (a) 10d upstream of bleed, (b) mid-way between 2 bleed patches (point b, Fig. 7), (c) 5d downstream of last row of bleed holes (C-C'), and (d) 15d downstream of last row of bleed holes.

Z = radial coordinate, Z_0 = local wall coordinate, d = bleed-hole diameter.

Figure 2.16 (cont'd)

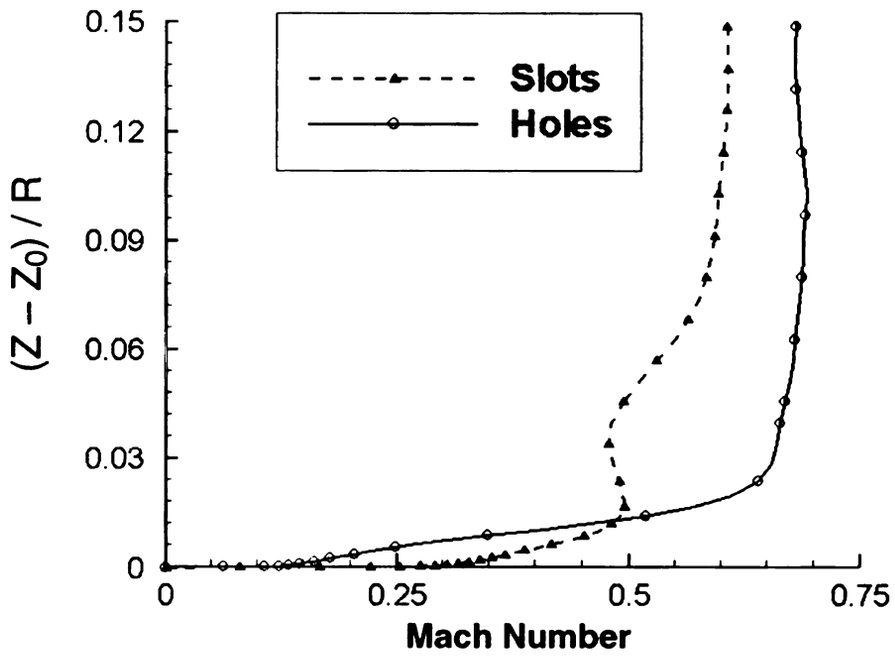

(c)

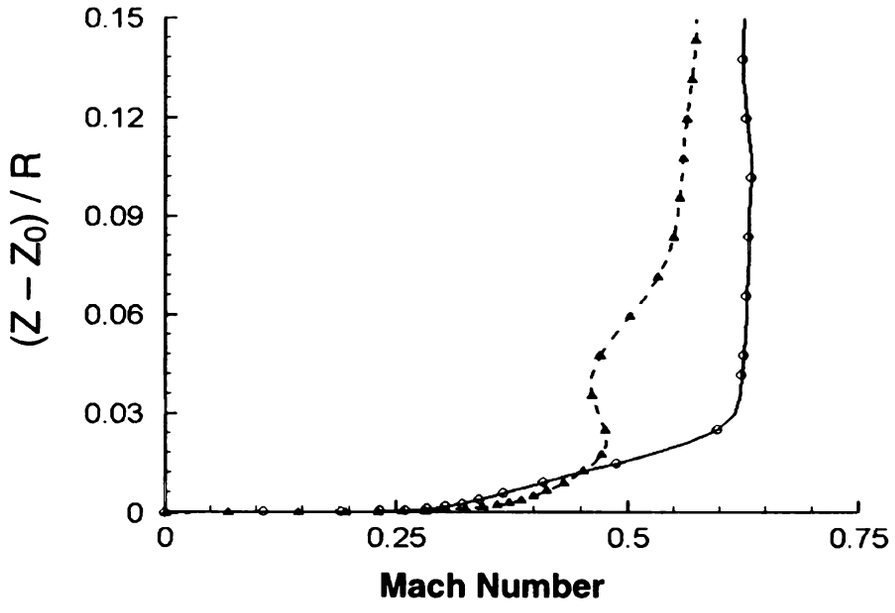

(d)

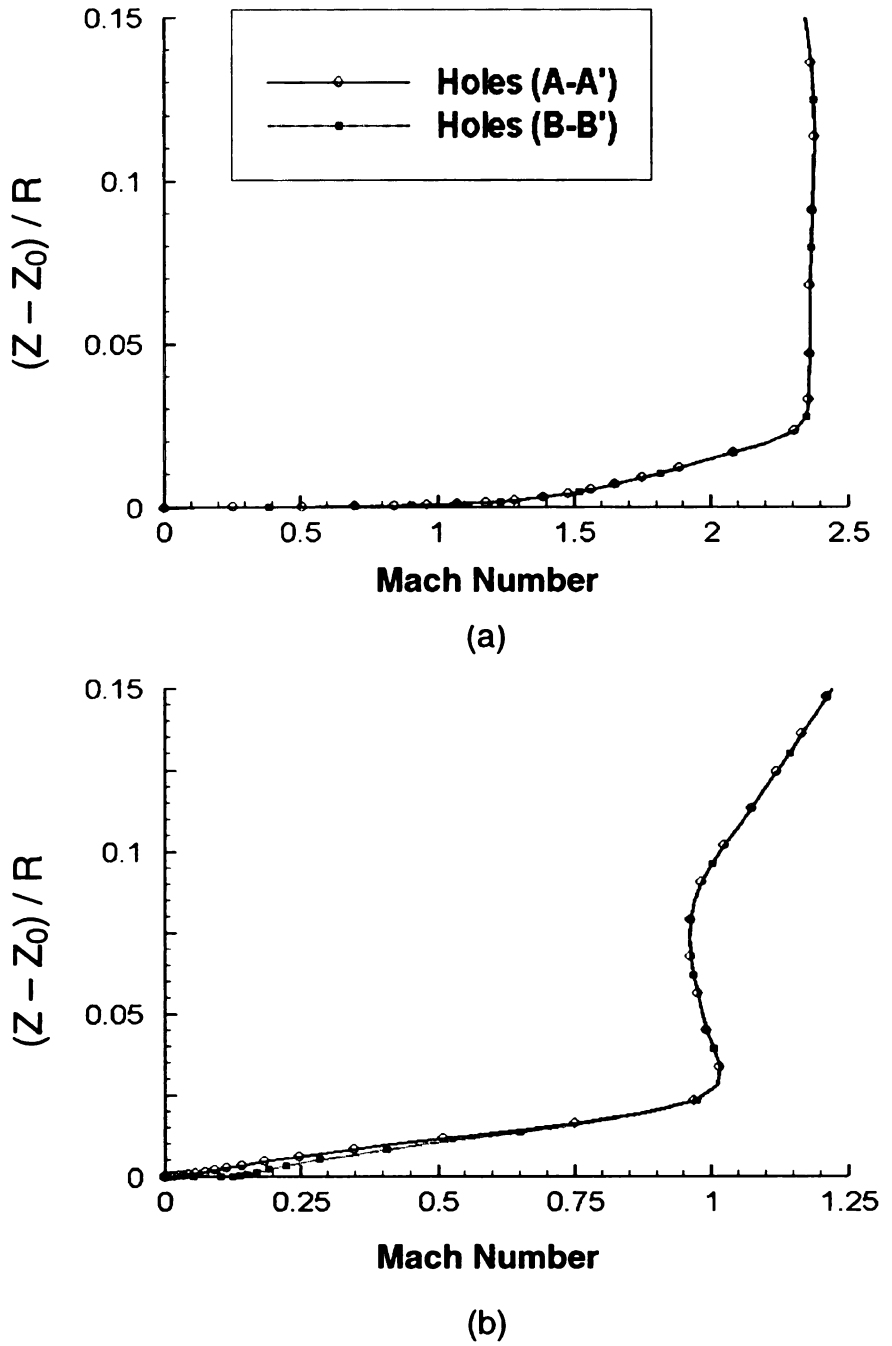

Figure 2.17 Mach number profiles on centerbody surface for the hole-discerning bleed BC along A-A′ and B-B′ (Fig. 8) at (a) mid-way between the two sets of bleed patches (point c, Fig. 7), (b) mid-way between 2 bleed patches (point b, Fig. 8), (c) 5d downstream of last row of bleed holes (C-C′).

Z = radial coordinate, Z_0 = local wall coordinate, d = bleed-hole diameter.

Figure 2.17 (cont'd)

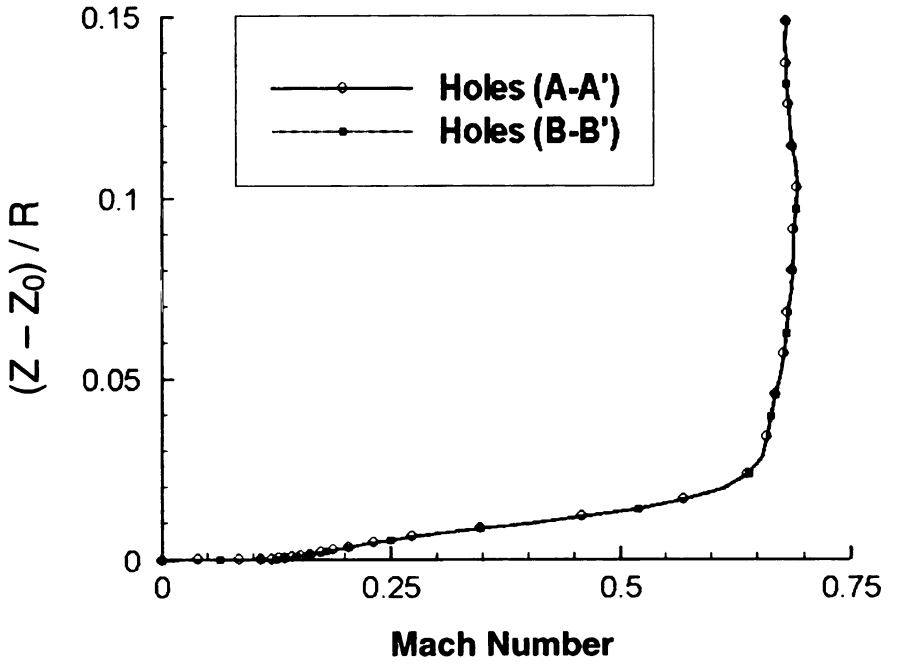

(c)

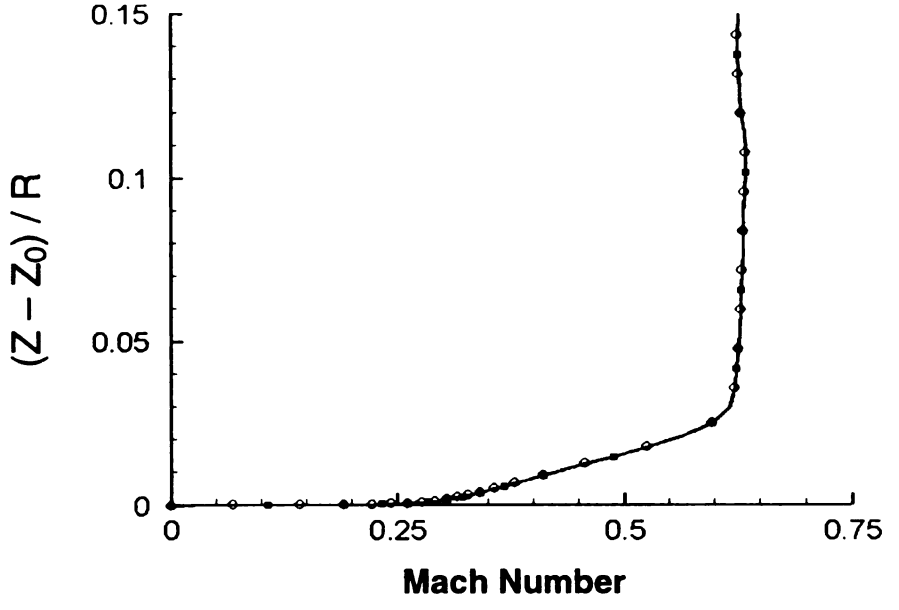

(d)

azimuthal plane. The results in this alternate azimuthal plane, **Figure 2.16**, are similar to the centerline results with only a slight difference in the near-wall behavior around the bleed holes. This difference is anticipated and explained by the presence of the discrete bleed holes. **Figure 2.17** displays the variation in the azimuthal direction for the hole-discerning bleed boundary condition. The results for the hole-discerning bleed boundary condition show significant differences existing in the azimuthal direction only in the region near the bleed holes and confined to near the surface. The data for the row-slot bleed boundary condition, however, displays no variation in the azimuthal direction and is not shown.

Figure 2.18 and **Figure 2.19** compare the pressure distributions predicted by the two different methods of implementing the bleed boundary condition on the cowl and centerbody. From these figures, it can be seen that at 10d upstream of the bleed region, the pressure distributions are identical for the hole-discerning and row-slot bleed boundary conditions. At a point midway between the two bleed patches, a considerable difference can be seen in the two profiles. At 5d and 15d downstream of the bleed region, both bleed boundary conditions gave similarly shaped distributions. At these locations, the row-slot bleed boundary condition yielded higher pressures than the hole-discerning bleed boundary condition, indicating that the row-slot bleed boundary condition created a stronger terminal shock than the hole-discerning bleed boundary condition.

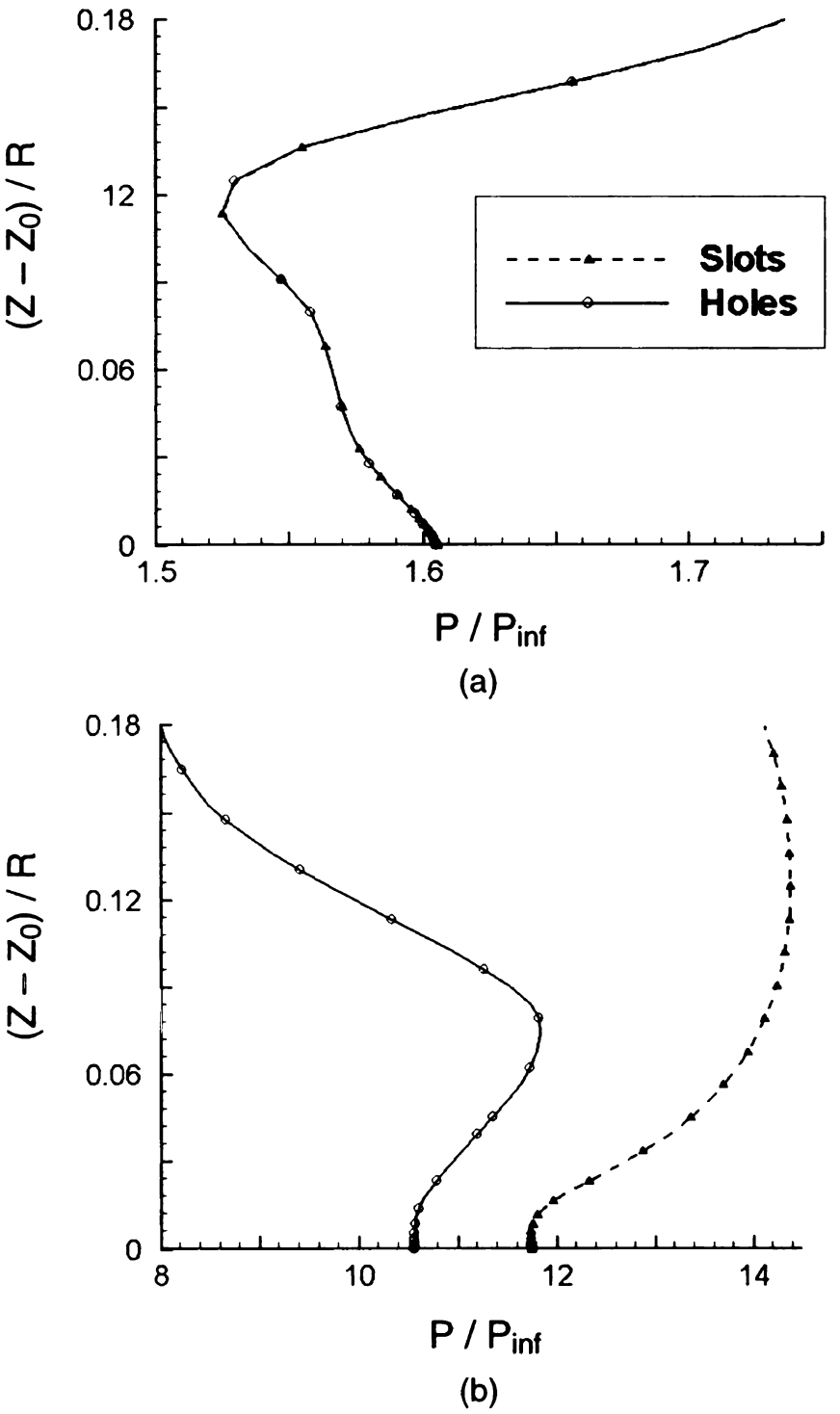

Figure 2.18 Pressure profile on centerbody surface along centerline (A-A′, Fig. 7) at (a) 10d upstream of bleed, (b) mid-way between 2 bleed patches (point a, Fig. 7), (c) 5d downstream of last row of bleed holes (C-C′), and (d) 15d downstream of last row of bleed holes.

Z = radial coordinate, Z_0 = local wall coordinate, d = bleed-hole diameter.

Figure 2.18 (cont'd)

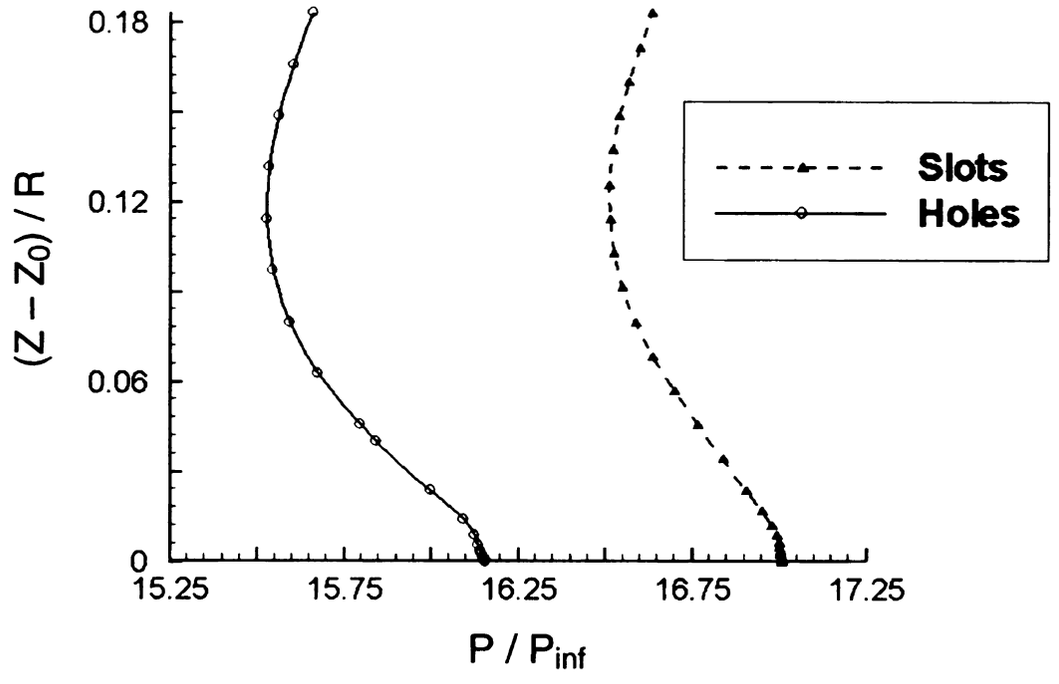

(c)

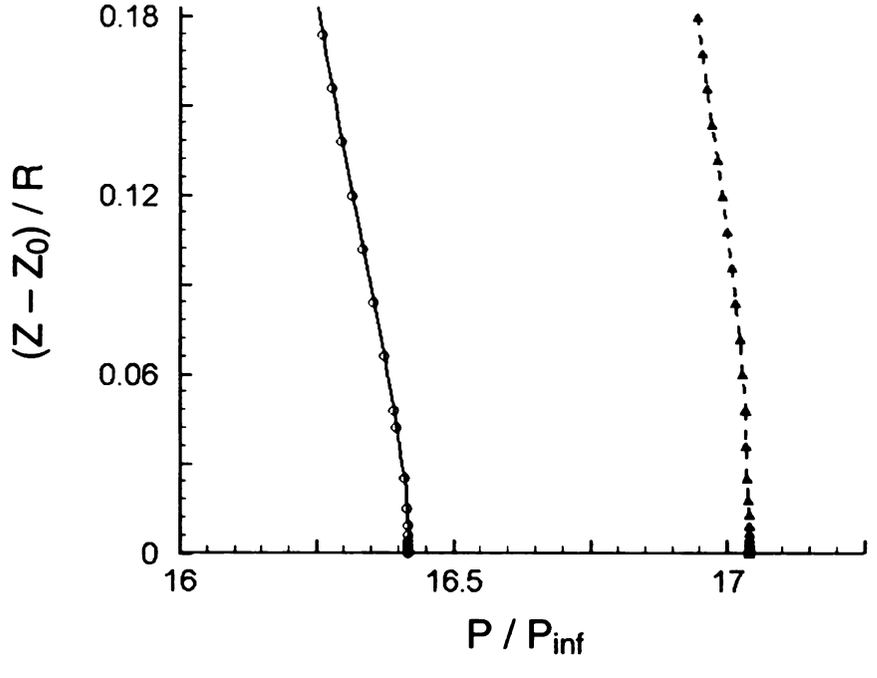

(d)

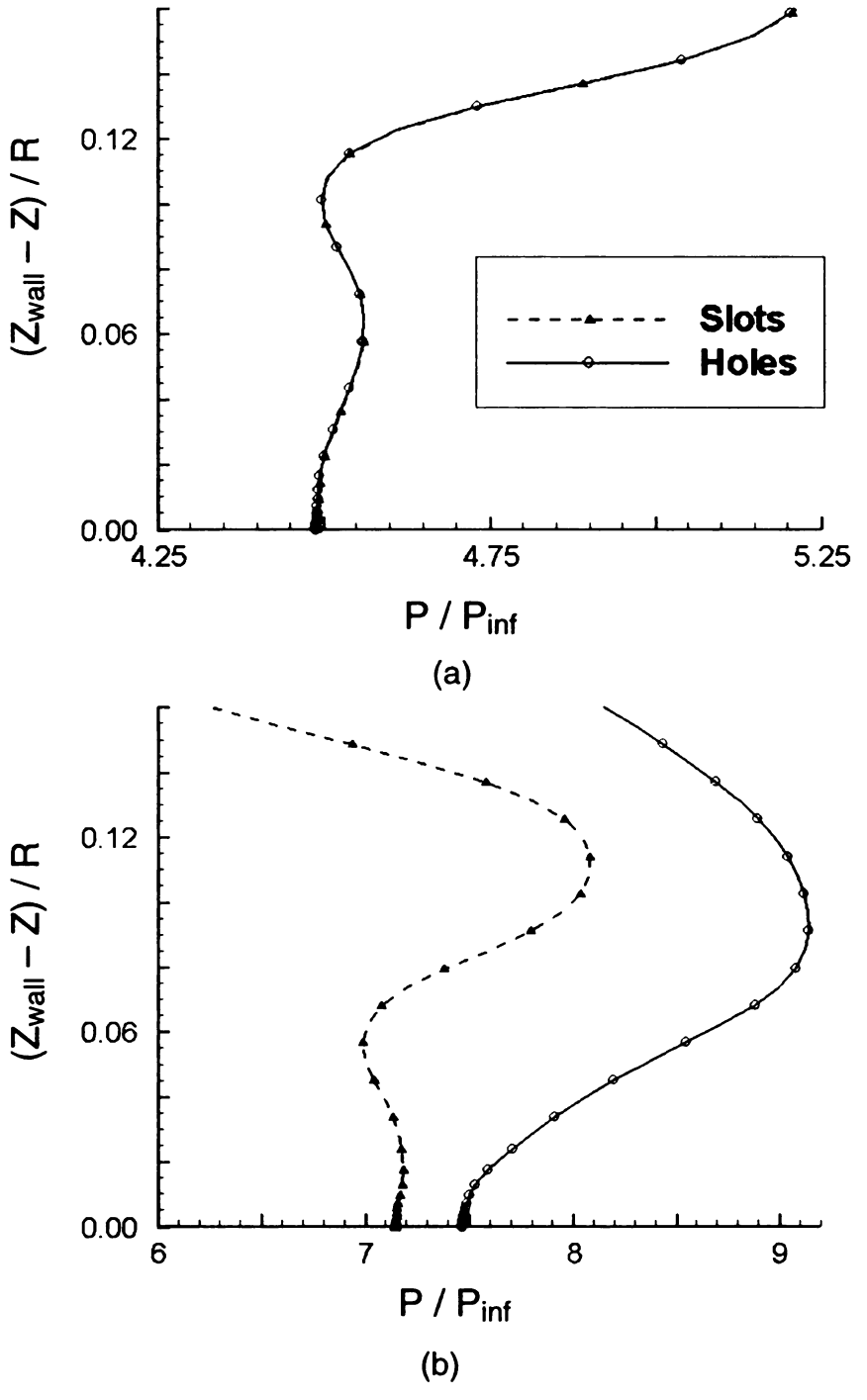

Figure 2.19 Pressure profile on cowl surface along centerline (A-A′, Fig. 8) at (a) 10d upstream of bleed, (b) mid-way between 2 bleed patches (point a, Fig. 7), (c) 5d downstream of last row of bleed holes (C-C′), and (d) 15d downstream of last row of bleed holes.

Z = radial coordinate, Z_{wall} = local wall coordinate, d = bleed-hole diameter.

Figure 2.19 (cont'd)

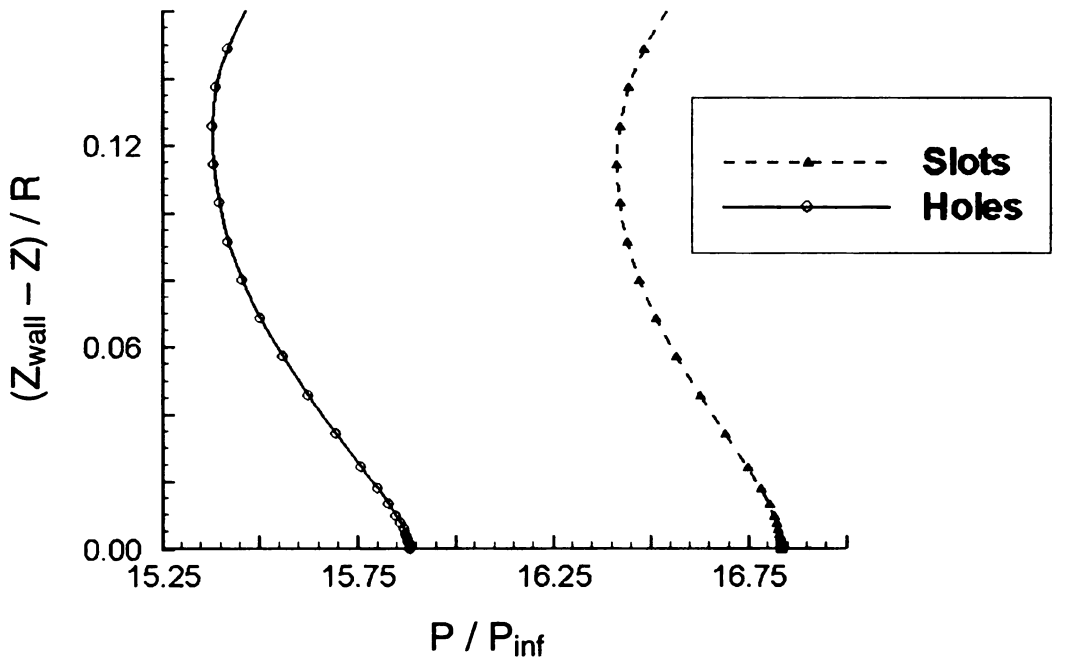

(c)

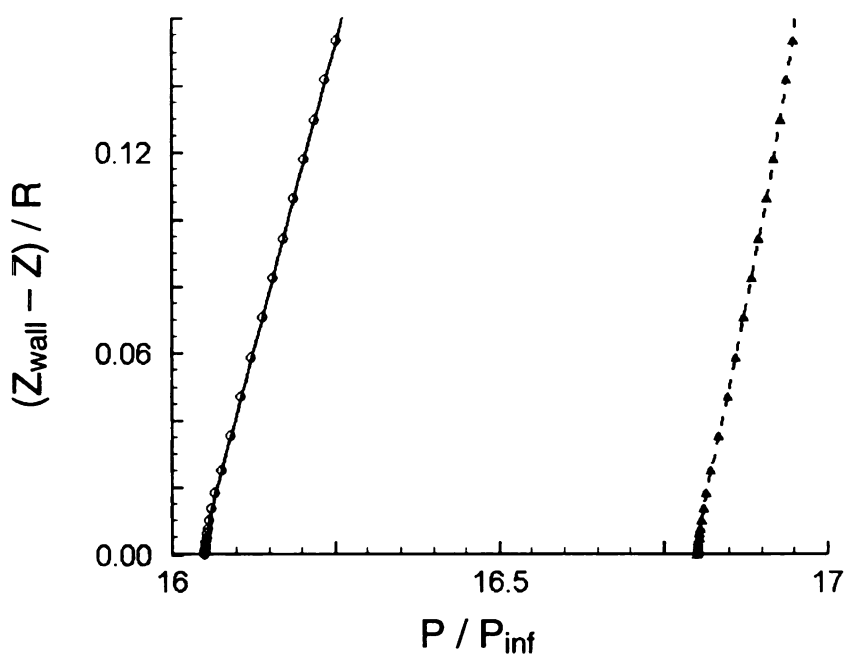

(d)

2.6 Conclusions

Computations were performed for an axisymmetric mixed-compression inlet at zero angle of attack in which a bleed boundary condition involving a discharge coefficient is implemented in two different ways. In one implementation, the locations of the bleed holes are discerned. In the other implementation, each row of bleed holes is modeled as a porous surface or slot, where the number of bleed holes in each row is accounted for by adjusting the discharge coefficient to give the correct bleed rate.

During these simulations, it was noted that the initialization of the flow through the mixed-compression inlet was complicated by several factors. To assist future CFD research into these types of inlets, a set of guidelines was generated for this type of flow. These guidelines outline and detail the major difficulties and propose methods for initializing the flow through the inlet. One key outcome of this method is the inclusion of a buffer in the placement of the terminal shock during the construction of the inviscid, critical flow solution. This buffer is intended to account for the effective-area changes that will occur when the viscous solution is initiated.

For critical flow through the mixed-compression inlet, stable solutions with no spillage were achieved for both the bleed hole (row-hole) and bleed-slot (row-slot) boundary conditions. Results from the simulations obtained show that although both implementations of the bleed boundary conditions gave the same overall bleed rate in approximately the same locations. The predicted Mach number profiles and pressure distributions downstream of the bleed region,

however, differed considerably between the row-hole and row-slot boundary conditions. These results indicate that the boundary layer development, the Mach number profile, the shock-wave/boundary-layer interaction, and the terminal shock strength are all affected by both the bleed rate and the bleed hole pattern.

The observations made regarding the role of the boundary layer growth during the initialization of the flow within the inlet have led to the proposal of a method of control that is especially suited for a mixed-compression inlet. This proposed method takes advantage of the fact that small changes in the boundary layer can result in significant changes to the properties of an inlet. This approach uses combined suction and bleed to create closed surfaces within the flow, thereby changing the effective-area ratio of an inlet.

CHAPTER 3

CFD Simulations of a Free Stream-Surface Control Method Using a Transverse Jet-in-Crossflow and Bleed Through Discrete Holes

3.1 Summary

CFD simulations were performed to demonstrate and investigate the general properties of a free stream-surface control method using jets injected transversally into a supersonic crossflow. In these simulations, a slightly underexpanded, supersonic jet is injected into a supersonic crossflow and, with the addition of bleed downstream of the injection port, closed surfaces are created in the crossflow. It is proposed that these surfaces, termed free stream-surfaces, can be used to control various aspects of the crossflow. For example, in a mixed-compression inlet these surfaces could be used to change the effective-area of the supersonic diffuser, thereby changing the location of the terminal shock in the inlet.

Results are presented for several cases to determine the general characteristics of the flow and the free stream-surface control mechanism. Estimates of the jet shape and penetration, as well as a description of the free stream-surface control mechanism are also provided. For these simulations, the

injection port is modeled as a simple square injection port in a periodic environment. The downstream bleed region is modeled using a bleed boundary condition that has been designed specifically to capture the physics of choked bleed through discrete holes: for example, barrier shock formation and the flow turning that occurs between holes.

This computational study is based on the Reynolds-averaged, thin-shear layer, compressible Navier-Stokes equations and the conservation equations of mass (continuity) and total energy closed by the one-equation model of Spalart-Allmaras. Solutions were generated by a cell-centered, finite-volume method that uses third-order accurate, flux-difference splitting of Roe with limiters and multigrid acceleration of a diagonalized ADI scheme with local time stepping on structured grids.

3.2 Introduction

In the simulation of mixed-compression inlet (Chapter 2), the interplay between the boundary layer height, the applied back pressure, the bleed rate, and the translation of the cowl proved to be difficult to model. During these simulations it was observed that slight changes in the area ratio of the inlet could very easily change the properties of the inlet so that the terminal shock would move forward of the throat and be expelled. These slight changes were often caused by the growth of the boundary layer in the supersonic diffuser section. In a physical inlet, the influence of the boundary layer on the effective-area in supersonic diffuser is addressed by placing one set of bleed holes far upstream

of the throat. In the simulations of the mixed-compression inlet (Chapter 2), the changes in the boundary layer height occurred during the initialization process, when the solid surfaces were transitioned to viscous walls, or when the upstream bleed rate was insufficient for the flow conditions. While these are both issues that are unique to the simulation process, in a physical inlet these changes could also be induced by a change in the angle of attack, an inappropriate placement of the upstream bleed holes, or by an insufficient amount of upstream bleed.

It is proposed that a free stream surface control method, implemented in this manner, can be used to address both of the main issues facing the operation of a mixed-compression inlet. For example, a free stream surface control method implemented in the converging portion of a mixed-compression inlet could be used to replace or reduce the amount of translation needed to bring the aircraft to its operational speed. By methodically changing the amount and/or angle of injection or by modifying the number of active bleed holes, the free stream-surface could be controlled in such a way as to replicate the necessary changing geometry of the inlet, mimicking the effect of the translating cowl. A free stream-surface control method could also be implemented in such a way as to respond to the initial stages of unstart by changing the effective-area ratio of the inlet upstream of the shock and re-establishing favorable operating conditions.

Since critical flow in an inlet occurs when the shock is held at or near the throat, the system is operating very close to a marginally stable state and would benefit from any additional control. The advantage of using the free stream-

surface control method is that only small changes in the boundary layer height are needed to effect large changes in the properties of the inlet. The current approach is to model the injection as an individual hole in a periodic environment and to model the downstream bleed using a bleed boundary condition that permits the simulation of bleed through discrete holes. In this manner, the free stream-surface control mechanism can be quickly studied and the overall features can be examined.

3.3 Description of the Problem Studied and the Methods Employed

3.3.1 Problem Description

The flow simulation studied involves a supersonic, underexpanded, square jet injected into a turbulent, supersonic crossflow. Depending on the simulation, the Mach number was within 1.2 to 2.0 and the jet was slightly underexpanded. For these simulations, the jet momentum ratio was typically between 1.1 and 1.4 and, as a result, the penetration of the jet into the crossflow was minimal. The angle of injection (θ) for these simulations was 135 degrees.

A schematic diagram of the three-dimensional system studied is shown in **Figure 3.1**. The system consists of a flat plate, a square injection port, and circular bleed openings with a diameter (d) of 2.5 mm. The location and pattern of the bleed holes and the injection port are shown in **Figure 3.2**. The injection port has a width equal to the bleed hole diameter and is located in the center of a computational domain that is two hole diameters in width (spanwise direction).

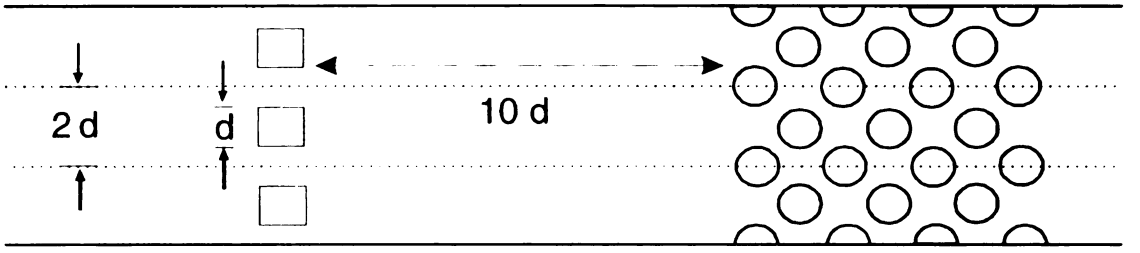

Figure 3.1 Schematic of computational domain for the free stream-surface simulations: top-down view of flat plate surface (dashed lines indicate periodic boundary planes).

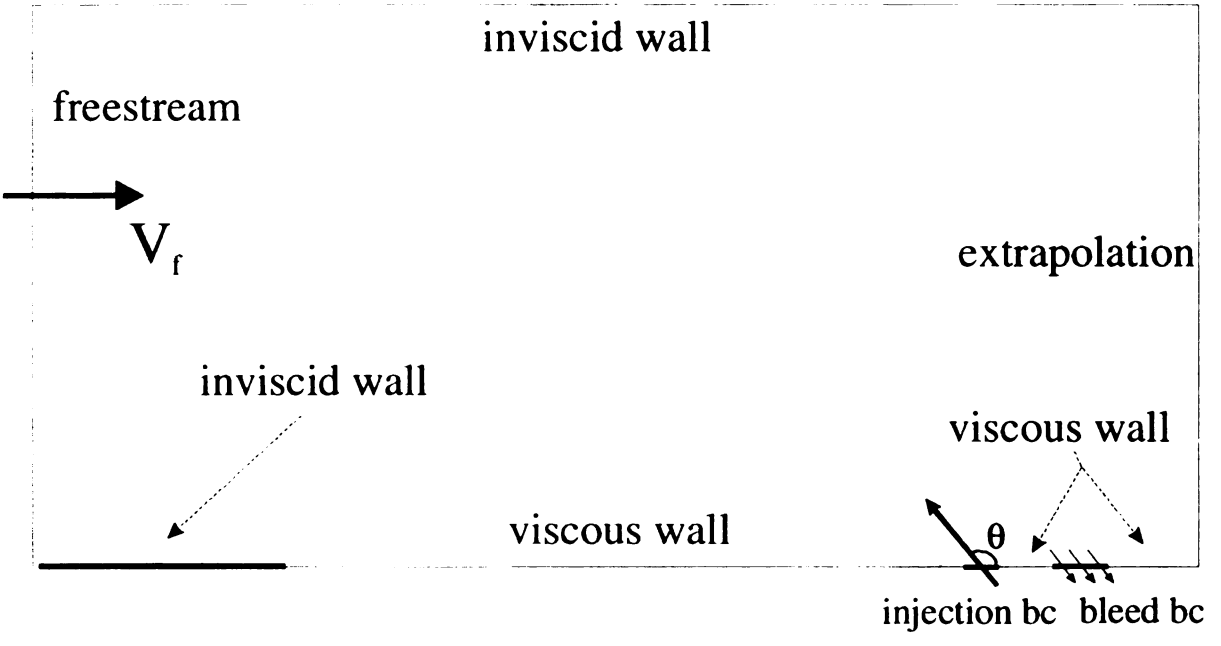

Figure 3.2 Boundary condition schematic for the free stream-surface simulations.

The flat plate is 2.32 m long and the approach length, the distance from the beginning of the viscous flat plate to the injection port, is 2.14 meters. This leads to a momentum thickness at the injection port, without injection, that is comparable to the width of the injection port. This thickness is also comparable to the actual momentum thickness in the near-throat region of a mixed-compression inlet that was used in a previous study. The bleed hole and injection port dimensions were also chosen so as to be comparable to the dimensions of the bleed holes used in an experimental study of a mixed-compression inlet.

Bleed is applied downstream of the injection port at several locations and, depending on the simulation, the number and location of the bleed holes could be varied. The center of the first row of holes was located at a distance of 11d downstream of the center of the injection port and the center of the last row of holes that could be used, the seventh row, was located 17d downstream of the injection port (**Figure 3.2**). Each hole is 1d in diameter and is modeled as a rough circle. The holes are arranged in a staggered fashion with no overlap between rows.

The boundary condition used is a discharge-coefficient, bleed boundary condition which permits the modeling of choked bleed through individual bleed holes. Since generating a zero net-mass flux is a difficult matter with this boundary condition, the bleed rate was permitted to float. For these simulations, the discharge coefficient for the bleed holes was fixed, based on previous research, at 0.75.

In the simulations described in this paper, the freestream static temperature, pressure, and Mach number are 173 K, 10.930 kPa, and 1.2 respectively. The Reynold's number-per-meter, based on the freestream conditions, is 3.495×10^7 m^{-1}. Flow conditions were designed to replicate the near-throat conditions of a mixed-compression inlet that was used in a previous study. The mixed-compression inlet problem described above was selected because experimental and computational data exists which can be used in future research to implement the results of this study.

3.3.2 Problem Formulation

The problem described in the previous section is modeled by the Reynolds-averaged, thin-shear layer, compressible Navier-Stokes equations and the conservation equations of mass (continuity) and total energy closed by the single equation model of Spalart-Allmaras. Additional details of the governing equations are available in the CFL3D User's Manual (Version 5.0) by Biedron et al. (1996).

3.3.3 Boundary Conditions

The boundary conditions applied at the boundaries of the flow domain (**Figure 3.2**) are as follows. At the inflow boundary, all flow variables are fixed at the supersonic freestream conditions. At the outflow boundary, a supersonic-outflow boundary condition is applied and all of the flow variables are extrapolated. The supersonic outflow boundary is situated far away from the

dynamic regions so that any influences resulting from incompatibility of the boundary condition with the outgoing boundary layer will not propagate into regions of interest. On the upper surface, the wall is set as an inviscid wall boundary. This was considered appropriate because the dynamics of the interaction of the upper wall boundary and the bow shock were not considered a part of this study. In the spanwise direction, periodic boundary conditions were imposed at the two boundaries to simulate a single element in a series of structures in an axisymmetric environment.

The solid surfaces in the simulations were treated as viscous, adiabatic walls and, at these surfaces, the no-slip condition and a zero normal-pressure gradient were imposed. At the injection inflow boundary, the flow was either sonic or supersonic, depending on the simulation, and all of the variables were specified. The bleed holes were modeled using a non-porous-wall bleed boundary condition (discharge coefficient boundary condition) as a model for bleed through discrete holes in which at least one grid point is located within each bleed hole. This is the same bleed boundary condition described in detail in Chapter 2.

3.3.4 Numerical Method of Solution

Solutions to the governing equations described in the previous section were obtained by using a cell-centered, finite-volume code called CFL3D. All inviscid terms were approximated by the flux-difference splitting of Roe (third-order accurate) with the slope limiter of Chakravarthy and Osher. All of the

diffusion terms were approximated conservatively by differencing derivatives at cell faces. In the steady-state solutions, time derivatives were approximated by the Euler implicit formula. The system of nonlinear equations that resulted from the aforementioned approximations to the space- and time-derivatives local time-stepping (local Courant number always set to unity) and three-level V-cycle multigrid.

3.3.5 Grid Structure

The single block, structured grid system used is shown in **Figure 3.3**. It has 1,225,105 grid points with the majority of the grid points clustered near the expected location of the bow shock and the injection and bleed holes. All of the grid dimensions were designed so that multigrid methods could be employed.

This grid, with dimensions 497 x 17 x 145, has 17 grid points in the spanwise direction. Depending on the simulation, the streamwise direction spans a distance between 10 and 40 injection hole diameters (10d - 40d) upstream of the injection region to 13d downstream of the injection port. Within the regions of interest, the aspect ratio is kept near unity so that the various shock structures could be reasonably captured. In the normal direction, the grid spacing was designed for use in a future simulation that would implement a k-ω turbulence model with the shear stress transport model of Menter. To resolve the boundary layer that forms adjacent to the flat plate surface, the grid is very densely clustered in the normal direction. With this structuring, the first grid point

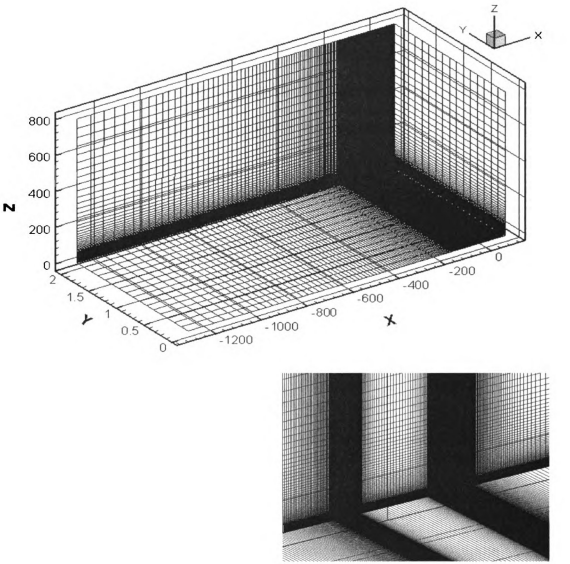

Figure 3.3 Single block grid system used in the free stream-surface simulations. The scale in the spanwise direction (y) has been expanded by a factor of 200. Top: Overall grid system. Bottom: Region around injection and suction (x = 0).

has a y+ value of less than unity. In addition, there were 5 grid points within a y+ of 10 and 25 grid points within a y+ of 100.

The injection port is modeled as a square measuring 8 cells on a side and the bleed holes are modeled as rough holes with 64 cells per hole. There are 4 cells between the injection port and each periodic boundary.

3.4 Results

Figure 3.4 shows the results from a two-dimensional simulation of the free stream-surface control mechanism. In this case, the two-dimensional grid was taken as the centerline plane of the three-dimensional problem. The injection jet is set at a Mach number of 1.6 and is only slightly underexpanded. In addition, the angle of injection is fixed at 135 degrees relative to the freestream flow direction. In this figure, the Mach number contours and several illustrative streamlines that emanate from both the freestream and the injection port are shown to illustrate the free stream-surface control mechanism. The jet, injected in to the crossflow, rises to a height of approximately 2.5d and then turns downstream. The majority of the injected fluid is recaptured by the bleed region, however, because the bleed rate was difficult to control with a discharge coefficient, there is a net injection of mass into the crossflow.

Downstream of the injection port a trapped recirculation region is clearly visible beneath the injection plume and, at the bleed location, the barrier shocks from the flow entering the holes (slots) coalesce into a single shock. Also visible on the downstream end of the control mechanism is a region of high Mach

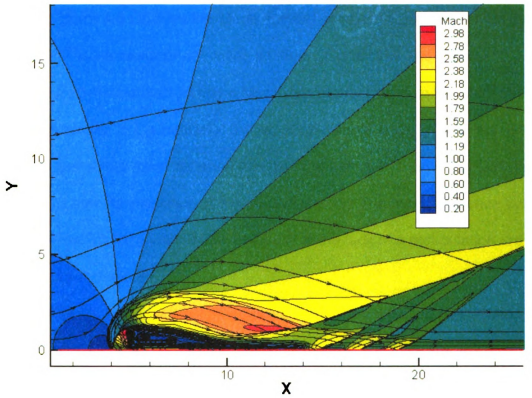

Figure 3.4 Mach number contours and selected streamlines for the two-dimensional simulations of the free stream-surface control structure. The freestream flow is from right to left.

number fluid. This is generated when the main flow expands as the injected jet is drawn back down towards the flat plate surface by the bleed. Within the jet itself, the expected expansion of the jet as it enters the crossflow is not apparent: this is a result of both the angle of injection and the slight underexpansion of the jet.

Figure 3.5 displays the Mach number contours along the centerline for one of the three-dimensional cases studied. In this case, the slightly-underexpanded injected jet has a Mach number of 1.4. In many respects, this profile is similar to the results of the two-dimensional study. The injected jet is seen to penetrate some distance into the fluid before it is turned by both the crossflow and the presence of the suction region. The main difference between this and the two-dimensional simulation is in the lack of a recirculation region downstream of the jet.

Figure 3.6 provides a perspective view of the injection port section of the free stream-surface control mechanism. Pressure contours are displayed along the flat plate and several selected streamlines for both the jet and crossflow are presented. The pressure contours on the plate surface show the pressure rise ahead of the jet and a low-pressure region forming the downstream side of the jet. **Figure 3.6** also shows how streamlines from the approaching flow are diverted past the injection plume. Some of the approaching flow is clearly entrained by the leading edge of the plume while the majority of the flow seems to be diverted around the injected fluid. Downstream of the injection port, the diverted flow is captured by the bleed process and removed from the crossflow.

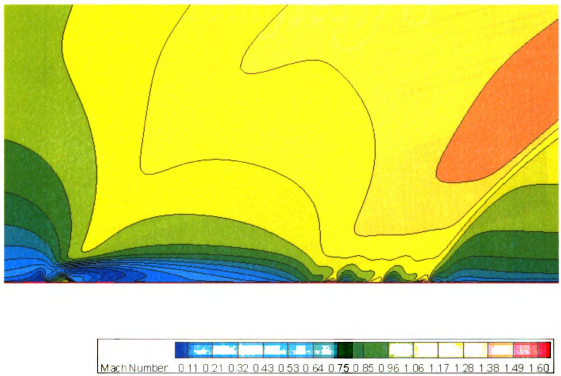

Figure 3.5 Mach number contours and selected streamlines along the centerline for a three-dimensional simulation of the free stream-surface control structure. The freestream flow is from right to left.

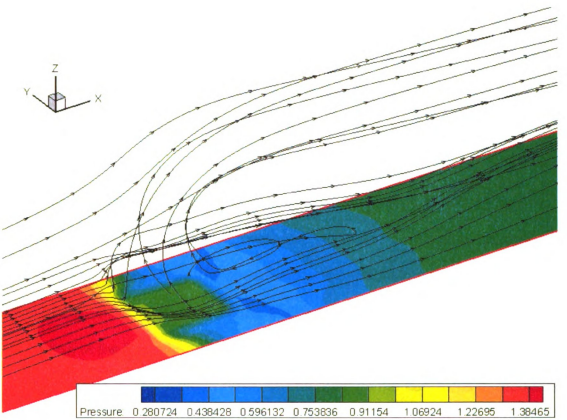

Figure 3.6 Pressure contours along the flat plate and selected streamlines from the crossflow and the injected jet. Freestream flow is from left to right.

Some of the diverted flow, however, reverses and is entrained by the downstream edge of the plume.

Figure 3.7 shows a series of streamlines from two heights within the approaching flow for the same case as described in **Figure 3.6**. These streamlines, especially the upper set, show the deformation of the freestream flow in response to the injected fluid. Also visible in this figure is the spanwise shape of the control surface: the injection of fluid from a square injection port yields a wavy control surface.

Figure 3.8 provides a perspective view of the injection-suction system. Mach number contours along the centerline plane and on the plate surface provide an overview of the free stream-surface control structure in three dimensions. On the left of the figure, the injection port is clearly seen, as is the stagnation of the fluid ahead of the injection port. Downstream of the injection port, the influence of the bleed holes can be seen as the flow turns to reconnect with the surface. Just past the last row of bleed holes, the barrier shocks from the bleed holes are seen to coalesce and the flow changes direction to follow the flat plate again. One of the interesting features of this plot is the region of high Mach number that is generated as the freestream flow turns to follow the suction.

Figure 3.9 shows the relationships between the injection Mach number and both the injected plume height and forward penetration of the jet for the three-dimensional cases studied. In this plot it is observed that there is a linear relationship between the injection Mach number and the maximum height achieved by the jet with a slope of 2.66.

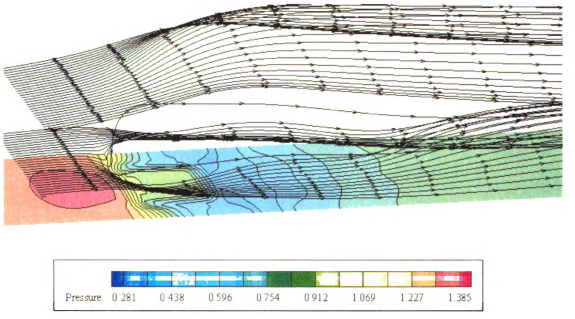

Figure 3.7 Pressure contours along the flat plate and selected streamlines from the crossflow.

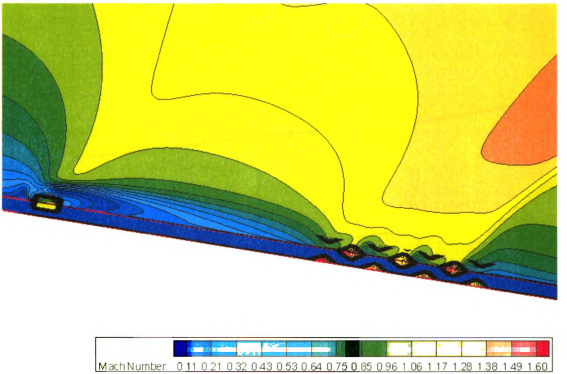

Figure 3.8 Mach number contours around the injection port and bleed region on the flat plate surface and along the centerline.

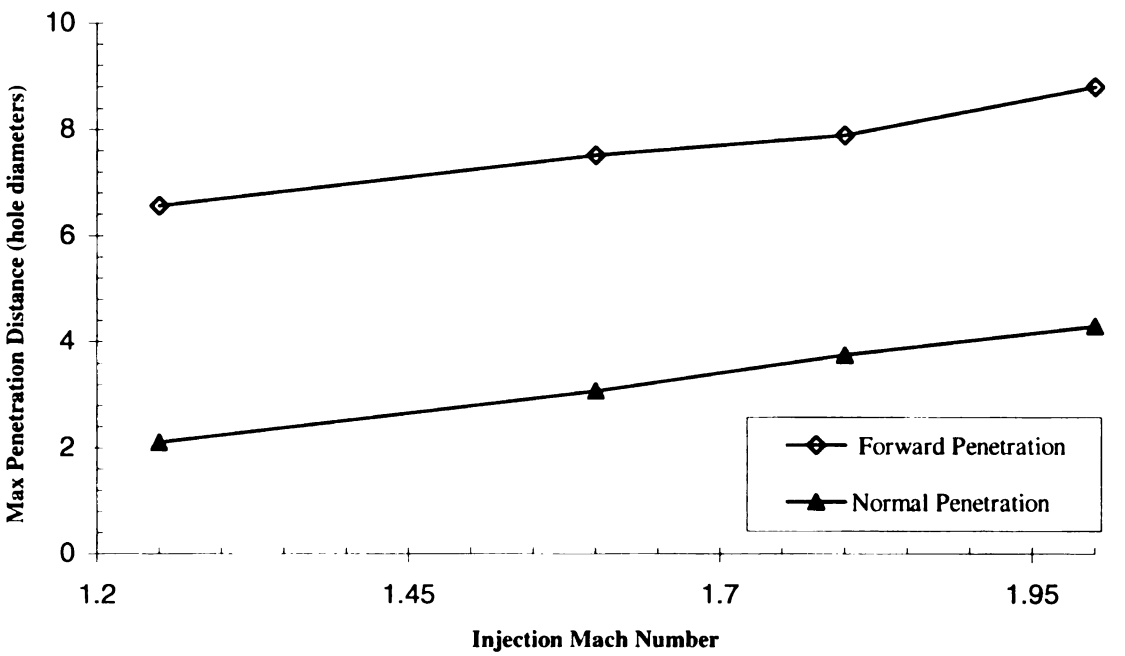

Figure 3.9 Relationship between injection Mach number and the forward and normal penetration of the jet for a typical case.

3.6 Conclusions

A number of simulations were conducted to investigate a proposed free stream-surface control structure using paired injection and suction to control the diversion of a crossflow. Simulations were conducted with a square, variable-Mach number, slightly-underexpanded jet exhausting into a supersonic crossflow. Downstream bleed was applied to alter the trajectory of the injected jet and to generate closed surfaces whose height and length are controllable. Initial results from a three-dimensional, turbulent case were presented which illustrate the three-dimensional properties of this flow and demonstrate the potential for use as a flow control mechanism.

The results from these simulations illustrate the main features of the free stream-surface control structure and provide information for the development of future studies. Items such as the location of the bow shock, the maximum penetration of the jet into the crossflow, and forward penetration of the jet were identified as important factors to be examined and addressed in future simulations.

In the simulations, it was observed that the injected plume clearly forms a free stream-surface whose reconnection can be improved by the proper choice of location for the suction. The injected jet was observed to penetrate into the crossflow before being turned by both the crossflow and the downstream suction and the jet's maximum height and forward penetration were acquired as a function of the Mach number of injection. From this, it was determined that the energy input required to effect meaningful control was significant and, potentially,

prohibitive. At the downstream bleed location, the jet reconnected to the flat plate surface and the flow realigned with the plate surface.

The main issue associated with the shape of the free stream-surface involves the manner by which the injected fluid is forced into the crossflow. Since the injection was conducted through a discrete hole, instead of a slot, much of the fluid that would be diverted by the jet in a slot configuration is, instead, either entrained into the jet or ends up being drawn out by the bleed holes. In other words, the injected plume fans out and is not completely recaptured by the bleed region, even if the discharge coefficient were set for a zero net-mass inflow. While this may be a disadvantage in controlling the shape of the free stream-surface, because of the flow turning at reconnection, this should act on the region downstream of the bleed as if there were tangential slot injection. One aspect of this, therefore, is that the boundary layer is energized by the expanding flow as the plume turns in response to the bleed.

During this research, two additional issues were identified as crucial for future investigation. The first issue deals with the control of the net bleed rate with the bleed boundary condition used in the simulations. Since the bleed boundary condition used models the bleed through each hole as a function of the local speed of sound, modifying the discharge coefficient to affect a given bleed rate is awkward. It is recommended that the bleed boundary condition subroutine be modified so that the mass flow rate through each hole can be tracked and adjusted.

The second issue involves the shape of the control structure when individual holes are used for injection. With the injection being accomplished by individual holes, the shape of the free stream-surface in the streamwise direction is highly distorted. In a mixed-compression inlet, this distortion will lead to local expansion and contraction of the flow and would be undesirable in practice.

Future work in this area should focus on further characterizing the profile of the jet as a function of the location of the bleed holes, the bleed hole configuration, and the Mach number and pressure of the injected fluid. Additional directions should also focus on alternative methods for shielding the injection from the high momentum crossflow. To this end, approaches such as injection behind a rearward facing step, tangential slot injection, or the injection of fluid into a recessed cavity would function starting points for alternative methods for generating free stream-surface control.

CHAPTER 4

CFD Simulations of a Free Stream-Surface Control Method Using a Driven Cavity

4.1 Summary

CFD simulations were performed to demonstrate and investigate the general properties of a free stream-surface control method using driven cavity flow. In these simulations, a subsonic jet is injected into cavity that is recessed within a turbulent, supersonic crossflow. By injecting fluid into the cavity, it is proposed that both the deflection of the separated crossflow and the downstream boundary layer profile can be controlled while, at the same time, shielding the injection process from the high-momentum crossflow fluid. With the addition of bleed downstream of the cavity, closed surfaces can be created which can be used to control various aspects of the crossflow. For example, in a mixed-compression inlet these surfaces could be used to change the effective area of the supersonic diffuser, thereby changing the location of the terminal shock in the inlet.

Results are presented for length-to-depth ratios (5.0, 8.0, 15.0, and 17.5) that cover both open and closed cavity flow. Mach number contours and profiles downstream of the cavity are presented to assess the impact of the driven cavity

on the crossflow. In addition, pressure profiles along the cavity floor are provided to assess the impact of the injection on the pressure gradient that would be experienced by stores enclosed in the cavity. Additional studies are conducted to examine the impact of the approaching boundary layer height on the dynamics of the driven cavity flow for L/h = 5.0 and to address the grid structure influences on the driven cavity flow.

This computational study is based on the Reynolds-averaged, thin-shear layer, compressible Navier-Stokes equations and the conservation equations of mass (continuity) and total energy closed by shear-stress transport (SST) turbulence model of Menter. Solutions were generated by a cell-centered, finite-volume method that uses third-order accurate, flux-difference splitting of Roe with limiters and multigrid acceleration of a diagonalized ADI scheme with local time stepping on structured grids.

4.2 Introduction

In the simulation of the mixed-compression inlet (Chapter 2), it was observed that the interplay between the boundary layer height, the applied back-pressure, the bleed rate, and the translation of the cowl was responsible for much of the instability that is experienced by mixed-compression inlets. When these influences are properly balanced within the inlet, efficient and effective operation is achieved. However, when any one of these items is out of balance, the natural response of the inlet is either inefficient operation, where the terminal shock is placed far downstream of the throat, or inlet unstart.

One potential method of control for a mixed-compression inlet involves modifying the properties of the inlet through the effective-area ratio profile upstream of the throat. During simulations of the mixed-compression inlet (Chapter 2), it was observed that slight changes in the boundary layer thickness in the supersonic diffuser section of the inlet, often caused by an improper pairing of the bleed rate and back-pressure, could change the properties of the inlet so that the terminal shock would move forward of the throat and be expelled. As a result, it was proposed that the insertion of a free stream-surface control mechanism, applied in the supersonic diffuser section or near the throat, could effectively control the thickness of the boundary layer and, therefore, provide a measure of control for the entire inlet.

In Chapter 3, it was observed that the generation of free stream-surfaces by combined injection and suction was very effective at generating controllable shapes and that, with some modification, true free stream-surfaces could be generated to control the diversion of the crossflow. The downside to this approach was that the injection of fluid directly into a supersonic crossflow is very expensive. In addition, the bow shock resulting from direct injection into a supersonic crossflow is a potential problem for flow control in a mixed-compression inlet environment. From these simulations, it was apparent that this type of control affects not only the boundary layer height of the fluid, but also the core flow.

The approach taken in this chapter is to generate the free stream-surface control using a driven-cavity flow field. In this iteration, a cavity would be placed

in the supersonic diffuser section of the inlet and the flow within the cavity would be driven by subsonic injection on the upstream face of the cavity. To close the surface, the bleed system used for normal inlet operation could be incorporated. By methodically changing the amount and/or angle of injection or selecting the geometry of the cavity, the free stream-surface can be used to control the effective-area ratio in such a way as to replicate the changing geometry of the inlet, thereby mimicking the effect of the translating cowl.

Early work on cavity insertion as a control device in supersonic flows focused primarily on reducing the heat transfer rate for protection of hypersonic vehicles. Chang (1976) reports that experimenters were able to reduce the heat transfer rate by a factor of two when a laminar cavity flow replaced a laminar boundary layer flow. However, Chang also that these same studies showed that the changes in the downstream heat transfer rates tended to nullify the positive effects of the injection into the cavity. In 1965, Nicholl (Chang, 1976) conducted experimental studies with helium injection in an annular cavity on a conic re-entry vehicle at Mach 11. Nicholl found that by increasing the height of the separation shoulder above the line of the conic surface, the injected fluid was able to pass into the downstream boundary layer flow and dramatically reduce the downstream heat transfer rates.

Current interest in cavity flow fields at supersonic speeds has focused on the issues associated with stores separation from high-speed aircraft. Recent developments in stealth technologies and the desire to reduce radar cross-section from the external store carriages in military aircraft are the motivating

factors in the examination of internal store carriages for supersonic aircraft. Simply modeled, these internal store carriages are cavities set into the airframe. Research by various authors (*cf.* Wilcox, 1990; Stallings *et al.*, 1991; Plentovich *et al.*, 1993) has focused on quantifying the flow field in the cavity by measuring the pressure, force and moment distributions on a generic store separating from within a box cavity. Various researchers have also proposed different methods to control of the moments and drag experienced by the stores. For example, Wilcox (1990) presented an approach using a cavity with a porous-floor to modify the cavity flow field. By venting the high-pressure fluid in the rear of the cavity to the low-pressure fluid in the front, the objective was to reduce the overall drag characteristics of the cavity. Each of these approaches, however, has involved the passive control of the fluid within the cavity for the purpose of drag reduction or the control of moments experienced by stores within the cavity.

For flow over cavities at supersonic speeds, there are two general types of cavity flow fields observed. In these flows, the type of flow field observed is determined primarily by the length-to-height ratio (L/h) of the cavity. For L/h greater than 13, the flow field is referred to as closed-cavity flow. In closed-cavity flow, the separating shear layer expands over the leading edge of the cavity and then, because of the length of the cavity, the shear layer impinges on the floor of the cavity before exiting the cavity ahead of the downstream face (**Figure 4.1**). In this case, the pressure distribution along the floor of the cavity contains a low-pressure region in the upstream portion of the cavity, in the area under the separated shear layer before it impinges on the floor of the cavity. The pressure

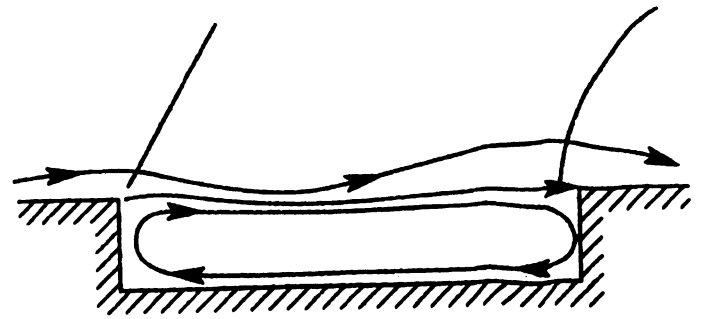

(a)

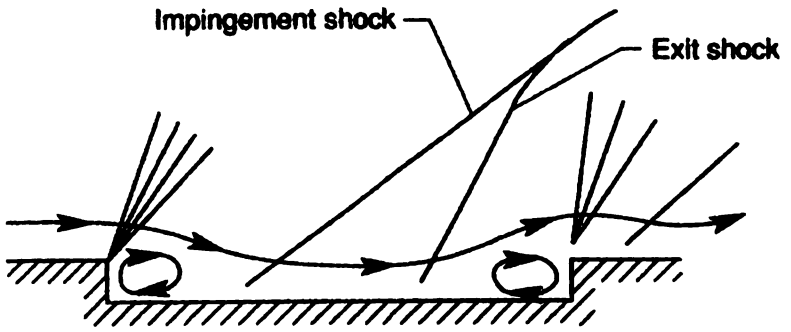

(b)

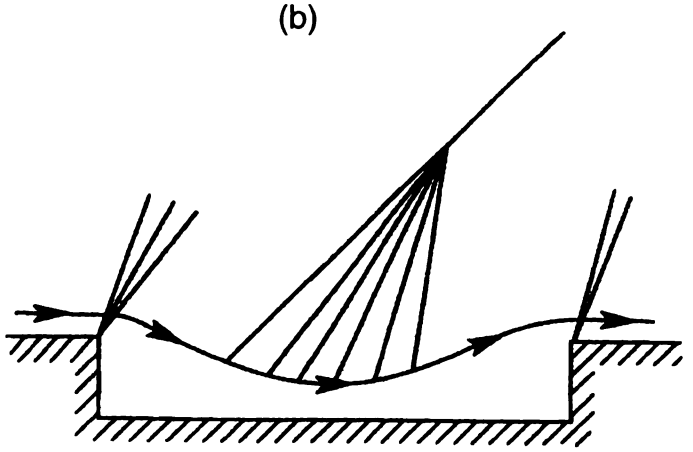

(c)

Figure 4.1 Description of the different types of cavity flow: (a) open cavity flow, (b) closed cavity flow, (c) transitional cavity flow (Plentovich *et al*, 1993 and Stallings *et al*, 1987).

then rises as the impingement location is reached and then it is observed to level off. As the downstream face of the cavity is approached, the pressure levels on the floor of the cavity rise again and reach a maximum value just ahead of the downstream face of the cavity.

An open cavity, on the other hand, is classified as a cavity with a length-to-height ratio (L/h) less than 10. In this case, the shear layer is able to bridge the cavity and does not impinge on the cavity floor. Across the floor of the cavity, the pressure recovery coefficient (C_p) is positive, however, it is very small for the majority of the cavity's length. In the supersonic crossflow cases studied by Stallings, *et al* (1987), the pressure recovery coefficient for the open cavities was below 0.05 in the leading edge of the cavity and jumped to only 0.2 at the downstream face of the cavity.

Between these two general cases for cavity flow is a region that has often been referred to as transitional cavity flow. In transitional cavity flow, the angle through which the shear layer turns to exit is such that the impingement shock and the exit shock coincide. Often, this range is further sub-divided into transitional-open cavity flow and transitional-closed cavity flow, depending on the degree to which the separated shear layer penetrates into the cavity. For this study, both open and closed-cavity type flows are investigated, however the transitional regimes are avoided because of their difficulty in classification.

4.3 Description of the Problem Studied and the Methods Employed

4.3.1 Problem Description

The flow simulation studied involves a subsonic jet injected into a cavity that is placed in a flat plate within a turbulent, supersonic crossflow. The freestream conditions are set so as to be representative of the flow within a mixed-compression inlet: the freestream Mach number, total pressure and static temperature are, respectively, 2.65, 1 atm and 129.772K. The boundary layer thickness at the leading edge of the cavity was fixed at 0.005 m. For the configurations studied, the depth of the cavity was fixed at 0.0127 m and the length-to-depth ratio of the cavity (L/h) was 5.0, 8.0, 15.0 and 17.5. Depending on the simulation, the Mach number for the injected jet either 0.4, 0.6 or 0.8. The angle of injection (θ), for each case, was either normal to the wall or at 45 degrees to the horizontal (streamwise direction). The amount of injected fluid was modified by changing the area of injection along the upstream wall. The different cases presented in this paper are summarized in **Table 4.1** and a schematic diagram of the system studied is shown in **Figure 4.2**. The system consists of a long flat plate on which the boundary layer is allowed to develop and a cavity recessed in the flat plate where the boundary layer was the desired thickness. In these simulations, the cavity is modeled as a two-dimensional structure and the injection occurs on the upstream sidewall of the cavity.

The momentum thickness at the leading edge of the cavity that is fixed at 0.005 m. This thickness is comparable to the actual momentum thickness in the near-throat region of a mixed-compression inlet that was used in a previous

Case Label	L/h	Injection Angle	Injection Mach Number	Injection Area (fraction of wall)	δ/h	Name
#1	5	-	0	0.8	0.4	5 - baseline
#2	5	45	0.26	0.8	0.4	5 - 45 - 0.26 - 8
#3	5	45	0.6	0.8	0.4	5 - 45 - 0.6 - 8
#4	5	45	0.6	0.8	0.8	
#5	5	45	0.26	0.4	0.4	5 - 45 - 0.26 – 4
#6	5	45	0.4	0.4	0.4	5 - 45 - 0.4 - 4
#7	5	45	0.6	0.4	0.4	5 - 45 - 0.6 - 4
#8	15	-	0	0.8	0.4	15 - baseline
#9	15	45	0.8	0.8	0.4	15 - 45 - 0.8 - 8

Table 4.1 Table listing relevant parameters of cases presented for the driven cavity simulations.

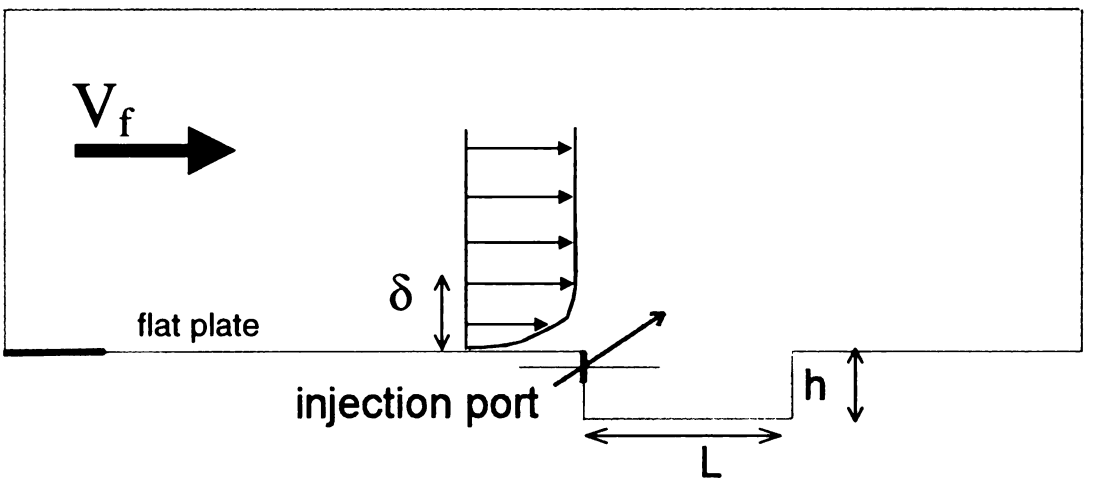

Figure 4.2 Schematic of computational domain for the driven cavity simulations.

study. The bleed hole and injection port dimensions were also chosen to be comparable to the dimensions of the bleed holes used in an experimental study of a mixed-compression inlet.

4.3.2 Problem Formulation

The problem described in the previous section is modeled by the Reynolds-averaged, thin-shear layer, compressible Navier-Stokes equations and the conservation equations of mass (continuity) and total energy closed by shear-stress transport (SST) turbulence model of Menter. Additional details of the governing equations are available in the CFL3D User's Manual (Version 5.0) by Biedron et al. (1996).

4.3.3 Boundary Conditions

The boundary conditions applied at the boundaries of the flow domain (**Figure 4.3**) are as follows. At the inflow boundary, all flow variables are fixed at the supersonic freestream conditions. By allowing the boundary layer to develop in the simulation, the environment into which the fluid is injected can be easily modified with minimal changes to the grid. At the outflow boundary, a supersonic-outflow boundary condition is applied and all of the flow variables are extrapolated. The supersonic outflow boundary is situated far away from the dynamic regions so that any influences of the incompatibility of the boundary conditions with the boundary layer will not propagate far into the domain and influence any measurements.

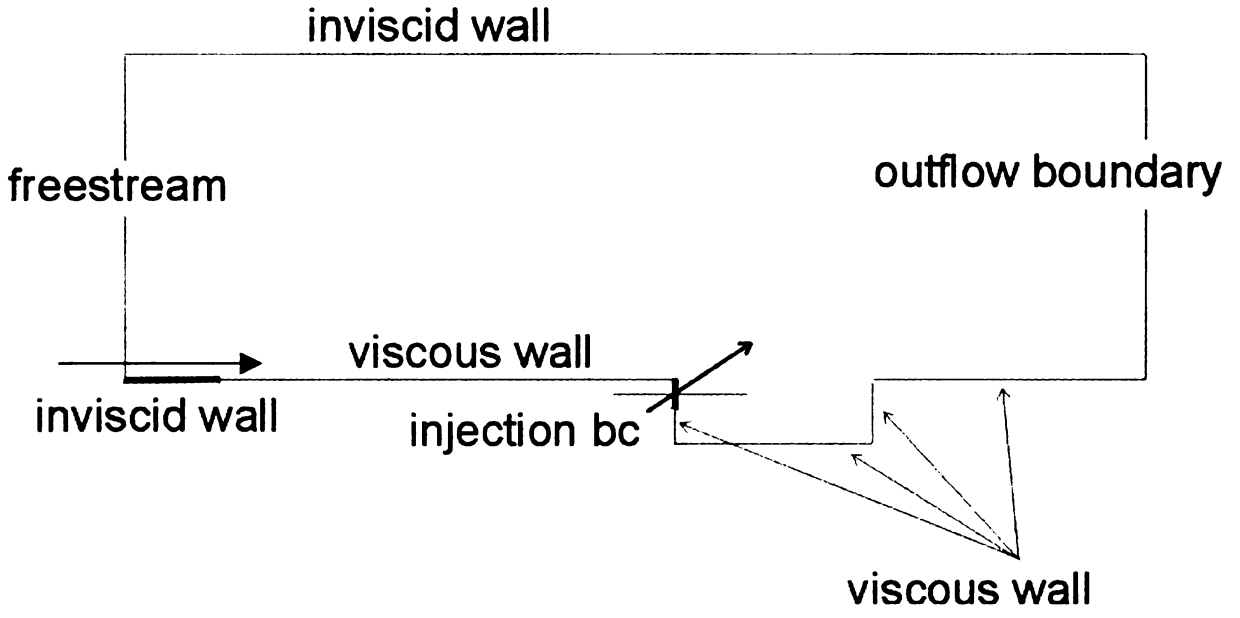

Figure 4.3 Boundary condition schematic for the driven cavity problem.

On the upper surface, the wall is set as an inviscid wall boundary. In the spanwise direction, symmetry boundary conditions were imposed at the two boundaries. The solid surfaces in the simulations were treated as viscous, adiabatic walls and, at these surfaces, the no-slip condition and a zero normal-pressure gradient were imposed. At the injection inflow boundary, the flow was subsonic. At this boundary, the velocity of the flow was fixed at the desired value and angle as was the mass flow rate. From this information, the pressure is extrapolated.

The boundary condition used for the bleed region is a discharge-coefficient, bleed boundary condition which permits the modeling of individual bleed holes. Since generating a zero-net mass-flux is a difficult matter with this boundary condition, the bleed rate was permitted to float. For these simulations, the discharge coefficient for the bleed holes was fixed, based on previous research, at 0.75.

4.3.4 Numerical Method of Solution

Solutions to the governing equations described in the previous section were obtained by using a cell-centered, finite-volume code called CFL3D. All inviscid terms were approximated by the flux-difference splitting of Roe (third-order accurate) with the slope limiter of Chakravarthy and Osher. All of the diffusion terms were approximated conservatively by differencing derivatives at cell faces. In the steady-state solutions, time derivatives were approximated by

the Euler implicit formula. The system of nonlinear equations that resulted from the aforementioned approximations to the space- and time-derivatives local time-stepping (local Courant number always set to unity) and three-level V-cycle multigrid.

4.3.5 Grid Structure

For each of the configurations studied, a four block, structured grid system is used to model the recessed cavity. The grid system used for L/h=5 is shown in **Figure 4.4**. The grid system used to model the cavity is a wrap-around grid system. It has 183,624 grid points and is made up of four blocks that are connected through one-to-one blocking. In addition, all dimensions are designed so that multigrid methods can be used and accommodations have been made so that each block can be fully included in the multigrid. Although the grid for these simulations is three-dimensional, the problem studied is two-dimensional: the extra grid point in the spanwise direction is required because the version of the code being used was unable to run two-dimensional simulations.

Block 1 is a wrap-around grid that conforms to the surface of the flat plate and the cavity. This grid has dimensions 675 x 3 x 57 (3 grid points in the spanwise direction) and, except in the corner regions, provides a fairly uniform distribution of grid points. While the aspect ratio and grid distortion of Block 1 is unavoidable at the corners of the cavity, the use of a wrap-around grid does reduce the issues associated with high aspect ratios or the need for grid patching at these points.

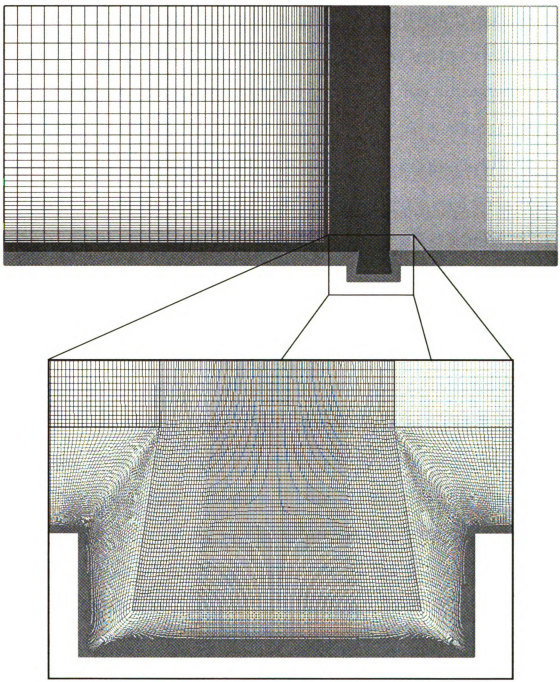

Figure 4.4 The four block, wrap-around grid system used for driven cavity flow problem.

Block 2 fills the region above the wrap-around grid (Block 1) upstream of the recessed cavity. Block 2 has dimensions 121 x 3 x 49 and has a fairly uniform distribution of grid points. The third grid, Block 3, has dimensions 119 x 3 x 57 and fills the region directly above the cavity. This grid is included because a wrap-around grid would have to stretch considerably within the cavity to encompass the majority of the cavity. One-to-one blocking is used along each interface with the wrap-around grid to permit efficient transfer of information across the interfaces.

The fourth grid, Block 4, fills the region above the wrap-around grid (Block 1) downstream of the recessed cavity. Block 4, with dimensions 233 x 3 x 49 and is included to permit the growth of the boundary layer downstream of the cavity beyond the height of Block 1. Block 4 is also included to permit the compression shock, expected from where the separated shear layer reconnects with the downstream edge of the cavity, to properly exit the flow domain.

For Block 1, the first grid point away from the surface has a y+ value less than unity and the first five grid points away from this wall are within a y+ value of ten. This grid spacing is required for the turbulence model of Menter's SST, where integration is to the wall. For these simulations, an initial value for y+ was determined by treating the inlet as a flat plate. As the simulations progressed, the value of y+ was re-assessed and corrections were made to the grid to provide appropriate adjustments.

4.4 Results

Figure 4.5 shows the Mach contours of the baseline case, no injection, for the open cavity flow where L/h= 5.0. This figure shows the boundary layer of the approaching flow and the separation of the crossflow at the cavity lip. Downstream of the cavity, the crossflow reconnects with the flat plate with the result that the boundary layer is thicker. A slight compression shock results where the flow reconnects to the plate and the boundary layer thickens. **Figure 4.6** shows pressure contours and several streamlines for the same case. Within the cavity, the flow is subsonic and it can be seen, from the deformation of the streamlines, that the separated flow penetrates the cavity only slightly for this configuration.

Figure 4.7 shows the Mach number contours for the L/h = 5.0 case where the injected fluid is at 45 degrees to the horizontal at Mach 0.8. In this case, the area of injection was the maximum studied (case #4). **Figure 4.8** shows the pressure contours and selected streamlines for the case. Although the differences between this case and the baseline for this geometry are minor, several differences do stand out. First, the injected fluid, seen clearly at the leading face of the cavity, appears to deflect the crossflow and prevents it from penetrating into the cavity. The deflection of the crossflow can also be seen in the presence of a weak compression shock above the leading edge of the cavity. In **Figure 4.8**, the injected fluid is also seen to deform the shape of the recirculating region within the cavity as it passes into the crossflow. Also visible

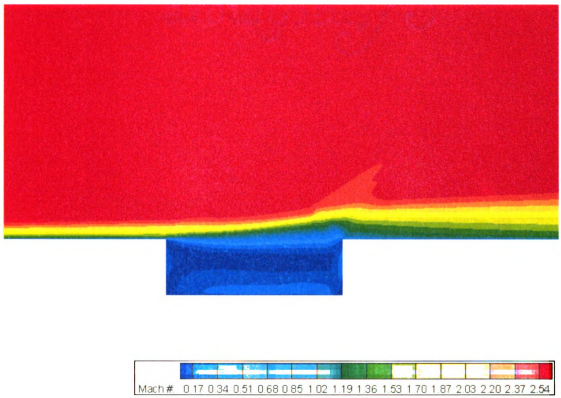

Figure 4.5 Mach number contours for case 1: baseline cavity (L/h = 5.0).

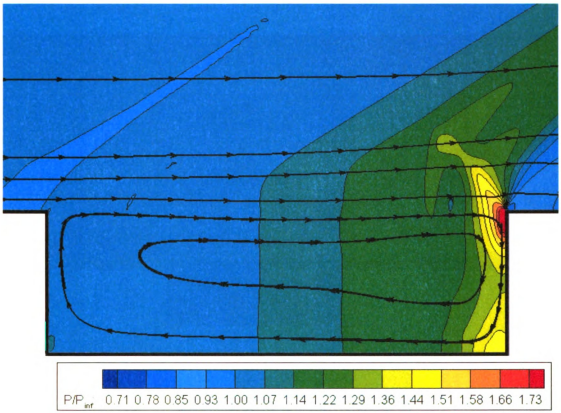

Figure 4.6 Pressure contours and selected streamlines for case 1: baseline cavity (L/h=5.0).

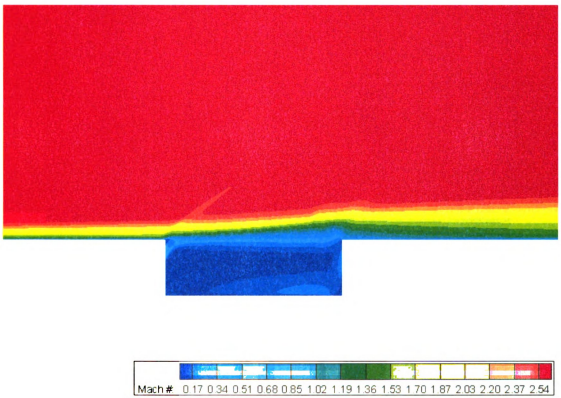

Figure 4.7 Mach number contours for case 2: M_{inj}= 0.6, θ= 45 degrees (L/h=5.0).

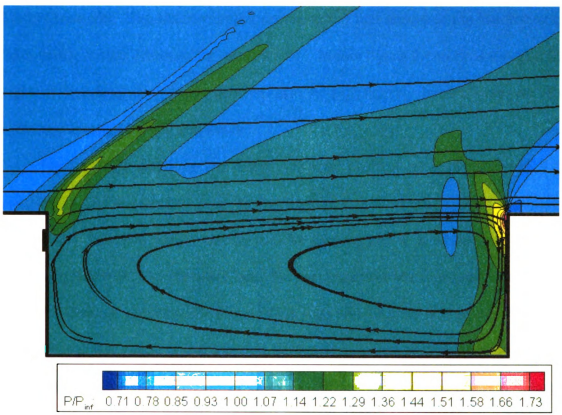

Figure 4.8 Pressure contours and selected streamlines for case 2: M_{inj}= 0.6, θ= 45 degrees (L/h=5.0).

in this figure is the pressure rise that occurs where the crossflow/injected fluid reconnects to the plate surface.

Figure 4.9 displays the Mach number profile at 1.0L and 1.5L downstream of the rear face of the cavity for the L/h=5.0 case with an injection Mach number of 0.60 (case #2). The Mach number profile at the just ahead of the leading edge of the cavity is also included for comparison. In this figure it can be seen that the height of the boundary layer downstream is significantly larger, however, the profile is also significantly shallower.

Figure 4.10 displays the Mach number profiles at a distance of 1.0L downstream of the injection port, for the baseline case in the L/h= 5.0 geometry and for two injection Mach numbers. In this figure, it is observed that the differences between the baseline and the two injection Mach number cases are minimal. All three produce shallow profiles with similar inflection points, however it is clear that the effect of the injected fluid was to primarily influence the profile in the region above the inflection point, in upper half of the boundary layer. Similar results are observed for the L/h = 8.0 case, however the effects are significantly damped out for the higher L/h ratio cases.

Figure 4.11 shows the relationship between the injection Mach number and the pressure across the cavity floor for the case where L/h = 5.0. The streamwise component, X/L, is zero at the leading edge of the cavity and one at the downstream face. In the baseline case there is no injection into the cavity and there exists a low-pressure region in the leading half of the cavity and a high-pressure region in the downstream half. When the injection is applied on the

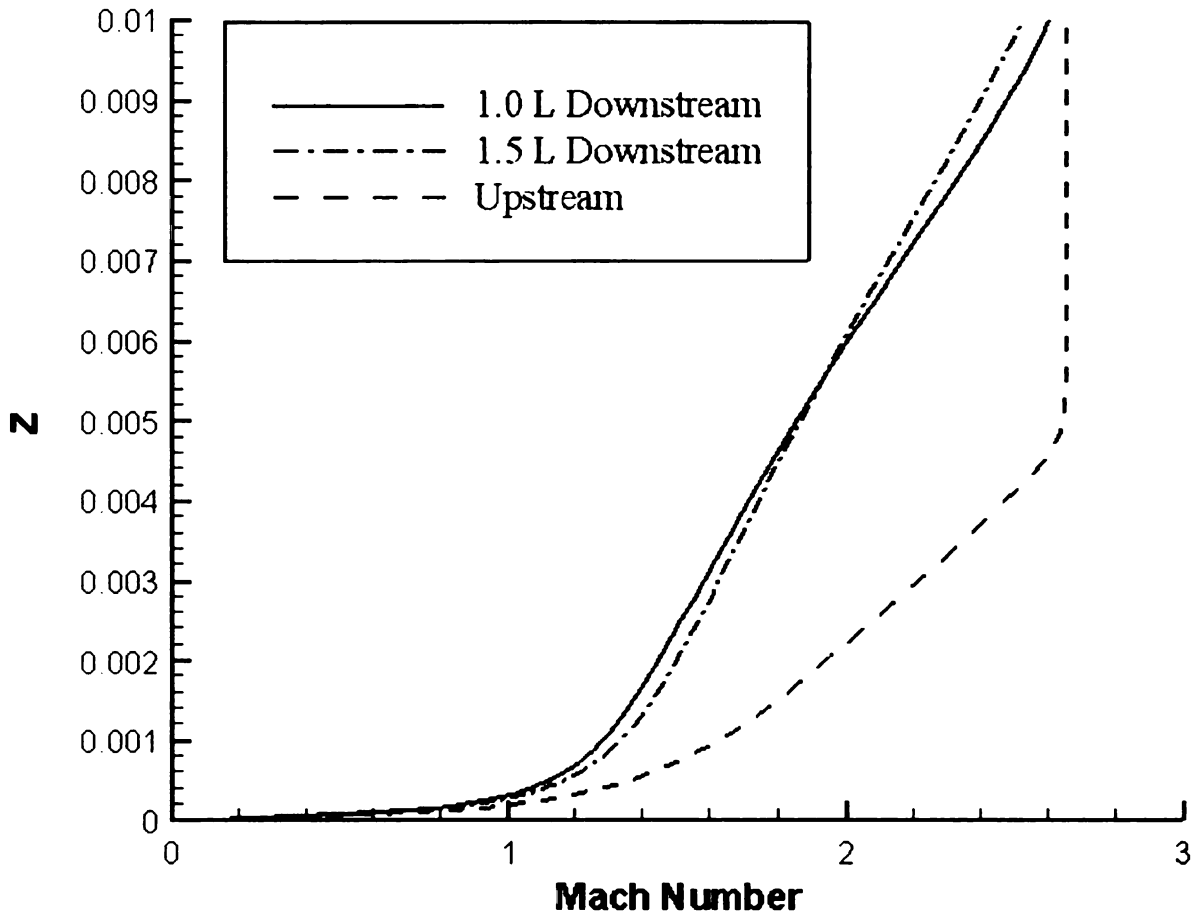

Figure 4.9 Mach number profiles normal to the plate surface at X/L = 1.5 and at X/L=1.0 for case 2: M_{inj}= 0.6, θ= 45 degrees (L/h=5.0).

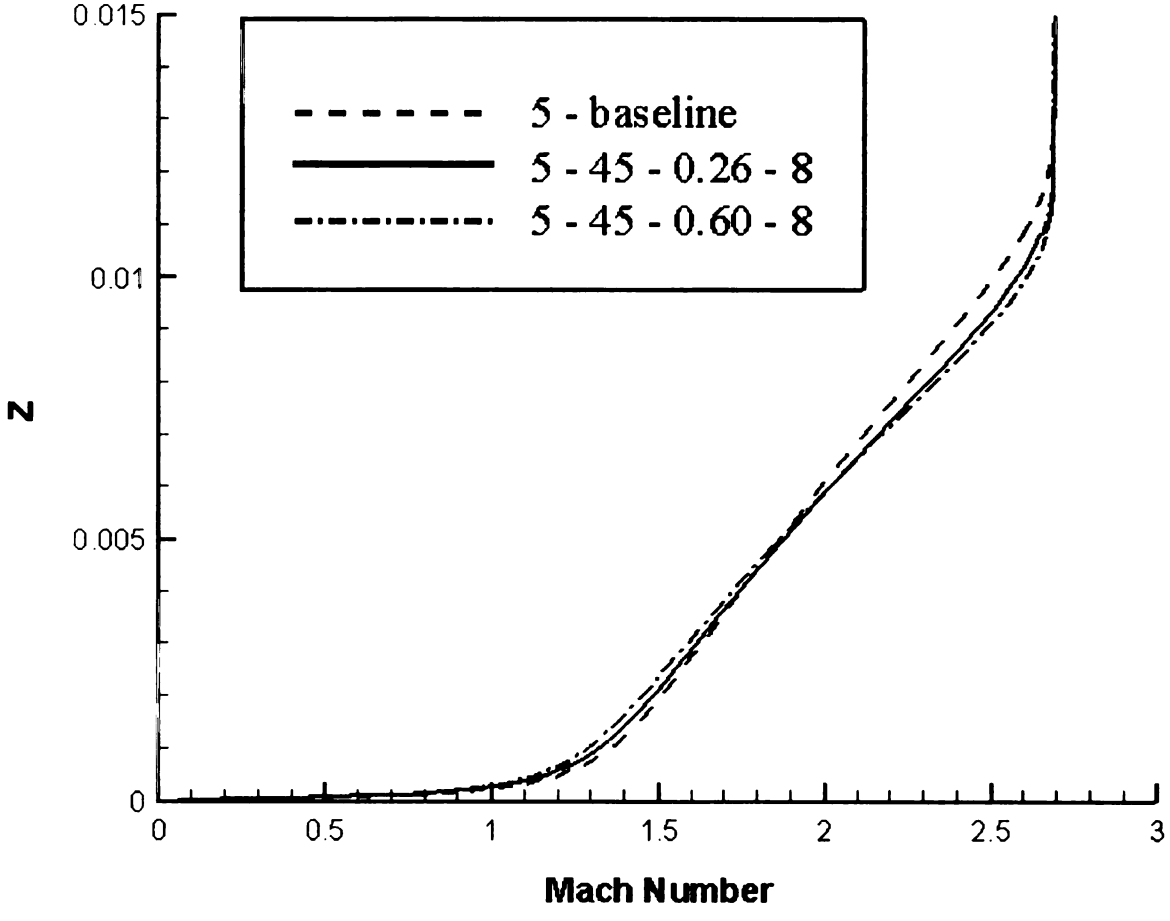

Figure 4.10 Mach number profiles normal to the plate surface at X/L = 1.5 for case 1, case 2 and case 3: M_{inj}= 0, M_{inj}= 0.26 and M_{inj}= 06, respectively (L/h=5.0).

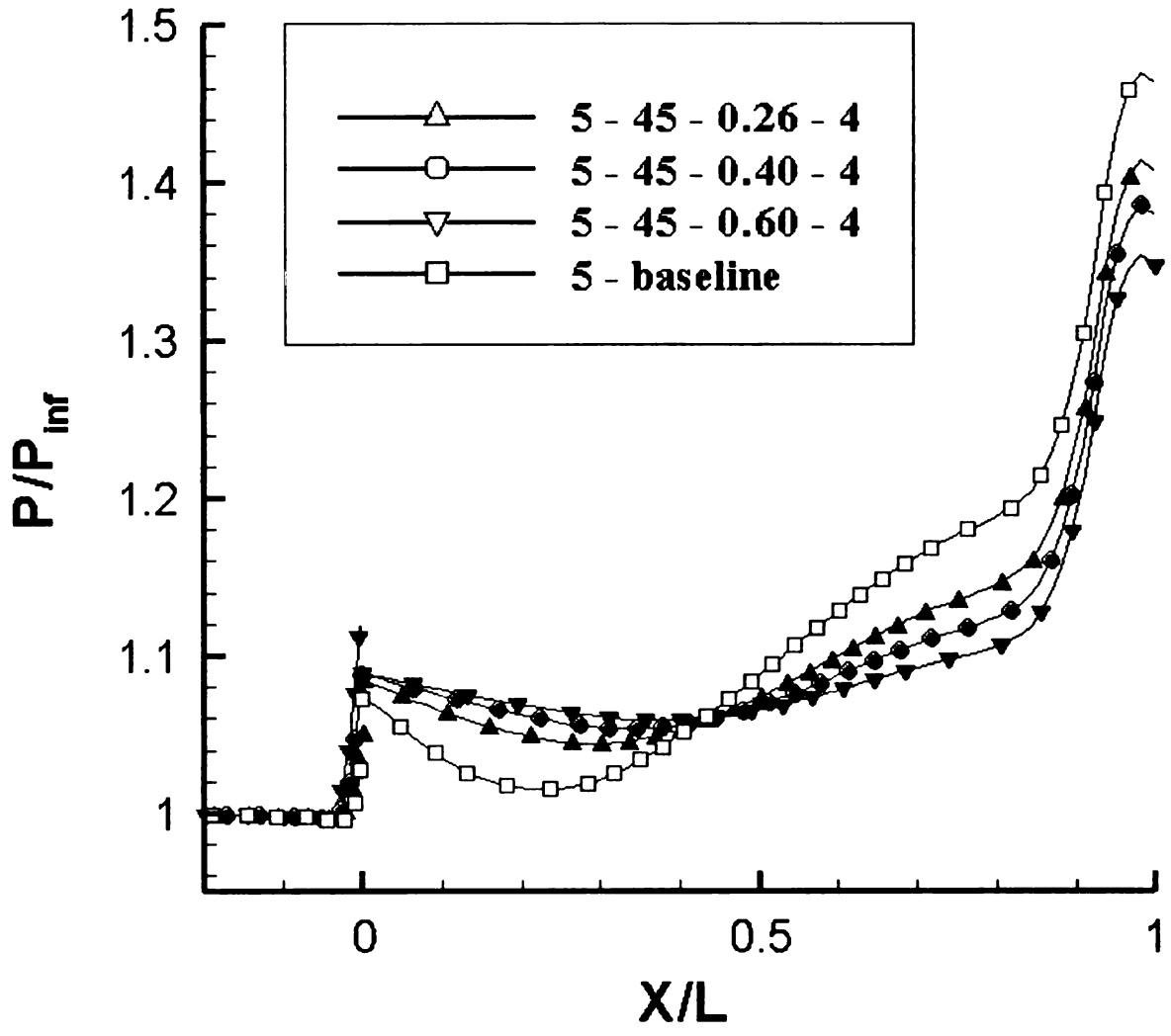

Figure 4.11 Pressure profiles (normalized) across the length of the cavity floor (streamwise direction) for case 5, case 6 and case 7: M_{inj}= 0, M_{inj}= 0.26 and M_{inj}= 06, respectively (L/h=5.0).

upstream face of the cavity, the effect is to even out the pressure distribution on the floor of the cavity. This trend is repeated for the L/h=8.0 case, however, the injection produced little to no effect on the floor pressure profiles in the L/h = 15.0 and L/h=17.5 cases (**Figure 4.12**).

Figure 4.13 shows a comparison when the height of the boundary layer is modified with respect to the cavity. In this figure, pressure profiles along the cavity floor are plotted for two ratios of the incoming boundary layer height to the depth of the cavity (delta/h) for a case where there is no injection. **Figure 4.14** shows the profile along the entire flat plate surface, including the cavity floor. Both cases yield the same pressure rise ahead of the cavity where the flow separates, but differ both along the cavity floor and downstream of the cavity. At most, they differ by approximately 10 percent, however, at distances far downstream of the cavity, they tend to even out.

Figure 4.15 details the grid system used to compare with the results from the wrap-around grid system. The grid system shown in **Figure 4.15** is a three block, patched grid system. The grid has a high aspect ratio across the entrance to the cavity due to the level of grid refinement needed to capture the boundary layer ahead of the cavity. **Figure 4.16** details the pressure profiles at three key points within the flow field: just ahead of the cavity, along the cavity floor, and just downstream of the cavity where the separated shear layer reconnects to the flat plate. In this figure, differences are observed to exist between the two grid methods.

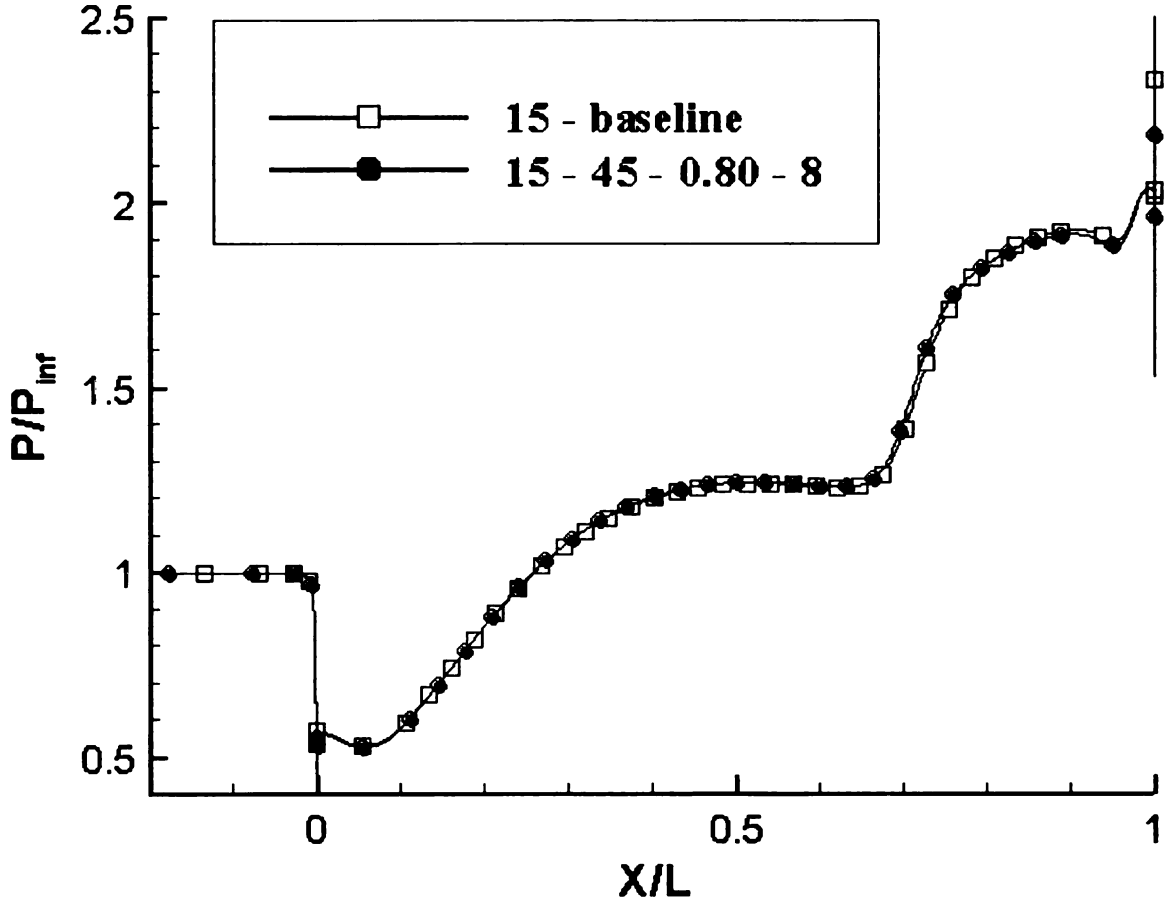

Figure 4.12 Pressure profiles (normalized) across the length of the cavity floor (streamwise direction) for case 8 and case 9: M_{inj}= 0, M_{inj}= 0.8, respectively (L/h=15.0).

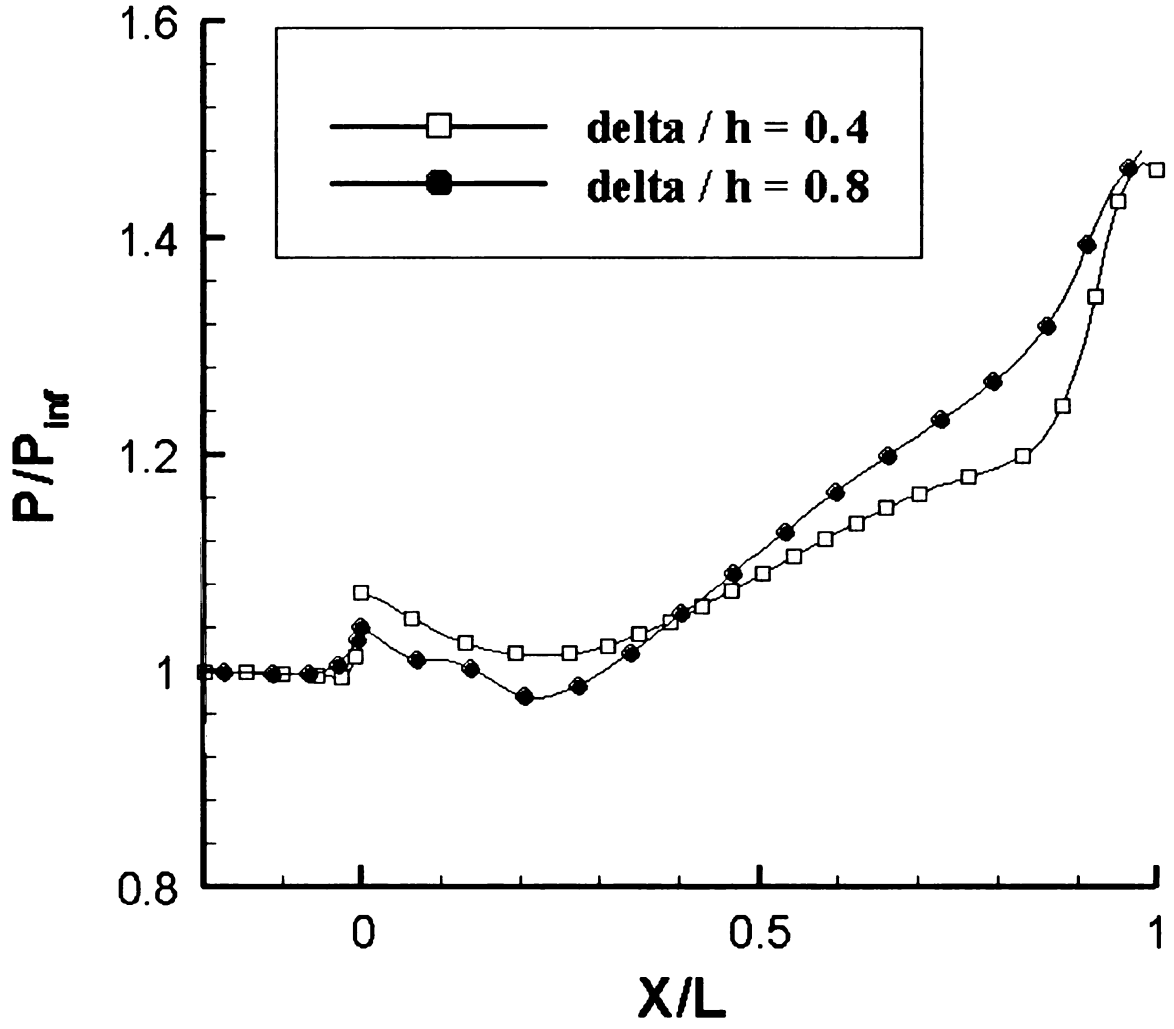

Figure 4.13 Pressure profiles (normalized) along cavity floor in the streamwise direction for delta/h = 0.8 and delta/h = 0.4: case 3 and case 4, respectively (L/h = 5.0).

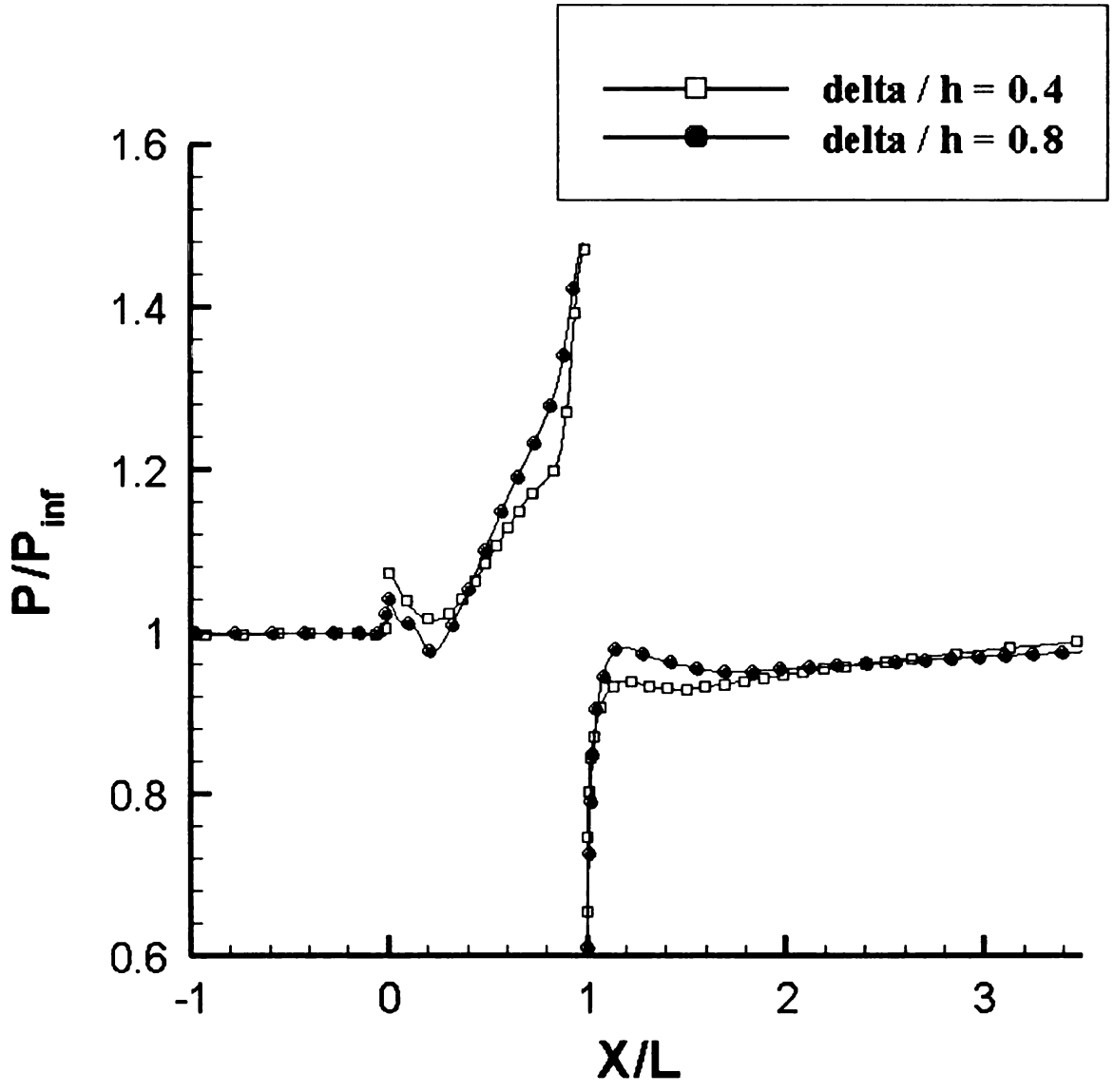

Figure 4.14 Pressure profiles (normalized) along flat plate surface in the streamwise direction for delta/h = 0.8 and delta/h = 0.4: case 3 and case 4, respectively (L/h = 5.0).

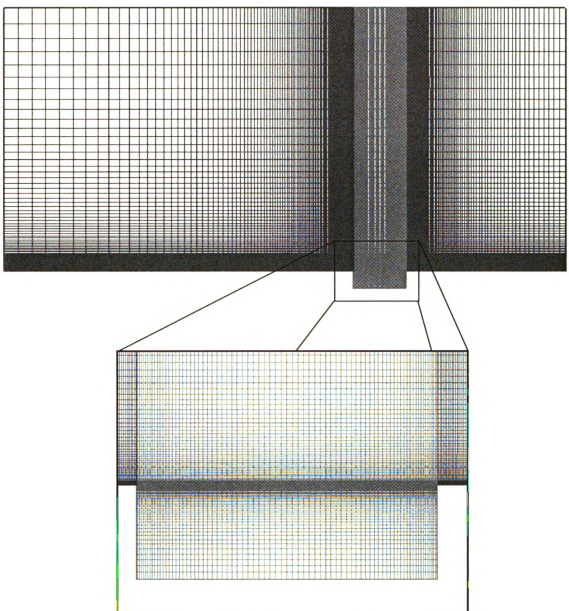

Figure 4.15 Patched-grid system used for comparison with the wrap-around grid system case (L/h = 5.0).

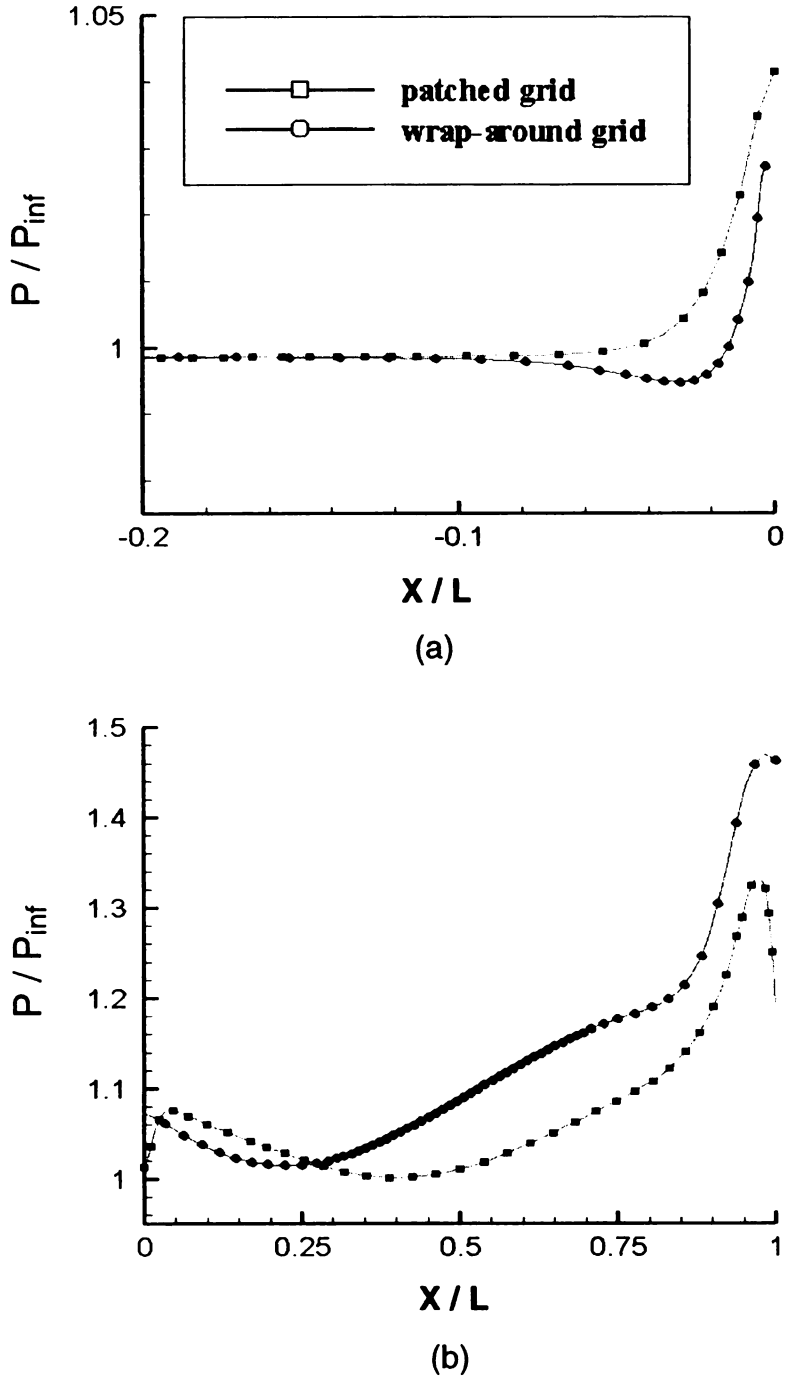

Figure 4.16 Normalized pressure profiles(a) ahead of the cavity, (b) along the cavity floor, and (c) just downstream of the cavity for the wrap-around grid and the patched grid in the L/h =5.0 case (case 1: no injection).

Figure 4.16 (cont'd)

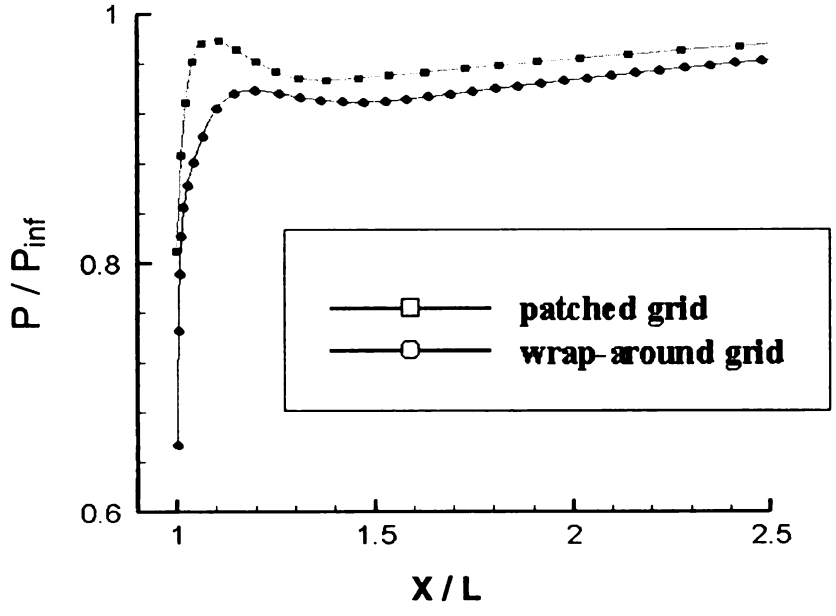

(c)

4.5 Conclusions

A number of simulations were conducted to investigate a proposed free stream-surface control structure generated by driving the flow within a cavity that is placed in a supersonic crossflow. Simulations were conducted to assess the dependence of the driven cavity flow field on the Mach number of the injected fluid and the mass flow rate of the injected fluid for length-to-depth (L/h) ratios that covered both open and closed cavity flow. In these simulations, the injection was implemented as a patch boundary condition and the total mass flow rate was controlled by the size of the injection boundary.

The results from the simulations on the closed cavity flows indicate that, for the situations examined, the injection on the upstream face of the cavity has little to no impact on the Mach number profiles downstream of the cavity. In this situation, the impingement of the separated shear layer on the floor of the cavity appears to wipe out any influences of the injected flow. In addition, the injected fluid has very little impact on the pressure profiles observed on the floor of the cavity and, therefore, is of little interest for the control of stores in aircraft. For the influence of the flow on the stores, however, bleed through the floor of the cavity combined with injection may result in the ability to tailor the location of the impingement and to change the character of the pressure profile in the leading edge of the cavity.

The results from the open cavity simulations provided a more direct assessment of the capabilities and potential for the driven cavity form of control. Without injection, an open-type cavity produces a dramatic jump in the boundary

layer thickness as the separated shear flow reconnects to the crossflow plate. In this case, although the pressure recovery coefficient on the cavity floor is positive and small, a pressure gradient does exist across the cavity floor. When fluid is injected on the leading edge of the cavity, the effect was to reduce the penetration of the separated crossflow into the cavity and to level the pressure profile along the cavity floor ahead of the jump that occurs at reconnection.

Downstream of the cavity, the influence of the injected jets is difficult to ascertain. In each case, the boundary layer profile was shallower than the upstream boundary layer profile and the boundary layer profile was observed to undergo an inflection near the halfway point. In these open geometry cases, the injection had the greatest impact on energizing the upper half of the boundary layer and not on the thickness of the boundary layer. The influence of the injected jet on the boundary layer profile can be further examined by increasing the total mass flow rate of the injected fluid. Since the depth of the cavity for the main cases studied was only slightly larger than the boundary layer height of the approaching fluid (often used as a bleed hole diameter measure), the injection port could conceivably take up the majority of the leading edge surface. This may result in a much larger boundary layer and a much fuller profile than was observed.

An additional assessment of the influence of the boundary layer height on the flow was conducted for the baseline case where L/h = 5.0. In these simulations, the height of the boundary layer in relation to the depth of the cavity

was shown to have a minor influence on the flow patterns that resulted. The largest impact seemed to occur on the reconnection face of the cavity.

Finally, a comparison the grid system (wrap-around vs. conventionally-structured grid) is presented. The results from this comparison indicate that the grid is a sensitive issue in the study of driven flow fields. With the patched grid, large aspect ratios exist directly in the region of the cavity where the separated shear flow undergoes its greatest amount of turning. In addition, patched grid boundaries exist at both the leading edge and reconnection lips of the cavities and both of these regions are where much of the dynamics of the flow take place. The wrap-around grid eliminates both of these issues, but instead introduces grid elements that are skewed and distorted.

CHAPTER 5

Conclusions and Recommendations

5.1 Conclusions

CFD simulations of a mixed-compression inlet and two methods for generating free stream-surfaces in a crossflow were conducted to motivate and initiate the development of a free stream-surface control method for use in the control of mixed-compression inlets. Where available, the results of these simulations were compared with experimental data to validate the methods employed and the conclusions reached. This research is presented to introduce a method of inlet control using free stream-surface structures and to address issues for future study. This includes items such as the location of bleed regions, methods for shielding the injection process from the high momentum of the crossflow, and areas for grid refinement.

During the simulation of flow through a mixed-compression inlet, several objectives were achieved. First, a method was developed for initiating critical flow in a simulation. Early on in this research one of the most difficult problems encountered was transitioning the flow from the initial conditions to the critical flow state. The flow initialization process was observed to be complicated by the interdependence of the shock location, applied back-pressure, bleed rate, and

bleed location. To assist with future simulations of these types of inlets, a method for initiating critical flow in a simulation of a mixed-compression inlet was developed. The key elements of this process are (1) the use of "slow-start" boundary conditions on the walls and (2) a method for positioning the terminal shock that anticipates the reduction in the effective-area that will occur when the solid surfaces are switched from inviscid walls to viscous walls.

A second outcome of these simulations was that a bleed boundary condition, designed to discern the flow through individual bleed holes, was implemented in the mixed-compression inlet. By modeling, instead of simulating, the flow through the bleed holes, the number of grid points needed to simulate critical flow was greatly reduced. In addition, this bleed boundary condition was designed to better capture the physics of the bleed process such as the barrier shocks and the flow turning that is characteristic of a bleed configuration.

In the simulations, this bleed boundary condition produced very different results from the bleed-slot boundary condition that is commonly used in practice. While both simulation of the bleed boundary condition and the slots led to separation, the bleed slots simulations led to steeper boundary layer profile and a stronger terminal shock. These differences highlight the influence of the bleed hole configuration and the effects of removing the azimuthal variation in the flow that is produced by bleed through discrete holes.

Finally, the simulations of the mixed-compression inlet have led to the proposal of a method of internal flow control that has been termed "free stream-surface control". In this approach, small changes in the effective-area of the inlet

are generated by the combination of injection and suction in the inlet. This process echoes the observations made during the development of the boundary layer of the mixed-compression inlet simulations. This free stream-surface control method could be used in mixed-compression inlets to mitigate the amount of cowl translation that is needed in initializing the flow or, possibly, to assist in the prevention of unstart.

After the simulations of the mixed-compression inlet were concluded, two different approaches to generating a free stream-surface control process were implemented to examine their potential for the control of a mixed-compression inlet. The objective of these simulations was to determine the relevant parameters of each method and to identify any issues associated with their use or implementation.

The first free stream-surface control mechanism that was examined used combined injection and suction to generate closed surfaces within the crossflow. In these simulations, the injection was modeled as a simple square injection port with a supersonic inflow boundary condition and the suction region was modeled with a boundary condition that permits bleed through discrete holes. Using this approach, it was observed that the combined injection and suction produced significant and easily recognizable free stream-surface control surfaces whose height could be adjusted by modifying the injection Mach number. The injected jet was observed to penetrate some distance into the crossflow and then turn and reconnect with the flat plate surface downstream of the bleed region.

Two issues associated with the method were identified. The first involves the degree to which the penetration of the crossflow was achieved with changes in Mach number. In these simulations it was observed that the maximum height achieved by the free stream-surface was linearly related to the injection Mach number. To affect meaningful control of the inlet profile with jets injected directly into the crossflow, this method would therefore require a significant energy input to achieve even modest results.

The second issue involves the generation of a zero net-mass flow and the bleed process used in the simulation. The discharge coefficient boundary condition for choked bleed through discrete holes does not permit the determination of the bleed rate as a part of the boundary condition. In addition, it was observed that the majority of the flow that was bled through the plate surface was from the fluid that was diverted by the jet rather than from the jet itself. The injected jet still responds to the bleed region, but it is not completely bled away by the suction region. This, however, may not be a negative issue for the system in that the boundary layer downstream of the bleed region is much fuller than it would have been without the free stream-surface control mechanism.

One other observation arising from these simulations is that the use of individual injection holes would lead to a distorted control shape and that a slot approach would be preferred even though the slot can only be implemented within an axisymmetric mixed-compression inlet in a modified form. To satisfy this issue, it was proposed that the slots could be replaced with closely packed,

elongated ellipses. While this system will have a distorted shape around the gaps in between the slots, it will, for the most part, behave as a uniform slot.

The second method for generating a free stream-surface involved the injection of fluid into a cavity that is recessed within the crossflow. In this approach, fluid injected through the sidewall of a cavity would drive the cavity flow and cause the separated of the crossflow to be diverted. In this manner, the injected fluid would be shielded from the high momentum of the supersonic crossflow and still be capable of altering the boundary layer profile downstream of the cavity. With a driven cavity, the downstream bleed needed to close the free stream-surface would be provided by the bleed holes that are normally used in the operation of the mixed-compression inlet.

Two different cavity geometry configurations were examined in this part of the research: open-cavity flow and closed-cavity flow. In the open-cavity flow, the length-to-depth ratio of the cavity was less than ten and the separated shear layer does not impinge of the floor of the cavity. In these simulations, the injected fluid was observed to affect the penetration of the crossflow into the cavity and to level out the pressure profile on the floor of the cavity, however, the impact of the injection on the downstream Mach number profiles and the boundary layer height was insignificant when compared with the action of an un-driven slot on the crossflow.

In the closed-cavity flow simulations, the injected jet had almost no impact on any of the examined parameters: pressure profile along the cavity floor, downstream Mach number profiles, boundary layer height. The strong effects of

the crossflow impinging on the floor of the cavity were too much for the injections studied. In this configuration, the injection on the leading edge of the cavity would most likely affect the location of the impingement.

5.2 Recommendations

This study is a first step in understanding the use of combined injection and suction to control flow throughout a mixed-compression inlet. The motivation for this study has been to identify and develop methods for controlling the location of the terminal shock within an inlet and preventing unstart. Continuing toward this goal, the next phase in this study should include several simulations involving the transverse injection of a jet into a supersonic crossflow to further identify the characteristics of the jet and this control method. In addition, further lines of investigation should address the shielding of the injection process and develop methods to achieve a boundary layer profile that is both thicker and fuller so that it will provide the desired level of control and resistance to separation. Future research would also involve implementing this control structure in a simulation of a mixed-compression inlet.

The first simulations conducted after this work should replace the coarse model of the injection port, presented in the third chapter, with a contoured nozzle for which experimental data exists as a basis for comparison. Although changing the method of injecting the fluid into the crossflow from a straight injection port to a nozzle would require significant additional grid generation, this would be necessary for a thorough examination of the jet-in-crossflow problem

and for generating injection boundary condition patches so that the free stream-surface control system can be implemented in a mixed-compression inlet simulation

Once these simulations are completed, the bleed through discrete holes can be implemented, and the general characteristics of the free stream-surface control structure can be examined in further detail for a round-hole injection. These simulations will benefit from the development of the discharge-coefficient bleed boundary condition and can utilize the same grid and solution from the previous studies. From these simulations, information about the shape and size of the control structure, as well as a functional relationship between the shape and the relevant parameters, can be acquired. As a additional study, if the turbulence characteristics of the jet-in-crossflow can be adequately modeled in simulations, it would be interesting to examine the effect that the addition of suction has on the mixing properties of the jet.

For the driven cavity method for controlling the flow through an inlet, future research should focus on examining the effect of increasing of the mass flow rate for the injection and on inserting injection within the driven cavity flow to control the reconnection of the separated shear layer. Methods also need to be established to generate a fuller velocity profile downstream of the cavity. To achieve this, experiments with supersonic injection into the subsonic cavity flow may lead to improvements in the boundary layer profiles.

For both of the approaches examined, an additional consideration that needs to be addressed in this research is the response of the system to oblique

and normal shocks. The environment where this system is envisioned to operate is complex in structure and rich in oblique shocks. When an oblique shock impinges on the structure, it is anticipated that the boundary layer would thicken appreciably, but the response of the system is unclear. As the boundary layer thickens, however, the profile above the downstream suction holes would be affected as well and it is important to characterize this response.

Finally, the stability of the suction-injection system in response to changes in the freestream conditions needs to be examined. This can be accomplished by imposing perturbations on the freestream boundary conditions in time-accurate simulations of a zero-net-mass flow system. Because of the grid spacing requirements near the solid surfaces, the time steps for these simulations will be very small. Although the perturbations will be in the streamwise direction, the variation and dynamics in the normal direction are significant and need to be addressed.

LIST OF REFERENCES

Abrahamson, K.W. and Bower, D.L., "An Empirical Boundary Condition for Numerical Simulation of Porous Plate Bleed Flows," AIAA Paper 88-0306, January 1988.

Adamson, T.C., and Nicholls, J.A., "On the Structure of Jets from Highly Underexpanded Nozzles into Still Air", Journal of Aero/Space Sciences, 1959, pp. 16-24.

Anderson, W.K., Thomas, J.L., and Whitfield, D.L., "Multigrid Acceleration of the Flux-Split Euler Equations," *AIAA Journal*, Vol. 26, No. 6, 1988, pp. 649-654

Benhachmi, D. Greber, I., and Hingst, W., "Experimental and Numerical Investigation of an Oblique Shock Wave/Boundary Layer Interaction with Continuous Suction," AIAA Paper 89-0357, January 1989.

Benson, D., Shih, T.I-P., Davis, D.O., "CFD Simulations of an Axisymmetric Mixed-Compression Inlet with Bleed Through Discrete Holes," FEDSM Paper 2003-45076, July 2003.

Benson, D., Shih, T.I-P., Davis, D.O., and Willis, B.P., "Boundary Conditions for CFD Simulations of Supersonic Boundary-Layer Bleed through Discrete Holes," AIAA Paper 2000-0888, Jan. 2000.

Benson, D.B., Shih, T.I-P., Davis, D.O., and Willis, B.P., "Bleed Boundary Conditions for CFD Simulations of Supersonic Flows with Embedded Shocks and Boundary-Layer Bleed," ASME Paper FEDSM-2001-18116, May 2001.

Beresh, S.J., Henfling, J.F. and Erven, R. J., "Flow Separation Inside a Supersonic Nozzle Exhausting into a Subsonic Compressible Flow," *Journal of Propulsion and Power*, vol.19, July/August 2003, pp 655-662.

Biedron, R.T., Krist, S.L., and Rumsey, C.L., *CFL3D User's Manual (Version 5.0)*, NASA Langley, 1996.

Bowersox, R.D., "Turbulent Flow Structure Characterization of Angled Injection into a Supersonic Crossflow", *Journal of Spacecraft and Rockets*, Vol. 34, No. 2, 1997, pp. 205-213.

Buggeln, R.C., McDonald, H., Kreskovsky, J.P., and Levy, R., "Computation of Three-Dimensional Viscous Supersonic Flow in Inlets," AIAA Paper 80-0194, 1980.

Chang, P.K., *Control of Flow Separation*, McGraw-Hill, New York, 1976.

Chakravarthy, S.R. and Osher, S., "High Resolution Applications of the Osher Upwind Scheme for the Euler Equations," AIAA Paper 86-1943, 1983.

Chen, L.T. and Caughey, D.A., "Calculation of Transonic Inlet Flowfields Using Generalized Coordinates," *Journal of Aircraft*, Vol. 17, 1980, pp. 167-174.

Chyu, W.J., Howe, G.W., and Shih, T.I-P., "Bleed Boundary Conditions for Numerically Simulated Mixed-Compression Supersonic Inlet Flows," AIAA Journal of Propulsion *and Power*, Vol. 8, No. 4, 1992, pp. 862-868.

Chyu, W.J., Kawamura, Y., and Bencze, D.P., "Calculation of External-Internal Flow Fields for Mixed-Compression Inlets," NASA TM-88362, 1986.

Chyu, W.J., Rimlinger, M.J., and Shih, T.I-P., "Control of Shock-Wave/Boundary-Layer Interactions by Bleed," *AIAA Journal*, Vol. 33, No. 7, 1995, pp. 1239-1247.

Flores, A.J., Shih, T.I-P., Davis, D.O., and Willis, B.P., "Bleed of Supersonic Boundary-Layer Flow through Rows of Normal and Inclined Holes," AIAA Paper 99-2112, June 1999.

Hahn, T.O., Shih, T.I-P., and Chyu, W.J., "Numerical Study of Shock-Wave/Boundary-Layer Interactions with Bleed," *AIAA Journal*, Vol. 31, No. 5, 1993, pp. 869-876.

Hamed, A. and Lehnig, T., "Effect of Bleed Configuration on Shock/Boundary Layer Interactions," *AIAA Journal of Propulsion and Power*, Vol. 11, No. 1, 1995, pp. 42-48.

Harloff, G.J. and Smith, G.E., "On Supersonic-Inlet Boundary-Layer Bleed Flow," AIAA Paper 95-0038, January 1995.

Huang, W., Yamasaki, N., Masanobu, N., "Numerical Study of Interaction of a Jet with a Supersonic Cross Flow", *Memoirs of the Faculty of Engineering, Kyushu University*, vol. 50, 1990, pp 467-488.

Hurley, D.G., "The Use of Boundary Layer Control to Establish Free Streamline Flows", *Boundary Layer and Flow Control*, G.V. Lachmann, ed., Pergamon Press, New York, 1961.

Joslin, R., Horta, L, Chen, F.-J., "Transitioning Active Flow Control to Applications", AIAA Paper 99-3575, June 1999.

Kawamura, T., Chyu, W.J., and Bencze, D.P., "Numerical Simulation of Three-Dimensional Supersonic Inlet Flow Fields," AIAA Paper 87-0160, 1987.

Knight, D.D., "Numerical Simulation of Realistic High-Speed Inlets Using the Navier-Stokes Equations," *AIAA Journal*, Vol. 15, 1977, pp. 1583-1589.

Lee, J., Sloan, M.L., and Paynter, G.C., "A Lag Model for Turbulent Boundary Layers Developing over Rough Bleed Surfaces," *AIAA Journal of Propulsion and Power*, Vol. 10, No. 4, 1994, pp. 562-568.

Lin, Y.-L., Stephens, M.A., Shih, T.I-P., and Willis, B.P., "Effects of Plenum Size on Bleeding a Supersonic Boundary Layer," AIAA Paper 97-0609, Jan. 1997.

Menter, F.R., "Performance of Popular Turbulence Models for Attached and Separated Adverse Pressure Gradient Flows," *AIAA J.*, Vol. 30, No. 8, 1992, pp. 2066-2071.

Menter, F.R., "Zonal Two-Equation k-ω Turbulence Models for Aerodynamic Flows," AIAA Paper 93-2906, 1993.

Ni, R.-H., "A Multiple Grid Scheme for Solving the Euler Equations," AIAA Paper 81-1025, 1981.

Paynter, G.C. and Chen, H.C., "Progress toward the Analysis of Supersonic Inlet Flows," AIAA Paper 83-1371, 1983.

Paynter, G.C., Treiber, D.A., and Kneeling, W.D., "Modeling Supersonic Inlet Boundary Layer Bleed Roughness," *AIAA Journal of Propulsion and Power*, Vol. 9, No. 4, 1994, pp. 622-627.

Presley, L.L., "Internal Flow Calculations for Axisymmetric Supersonic Inlets at Angle of Attack," AIAA Paper 75-1214, 1975.

Plentovich, E.B., Stallings, R.L., Tracy, M.B., "Experimental Cavity Measurements at Subsonic and Transonic Speeds: Static Pressure Results", NASA TP-3358, 1993.

Pulliam, W.R. and Chaussee, D.S., "A Diagonal Form of an Implicit Approximate Factorization Algorithm," *Journal of Computational Physics*, Vol. 39, 1981, pp. 347-363.

Rimlinger, M.J., Shih, T.I-P., and Chyu, W.J., "Shock-Wave/Boundary-Layer Interactions with Bleed through Rows of Holes," *AIAA Journal of Propulsion and Power*, Vol. 12, No. 2, 1996, pp. 217-224.

Rimlinger M.J., Shih, T.I-P., Chyu, W.J., Willis, B.P., and Davis, D.O., "Computations of Shock-Wave/Boundary-Layer Interactions with Bleed," AIAA Paper 96-0432, Jan. 1996.

Roe, P.L., "Approximate Riemann Solvers, Parameter Vector and Difference Schemes," *J. of Computational Physics*, Vol. 43, 1981, pp. 357-72.

Roe, P.L., "Characteristic Based Schemes for the Euler Equations," *Annual Review of Fluid Mechanics*, Vol. 18, 1986, pp. 337-65.

Rumsey, C.L. and Vatsa, V.N., "A Comparison of the Predictive Capabilities of Several Turbulence Models Using Upwind and Central-Difference Computer Codes," AIAA Paper 93-0192, Jan. 1993.

Santiago, J.G. and Dutton, J.C., "Velocity Measurements of a Jet Injected into a Supersonic Crossflow", *AIAA Journal of Propulsion and Power*, Vol. 13, No. 2, 1997, pp. 264-273.

Schetz, J.A. and Billig, F.S., "Penetration of Gaseous Jets Injected into a Supersonic Stream", *Journal of Spacecraft and Rockets*, Vol. 3, No. 11, 1966, pp. 1658-1665.

Seddon, J. and Goldsmith, E.L., *Intake Aerodynamics*, AIAA, New York, 1985.

Shih, T.I-P., Rimlinger, M.J., and Chyu, W.J., "Three-Dimensional Shock-Wave/Boundary-Layer Interaction with Bleed," *AIAA Journal*, Vol. 31, No. 10, 1993, pp. 1819-1826.

Shih, T.I-P., Benson, T.J., Willis, B.P., Rimlinger, M.J., and Chyu, W.J., "Structure of Shock-Wave/Boundary-Layer Interaction with Bleed through Rows of Circular Holes," AIAA Paper 97-0508, Jan. 1997.

Smeltzer, D.B. and Sorensen, N.E., "Test of a Mixed Compression Axisymmetric Inlet with Large Transonic Mass Flow at Mach Numbers 0.6 to 2.65," NASA TN D-6971, 1972.

Spaid, F.W. and Zukoski, E.E., "A Study of Secondary Injection of Gaseous Jets from Transverse Slots with Supersonic External Flows," *AIAA Journal*, Vol. 6, 1968, pp. 205-212.

Stallings, R.L., Wilcox, F.J., "Experimental Cavity Pressure Distributions at Supersonic Speeds", NASA TP-2683, 1987.

Stallings, R.L., Wilcox, F.J., and Forrest, D.K., "Measurements of Forces, Moments, and Pressures on a Generic Store Separating from a Box Cavity at Supersonic Speeds", NASA TP-3110, 1991.

Thomas, J.L., Krist, S.T., and Anderson, W.K., "Navier-Stokes Computations of Vortical Flows over Low-Aspect-Ratio Wings", *AIAA .lournal*, Vol. 28, No. 2, 1990, pp. 205-212.

Vadyak, J., Hoffman, J.D., and Bishop, A.R., "Three-Dimensional Flow Simulations for Supersonic Mixed-Compression Inlets at Incidence," *AIAA Journal*, Vol. 22, 1984, pp. 873-881.

Vadyak, J., Smith, M.J., and Schuster, D.M., "Navier-Stokes Simulations of Supersonic Fighter Intake Flowfields," AIAA Paper 87-1752, 1987.

VanLerberghe, W., Santiago, J., Dutton, J., Lucht, R., "Mixing of a Sonic Transverse Jet Injected into a Supersonic Flow", *AIAA Journal*, vol. 38, 2000, pp. 470-479.

Wilcox, F.J., "Experimental Investigation of Porous-Floor Effects on Cavity Flow Fields at Supersonic Speeds", NASA TP-3032, 1990.